ISSN 2413-9432

BIOMEDICAL PHOTONICS

Volume 14, #1, 2025

In the issue:

BMP

Российская Фотодинамическая Ассоциация

www.pdt-association.com

BIOMEDICAL PHOTONICS

BIOMEDICAL PHOTONICS –
research and practice, peer-reviewed, multidisciplinary journal.
The journal is issued 4 times per year.
The circulation – 1000 copies., on a quarterly basis.

The journal is included into the List of peer-reviewed science press of the State Commission for Academic Degrees and Titles of Russian Federation
The journal is indexed in the international abstract and citation database – Scopus.

The publisher «Agentstvo MORE».
Moscow, Khokhlovskiy lane, 9

Editorial staff:

Chief of the editorial staff	Ivanova-Radkevich V.I.
Science editor professor	Mamontov A.S.
Literary editor	Moiseeva R.N.
Translators	Kalyagina N.A.
Computer design	Kreneva E.I.
Desktop publishing	Shalimova N.M.

The Address of Editorial Office:
Russia, Moscow, 2nd Botkinskiy proezd, 3
Tel. 8 (495) 945–86–60
www: PDT-journal.com
E-mail: PDT-journal@mail.ru

Corresponding to:
125284, Moscow, p/o box 13

Registration certificate ПИ № ФС 77–51995, issued on 29.11.2012 by the Federal Service for Supervision of Communications, Information Technology, and Mass Media of Russia

The subscription index of «Rospechat» agency – 70249

BIOMEDICAL PHOTONICS

BIOMEDICAL PHOTONICS –
научно-практический, рецензируемый,
мультидисциплинарный журнал.
Выходит 4 раза в год.
Тираж – 1000 экз., ежеквартально.

Входит в Перечень ведущих рецензируемых научных журналов ВАК РФ.
Индексируется в международной реферативной базе данных Scopus.

Издательство «Агентство МОРЕ».
Москва, Хохловский пер., д. 9

Редакция:

Зав. редакцией	Иванова-Радкевич В.И.
Научный редактор	проф. Мамонтов А.С.
Литературный редактор	Моисеева Р.Н.
Переводчики	Калягина Н.А.
Компьютерный дизайн	Кренева Е.И.
Компьютерная верстка	Шалимова Н.М.

Адрес редакции:
Россия, Москва, 2-й Боткинский пр., д. 3
Тел. 8 (495) 945–86–60
www: PDT-journal.com
E-mail: PDT-journal@mail.ru

Адрес для корреспонденции:
125284, Москва, а/я 13

Свидетельство о регистрации ПИ
№ ФС 77–51995, выдано 29.11.2012 г.
Федеральной службой по надзору в сфере связи, информационных технологий и массовых коммуникаций (Роскомнадзор)

Индекс по каталогу агентства «Роспечать» – 70249

ORIGINAL ARTICLES

REVIEWS OF LITERATURE

ОРИГИНАЛЬНЫЕ СТАТЬИ

ОБЗОРЫ ЛИТЕРАТУРЫ

POSSIBILITIES OF INTERSTITIAL PHOTODYNAMIC THERAPY IN THE TREATMENT OF BRAIN GLIOBLASTOMA

Rynda A.Yu., Olyushin V.E., Rostovtsev D.M., Zabrodskaya Yu.M., Papayan G.V.
Russian Neurosurgical Institute named after prof. A.L. Polenov – a branch of the National Medical Research Center named after V.A. Almazov Ministry of Health of Russia, St. Petersburg, Russia

Abstract

Interstitial photodynamic therapy (iPDT) is a minimally invasive treatment method based on the interaction of light, a photosensitizer (PS) and oxygen. In brain gliomas, iPDT involves the stereotactic introduction of one or more light guides into the target area to irradiate tumor cells and tissues that have accumulated PS, which subsequently causes necrosis and/or apoptosis of tumor cells, destruction of the tumor vascular network and causes an inflammatory reaction that triggers stimulation of the antitumor immune response.

The aim of the study was to analyze the possibility of using iPDT in the treatment of unifocal, small-sized (up to 3.5 cm) glioblastomas.

The study with iPDT included 7 patients with a unifocal variant of glioblastoma with a maximum tumor size of up to 3.5 cm and a Karnofsky score of at least 70 points. In 5 patients (71.4%) there was a relapse of glioblastoma, in 2 cases (28.6%) the tumor was diagnosed for the first time. As a PS, PS photoditazine was used, administered intravenously by drip at a dose of 1 mg/kg. Interstitial irradiation was performed using a laser (Latus 2.5 (Atkus, Russia)) with a wavelength of 662 nm and a maximum power of 2.5 W and cylindrical scattering fibers. The target tumor volume was determined after combining multimodal CT images (contrast-enhanced scanning, axial slices of 0.6 mm) with preoperative MRI, PET. Spatial precise interstitial irradiation of the tumor volume was planned using special software. The duration of irradiation did not exceed 15 min. The light dose was from 150 to 200 J/cm^2. Transient clinical deterioration was recorded in about 2 patients (28.6%). These 2 patients had worsening neurological deficits in the early postoperative period (increase in hemiparesis from 4 points to 2 points in one patient and development of dysarthria and dysphasia in the second patient). The median overall survival from the first diagnosis of malignant glioma to death was 28.3 months. The median relapse-free survival was 13.1 months. MGMT status played a significant role in the outcome of patients treated with iPDT. Patients with a methylated MGMT promoter survived longer than patients with an unmethylated MGMT promoter by a median of 22.1 months, and they did not experience disease progression for an additional 9.3 months.

iPDT may be a promising treatment option in a population of patients at high risk of postoperative neurological deficit. It does not interfere with, but rather may complement, other treatment options for this disease, such as repeat radiation therapy and chemotherapy. iPDT remains a potential option for deep-seated gliomas in patients with high surgical risk and in case of tumor recurrence.

Key words: glioblastoma, interstitial photodynamic therapy, new technologies, results, glioma.

For citations: Rynda A.Yu., Olyushin V.E., Rostovtsev D.M., Zabrodskaya Yu.M., Papayan G.V. Possibilities of interstitial photodynamic therapy in the treatment of brain glioblastoma, *Biomedical Photonics*, 2025, vol. 14, no. 1, pp. 4–19. doi: 10.24931/2413–9432–2025–14–1–4–19

Contacts: Rynda A.Yu., e-mail: artemii.rynda@mail.ru

ВОЗМОЖНОСТИ ИНТЕРСТИЦИАЛЬНОЙ ФОТОДИНАМИЧЕСКОЙ ТЕРАПИИ В ЛЕЧЕНИИ ГЛИОБЛАСТОМ ГОЛОВНОГО МОЗГА

А.Ю. Рында, В.Е. Олюшин, Д.М. Ростовцев, Ю.М. Забродская, Г.В. Папаян
Российский нейрохирургический институт имени проф. А.Л. Поленова – филиал ФГБУ «Национальный медицинский исследовательский центр имени В.А. Алмазова» Минздрава России, Санкт-Петербург, Россия

Резюме

Интерстициальная фотодинамическая терапия (иФДТ) — это минимально инвазивный метод лечения, основанный на взаимодействии света, фотосенсибилизатора (ФС) и кислорода. При глиомах головного мозга иФДТ включает стереотаксическое введение одного или нескольких световодов в целевую область для облучения опухолевых клеток и тканей, накопивших ФС, что вызывает в дальнейшем некроз и/или апоптоз опухолевых клеток, разрушение сосудистой сети опухоли и воспалительную реакцию, запускающую противоопухолевый иммунный ответ.

Целью исследования являлся анализ возможности применения иФДТ при лечении одноочаговых, небольших по размерам (до 3,5 см) глиобластом.
В исследование были включены 7 пациентов с одноочаговым вариантом глиобластомы с максимальным размером опухоли до 3,5 см и оценкой по шкале Карновского не менее 70 баллов. У 5 (71,4%) пациентов был рецидив глиобластомы, в 2 (28,6%) случаях опухоль была впервые диагностированной. В качестве ФС использовали фотодитазин, вводимый внутривенно капельно в дозе 1 мг/кг веса тела. Внутритканевое облучение выполняли с использованием лазера (Латус 2,5 (Аткус, Россия)) с длиной волны 662 нм и максимальной мощностью 2,5 Вт и цилиндрических рассеивающих волокон. Целевой объем опухоли определяли после объединения мультимодальных изображений КТ (сканирование с контрастным усилением, аксиальные срезы 0,6 мм) с предоперационной МРТ, ПЭТ. Пространственное точное внутритканевое облучение объема опухоли планировали с использованием специального программного обеспечения. Длительность облучения не превышала 15 мин. Световая доза составила от 150 до 200 Дж/см^2.
Транзиторное клиническое ухудшение было зафиксировано у 2 (28,6%) пациентов. У них наблюдали нарастание неврологического дефицита в раннем послеоперационном периоде (нарастание гемипареза с 4 баллов до 2 баллов у одного пациента и появление дизартрии и дисфазии у второго пациента). Медиана общей выживаемости от первого диагноза злокачественной глиомы до смерти составила 28,3 мес. Медиана безрецидивной выживаемости составила 13,1 мес. Статус MGMT сыграл значительную роль в результатах лечения пациентов с иФДТ. Пациенты с метилированным промотором MGMT жили дольше, чем пациенты с неметилированным промотором MGMT, в среднем на 22,1 мес, и у них не наблюдали прогрессирования заболевания в течение дополнительных 9,3 мес.
иФДТ может быть многообещающим вариантом лечения в популяции пациентов с высоким риском послеоперационного неврологического дефицита. Это не мешает, а скорее может дополнять другие варианты лечения данного заболевания, такие как повторная лучевая терапия и химиотерапия. иФДТ остается потенциальным вариантом при глубоко расположенных глиомах у пациентов с высоким хирургическим риском и при рецидиве опухоли.

Ключевые слова: глиобластома, интерстициальная фотодинамической терапии (иФДТ), новые технологии, результаты, глиома.

Для цитирования: Рында А.Ю., Олюшин В.Е., Ростовцев Д.М., Забродская Ю.М., Папаян Г.В. Возможности интерстициальной фотодинамической терапии в лечении глиобластом головного мозга // Biomedical Photonics. – 2025. – Т. 14, № 1. – С. 4–19. doi: 10.24931/2413–9432–2025–14–1–4–19

Контакты: Рында А.Ю., e-mail: artemii.rynda@mail.ru

Introduction

Glioblastoma (2021 WHO CNS, Grade IV) is the most common primary malignant tumor of the central nervous system [1-4]. Despite advances in oncology and the introduction of new methods and regimens for the treatment of malignant neoplasms of the central nervous system into clinical practice in recent decades, significant progress in achieving stable remission and increasing life expectancy in this category of patients has not been achieved [5-9]. A very low median overall survival of 12-16 months, persistent tumor resistance to drugs, and a high degree of diffuse, aggressive, and invasive tumor growth indicate that the treatment of glioblastomas remains a difficult task [10-17].

The current standard of treatment includes maximally safe tumor resection followed by adjuvant chemotherapy and radiotherapy [1, 2, 18-22]. Thus, even new advances in glioblastoma surgery (using fluorescence-guided surgery) have not fundamentally changed the prognosis of patients, and it still remains disappointing. In addition, patients with tumors localized in functionally significant or deep areas of the brain are often not prescribed surgical treatment using fluorescence navigation due to the high risk of aggravation or occurrence of neurological deficit in the postoperative period. To solve this problem and potentially prolong survival while maintaining adequate quality of life, several new approaches based on minimally invasive or non-invasive procedures such as brachytherapy, immunotherapy, radiosurgery, transcranial focused ultrasound or chemoradiation therapy have been investigated [4, 6, 9, 22-29].

Among these approaches, interstitial photodynamic therapy (iPDT) can be considered as a promising option based on the standard stereotactic procedure [30-33]. Patients receive PS orally or intravenously, which results in the appearance of the active substance in the intravascular space of the target tissue (tumor). Due to the dysfunction of the blood-brain barrier in the tumor area and impaired metabolism in tumor cells, PS selectively accumulates in malignant cells. Minimally traumatic access is performed from one trephination hole, no more than 1.5 cm in diameter. Then, along a pre-planned trajectory (stereotactic marking), the fibers of the optical diffuser are immersed in the target tumor tissue and the tumor is irradiated with a laser source. Excitation of PS by light causes the production of active oxygen species (in particular, singlet oxygen), which damage and ultimately destroy neoplastic cells. Compared to standard PDT, standard craniotomy is not required, and the tumor is accessed through a trephination hole. Thus, dead tumor tissue remains inactivated *in situ* [34-41]. Another advantage of the method is that normal brain tissue is preserved due to the selective accumulation of PS in the tumor (Fig. 1).

The effects of iPDT on tumor tissue and its environment are still being studied due to the abundance of processes involved. In particular, the activation of the immune response to the use of PDT plays a significant role. At

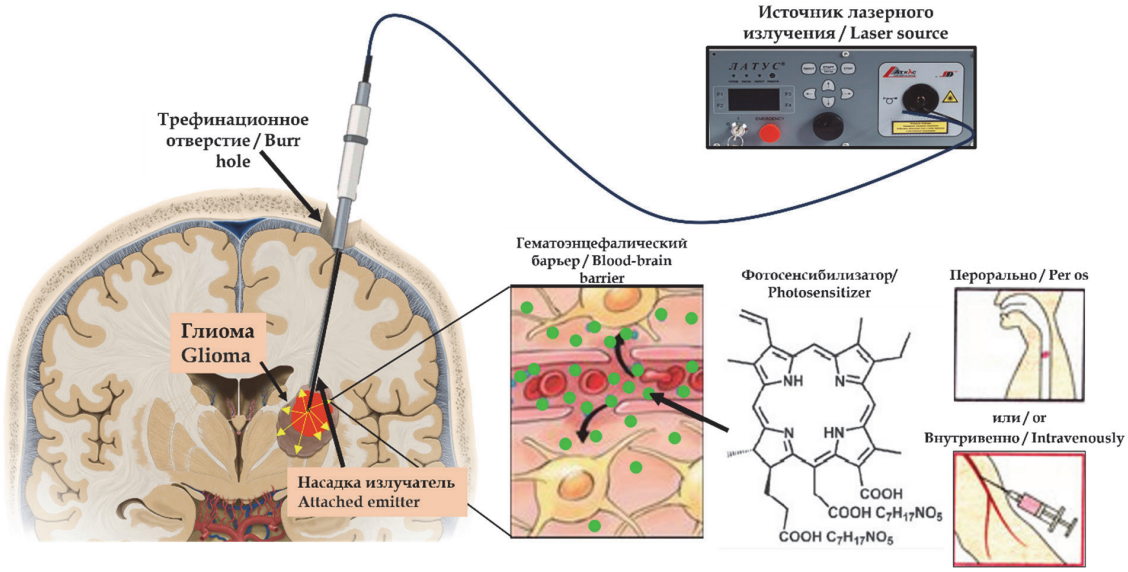

Рис. 1. Блок схема метода интерстициальной фотодинамической терапии.
Fig. 1. Block diagram of the interstitial photodynamic therapy method.

present, there is a relatively small number of clinical studies describing the use of this technique in patients with glioblastoma and presenting long-term results of the study after its use [3, 8, 11, 25, 42-46].

To determine the capabilities of this technique, we studied the intraoperative iPDT and the long-term results of its use in a cohort of patients with glioblastoma.

Materials and Methods

A single-center, cohort prospective study with elements of retrospective analysis was conducted at the Department of Neurooncology of the Russian Research Institute of Neurosurgery named after prof. A.L. Polenov. The study included 7 patients of different genders and ages.

All patients signed voluntary informed consent to participate in the study in accordance with Good Clinical Practice (GCP) (Clinical Trials Directive 2001/20/EC; GCP Directive 2005/28/EC; Clinical Trials Regulation 536/2014; Executive Commission (Regulation 2017/556)), Good Manufacturing Practice (GMP) standards and the principles of the Helsinki Declaration, 7th revision of 2013. The study was approved by the local ethics committee at the Russian Research Institute of Neurosurgery named after prof. A.L. Polenova No. 4 from 12/17/2013.

The inclusion criteria for the study were:

- written informed consent;
- age 18–75 years;
- Karnofsky performance status (KPS) ≥70 points;
- radiologically suspected diagnosis (according to RANO criteria [47]) of the first recurrence of glioblastoma located in the cerebral hemisphere, including the insular and intermediate lobes of the brain; tumors in the brainstem were excluded; the first MRI (magnetic resonance imaging) with signs of first recurrence (radiological RANO criteria for disease progression [47]) within 8 weeks before informed consent, not necessarily identical to the primary tumor location, or primary glioblastoma with deep localization without the possibility of complete tumor removal due to the high risk of postoperative neurological deficit;
- single or single progressive presence of contrast enhancement according to MRI, the largest tumor diameter no more than 3.5 cm.

Exclusion criteria:

- multifocal disease (more than 2 sites);
- patients with significant non-contrasting areas of tumor;
- previous treatment for relapse;
- presence of another malignancy;
- hypersensitivity to porphyrins;
- porphyria;
- HIV infection, active hepatitis B or C infection;
- patients with poor prognosis, such as severe ischemic heart disease, heart failure (NYHA III/IV), severe poorly controlled diabetes, immunodeficiency, residual neurological deficit after stroke, severe mental retardation or other serious concomitant systemic disorders incompatible with the study;
- any active infection;
- any psychological, cognitive, family, social condition that, in the opinion of the researcher, compromises the patient's ability to understand health information and the procedure, to give informed consent or to comply with the study protocol;
- previous antiangiogenic therapy;
- participation in another interventional clinical trial

during this study or within 4 weeks before the start of this study;
- pregnancy or breastfeeding.

The tumor size did not exceed the maximal extension of 3.5 cm, determined by gadolinium enhancement of the tumor on T1-weighted MRI. Viability of the tumor tissue was previously confirmed by a minimally invasive stereotactic biopsy procedure with subsequent morphological examination to exclude treatment-related effects or pseudoprogression of the tumor. The size limitation was based on the maximum number of light fibers per laser, since the optimal distance between

Таблица 1
Клиническая характеристика пациентов
Table 1
Clinical characteristics of patientsy

Характеристики пациентов с иФДТ Characteristics of patients with iPDT	Пациент Patient						
	1	2	3	4	5	6	7
Возраст (лет) **Age (years)**	45	61	47	58	53	60	49
Пол **Gender**	м m	м m	ж f	м m	ж f	м m	ж f
Индекс Карновского **Karnofsky index**	80	80	90	80	80	80	90
Симптомы заболевания **Symptoms of the disease**							
общемозговая симптоматика general cerebral symptoms	+	+	+	+	+		+
судорожный синдром convulsive syndrome	+						
афазия без парезов aphasia without paresis	+				+		
парез без афазии paresis without aphasia		+				+	
афазия и парез aphasia and paresis							
Сторона полушария **Side of the hemisphere**	правая right	левая left	правая right	правая right	левая left	левая left	правая right
Локализация, доля мозга **Localization, brain lobe**							
лобная frontal			+				
височная temporal	+				+		
теменная parietal		+					+
затылочная occipital						+	
таламическая область thalamic region				+			
Клиническая характеристика опухоли **Clinical characteristics of the tumor**							
Максимальный размер опухоли, мм **Maximum tumor size, mm**	29	25	20	23	19	22	27
первичная опухоль primary tumor		+			+		
первый рецидив опухоли first tumor recurrence	+		+	+		+	+

Степень злокачественности опухоли по ВОЗ **Grade,WHO**	IV	IV	IV	IV	IV	IV	IV
Степень ВОЗ при первоначальном диагнозе **WHO grade at primary diagnosis**	IV		IV	IV		IV	IV
Статус метилирования промотора MGMT **MGMT promoter methylation status**							
метилированный methylated	+				+	+	
неметилированный unmethylated		+	+	+			+
Мутация IDH **IDH mutation**							
дикий тип wild type	+		+	+	+	+	+
мутировал mutated		+					
Время пребывания в стационаре, дни **Duration of hospital stay, days**	6	5	7	5	4	5	6
Количество операций **Number of operations**	3	2	2	3	2	2	3
Лучевая терапия, СОД Гр **Radiation therapy, STD Gr**	60	120	180	120	60	90	120
Гамма нож, Кибер нож **Gamma knife, Cyber knife**		да / yes		да / yes			
Химиотерапия **Chemotherapy**							
первая линия, количество курсов first line, number of courses	7 тмз 7 tmz	5 тмз 5 tmz	10 тмз 10 tmz	8 тмз 8 tmz	7 тмз 7 tmz	11 тмз 11 tmz	9 тмз 9 tmz
вторая линия, количество курсов second line, number of courses	2 тмз + авастин 2 tmz + avastin	PCV	ломустин + винкристин lomustine + vincristine	3 тмз + авастин 3 tmz + avastin	PCV	авастин + иринотекан avastin + irinotecan	4 тмз 4 tmz
третья линия, количество курсов third line, number of courses	3 тмз 3 tmz		авастин + иринотекан avastin + irinotecan	PCV			PCV
Безрецидивная выживаемость, мес **Progressive-free survival (PFS), months**	15	10	9	6	12	29	11
Общая выживаемость, мес **Overall survival (OS), months**	36	19	21	17	28	61	22

light diffusers is about 7–9 mm, which is necessary for precise tissue irradiation without causing critical thermal effects. Detailed clinical characteristics of the patients are presented in Table 1.

Technique of the conducted interstitial photodynamic therapy

Photoditazine (OOO Veta-Grand, Russia) (Fig. 2A) with the active substance chlorin e6, diluted in 200 ml of physiological solution at the rate of 1 mg of the drug per 1 kg of the patient's body weight, administered to the patient intravenously 2 hours before the expected placement of the trephination hole for PDT, was used as the PS.

Preoperative planning was performed using software for spatially precise intra-tissue irradiation of the tumor volume. The target tumor tissue volume to be irradiated was determined after combining multimodal CT (computed tomography) images (contrast-enhanced

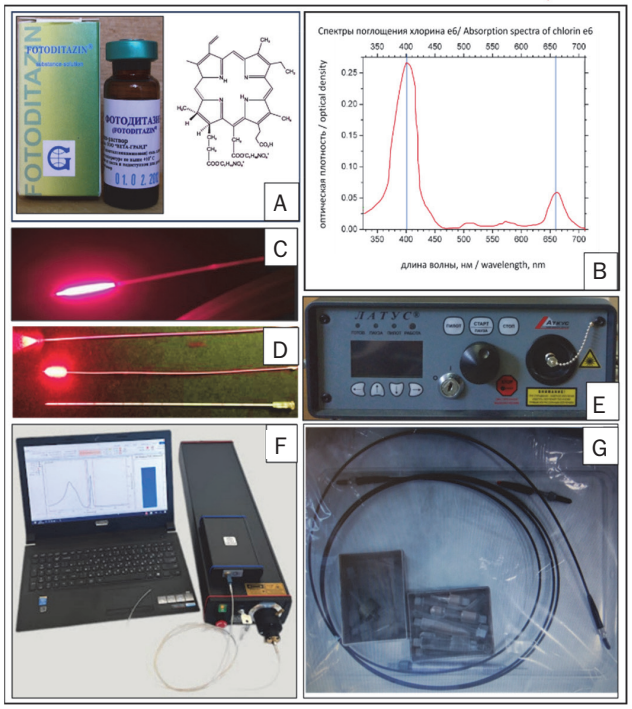

Рис. 2. Оснащение для иФДТ: А – фотодитазин; В – спектр поглощения хлорина е6; С – цилиндрический диффузор лазерного излучения в рабочем состоянии; D – формы диффузоров; Е – источник излучения полупроводниковый лазер «Латус 2,5»; F – спектроанализатор ЛЭСА-01-БИОСПЕК; G – световод.
Fig. 2. Equipment for iPDT: A – photoditazine; B – absorption spectrum of chlorin e6; C – cylindrical diffuser of laser radiation in working condition; D – shapes of diffusers; E – radiation source semiconductor laser "Latus 2.5"; F – spectrum analyzer LESA-01-BIOSPEC; G – light guide.

scanning, 0.6 mm axial slices) with preoperative gadolinium-enhanced MRI and PET-CT (positron emission tomography) (Fig. 3). The images were loaded into a computer and processed using the Gamma Multivox 2D/3D automated workplace software (AWP) for image summation and construction of a 3D tumor model.

At the next stage, simulations were performed for the iPDT parameters taking into account the obtained tumor volume and its spatial location according to the 3D simulation at the previous stage. Thus, for iPDT simulation, the software of the integrated Monte Carlo simulation platform was used for light delivery from the laser source and control of the thermal effect from laser radiation exposure. Figure 4A shows an overview of the integrated Monte Carlo simulation platform. The simulation platform processes the parameters from the user and performs an analysis of heat dissipation, light propagation and energy absorption. It is possible to determine the best PDT mode, which will be most effective for activating the photosensitizer. The software of the integrated Monte Carlo simulator made it possible to carry out iPDT taking into account five important criteria, including: the degree of light penetration; the rate of energy absorption; the level of uniform energy absorption in the tumor tissue; the time required to deliver the target volume of light energy; the range of temperature change.

Thus, using the software interface based on the integrated Monte Carlo modeling platform, a numerical analysis of the propagation and absorption of light (photon) and heat dissipation in the brain tissue and tumor (Fig. 4A, B) was performed. The platform allowed to select the number of laser radiation sources, the light spectrum (wavelength of the radiation spectrum), and the formation of an integrated analysis of the obtained data, taking into account the photosensitizer. Using the program, results for assessing heat dissipation, light absorption, and delivery of light energy to the target tissue were obtained, which made it possible to select the most effective iPDT mode. Figures 4B–F show the results for the photosensitizer chlorin e6 (photoditazine), which has an absorption peak at 400 and 662 nm, respectively. For the calculations, we used a three-dimensional spherical tumor model obtained from the preoperative

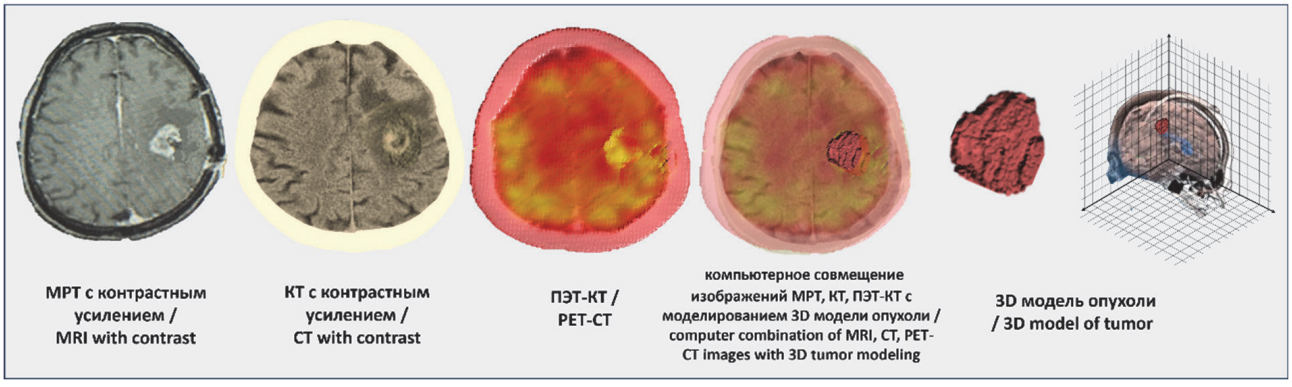

Рис. 3. Планирование предполагаемого объема облучения по данным нейровизуализационных методик с последующей суммацией изображений и построения 3D модели, загрузкой последней в программное приложение для расчета параметров иФДТ и интраоперационного планирования доступа к опухоли.
Fig. 3. Planning the expected volume of irradiation based on neuroimaging data, followed by image summation and construction of a 3D model, loading the latter into a software application for calculating iPDT parameters and intraoperative planning of access to the tumor.

3D modeling data. Figure 4C shows heat maps and heat dissipation graphs depending on the wavelength under constant (upper figure) and cyclic illumination (lower figure). The results showed that there was no detectable temperature change at any given setting, limiting damage to surrounding normal brain tissue due to thermal scattering from the laser sources during device operation in the cycling setting. Figures 4E,F summarize the performance comparisons across five criteria (degree of light penetration into target tumor tissue; energy absorption rate; level of energy absorption uniformity across the tumor volume; time required to deliver the target light energy; and range of temperature change) and show the light absorption distribution across the tumor volume for chlorin e6 (Figure 4E). We specified and calculated these variables in the simulations to provide detailed information on the critical variables in obtaining the results. Specifically, we assessed the ability of light to penetrate different types of media, such as gray and white matter, perifocal brain edema, and tumors (including cystic and solid components), for each light source. The energy absorption coefficient in the tumor was calculated in accordance with the light spectra, as well as the time to reach the threshold energy significant for tumor growth suppression. The results obtained under different conditions (wavelength) showed that the optimal condition for chlorin e6 is achieved with a combination of wavelengths of 400 and 662 nm and 25% of the irradiation working cycle.

The actual iPDT technique was as follows. After accessing the tumor along a special, pre-set trajectory of preoperative marking, an intraoperative analysis was performed for the presence of photosensitizer accumulation in the tumor tissue and the intensity of its luminescence. After receiving a positive result (maximum light emission by chlorin e6), a biopsy of the tumor was taken and sent to the histological express laboratory at the research laboratory of pathomorphology of the nervous system of the Russian Scientific Research Institute named after prof. A.L. Polenov located in the same building. Within 15-20 minutes, the morphological result of the biopsy was obtained. After confirmation that

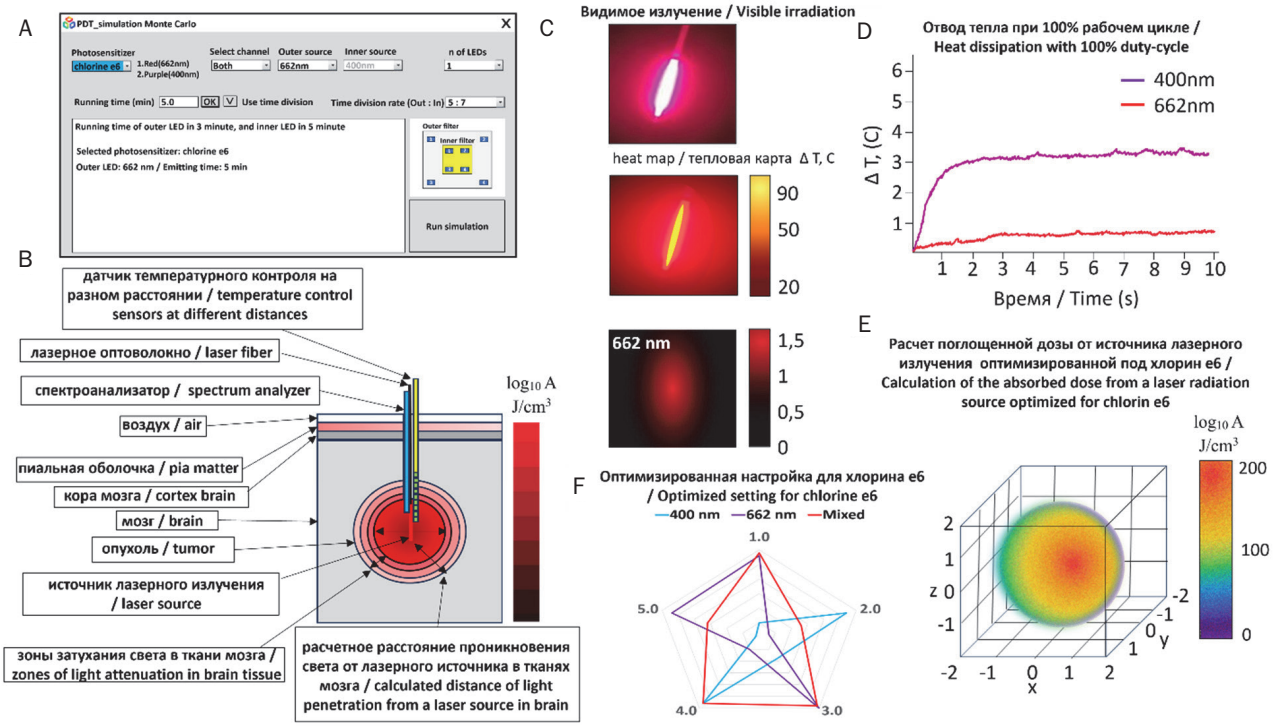

Рис. 4. Схема моделирования параметров для проведения сеансов иФДТ: A – обзор интегрированного симулятора программного обеспечения для проведения иФДТ – PDT simulation Monte Carlo; B – поперечное сечение модели опухолевой ткани для расчета проведения сеанса иФДТ и контроля параметров; C – рассеивание света и тепловая карта на длине волны 662 нм для активации хлорина е6; D – график температуры отведения тепла в режиме полноценного рабочего цикла; E – расчет поглощенной дозы от источника лазерного излучения в зависимости от расстояния от источника излучения, и учета эффекта затухания света в мозговой ткани; F – лучший режим иФДТ для активации хлорина е6 с учетом оптимизации.

Fig. 4. Schematic diagram of the simulation of parameters for conducting iPDT sessions. A – overview of the integrated software simulator for conducting iPDT – PDTsimulation Monte Carlo; B – cross-section of the tumor tissue model for calculating the iPDT session and parameter control; C – light scattering and heat map at a wavelength of 662 nm for the activation of chlorin e6; D – graph of the heat removal temperature in the full-duty cycle mode; E – calculation of the absorbed dose from the laser source depending on the distance from the radiation source, and taking into account the effect of light attenuation in the brain tissue; F – the best iPDT mode for chlorin e6 activation taking into account the optimization.

the biopsy material contained a tumor (glioblastoma), the next stage of iPDT was performed. Thus, the viability of tumor tissue was confirmed before iPDT using a minimally invasive stereotactic biopsy procedure with subsequent morphological examination to exclude treatment-related effects or tumor pseudoprogression.

When planning the procedure for introducing the laser radiation source with subsequent tumor irradiation, special equipment was used. Technically, the procedure was feasible in all expected cases. Intratissue irradiation was performed (from the target point with maximum luminescence emission according to spectroscopy data) using a laser (Latus 2.5 (Atkus, Russia)) (Fig. 2E) with a wavelength of 662 nm and a maximum power of 2.5 W, an optical fiber cable (Fig. 2D) and using cylindrical scattering fibers (Fig. 2C). The fibers for delivering light from the laser radiation source consisted of 4-6 cylindrical diffusers with a diameter of 600 μm and a length of 20 or 30 mm. The length of the diffuser was at least equal to the extent of the tumor along the trajectory of introduction. These fibers were introduced into the tumor tissue using a stereotaxic approach. The energy illumination was assessed using the "Optical power meter QB230" (ADVANTEST Corp., Japan).

Using the intraoperative spectral online monitoring technique (LESA-01-BIOSPEC laser electron-spectral system (Russia) (Fig. 2F)), it was possible to monitor the transmission of emitted light between the fibers and the fluorescent light of chlorin e6. The system consists of a laser source for excitation of the photosensitizer and a miniature universal spectrometer for recording and analyzing the fluorescent signal. During most irradiation sessions, chlorin e6 fluorescence before illumination was characterized as "good" and then decayed during irradiation. This fact, at least in cases with good postoperative gradation of light transmission, indicated a significant consumption of chlorin e6, as expected, due to photobleaching of this photosensitizer. The technique of spectral online monitoring allowed local determination of the degree of accumulation of the photosensitizer in the tumor tissue and normal brain tissue accessible to the fiber-optic probe. For the assessment, special software running in the Windows operating system was used, which made it possible to compare the degree of accumulation of the photosensitizer in the tumor tissue with the standard or with normal brain tissue. The procedure for collecting tissue samples was carried out under the guidance of intraoperative smear preparations, which usually guaranteed the selection of both solid and necrotic areas of the tumor. For histopathological examination, tissue probes were used and the density of tumor cells, the presence of necrosis, vascular proliferation, tissue proliferation of the tumor (Ki-67 index, P53), and molecular genetic analyses, such as determining the methylation status of the MGMT promoter, and IDH status were analyzed.

At each target point (according to both preoperative planning and intraoperative spectroscopy data) along

Таблица 2
Индивидуальные параметры лазерного излучения
Table 2
Individual parameters of laser radiation

Пациент Patient	Вариант глиобластомы Variant of glioblastoma	Доза ФС мг/кг Dose of PS mg/kg	Длина волны излучения, нм Radiation wavelength, nm	Диаметр оптического волокна, мкм Optical fiber diameter, microns	Выходная оптическая мощность, Вт Output optical power, W	Экспозиционная доза света в Дж/см^2 / Exposure dose of light in J/cm^2	Плотность мощности излучения в мВт/см^2 Radiant power density in mW/cm^2	Время облучения, мин. Irradiation time, min.	Число использованных световодов Number of used light diffusers
1	рецидив recurrence	1	665	600	2	200	200	15	6
2	первичная primary	1	665	600	3	150	200	9	4
3	рецидив recurrence	1	665	600	2	200	200	15	6
4	рецидив recurrence	1	665	600	2	180	200	11	5
5	первичная primary	1	665	600	3	150	200	9	4
6	рецидив recurrence	1	665	600	3	180	200	11	5
7	рецидив recurrence	1	665	600	3	200	200	15	6

the route of the light emitter, at least one irradiation session was performed. In case there was a residual level of photosensitizer accumulation after irradiation, according to spectroscopy data, a repeat irradiation session was performed in this area. The total irradiation duration did not exceed 15 min (Fig. 2G). The exposure dose of light was calculated based on the geometry and size of the tumor using the integrated Monte Carlo modeling platform. The light dose averaged 180 J/cm^2 (Table 2).

After the session, to avoid light damage to the retina due to the presence of traces of chlorin e6, the patient was in opaque glasses and a dimly lit room for the next 24 hours.

Assessment of the safety and tolerability of the treatment method

Complications that developed during iPDT treatment were considered any postoperative complications that developed within 2 months after surgery. The severity of the reaction and frequency were assessed in accordance with the unified terminology criteria for assessing the severity of adverse events (CTCAE) (version 5) dated 11/27/2017 [48]. In the postoperative period, the patient's complaints were assessed (daily, until discharge), somatic (including dermatological manifestations) and neurological status (daily, until discharge), ophthalmologist examination (at least 2 times before discharge, 1 and 2 months after surgery), electroencephalogram and electrocardiogram (at least 1 time before discharge) were assessed. Laboratory tests (clinical blood test, clinical urine test, biochemical blood test, coagulogram) were also performed on the 1st, 3rd and 7th day after surgery, before discharge from the hospital, 1 month and 2 months after surgery.

Statistical analysis

All analyses were performed using SPSS (version 20, IBM Corp.). Descriptive survival was analyzed using the Kaplan-Meier method, p-values <0.05 were considered significant.

Results

Before iPDT fiber placement, 7–13 tissue samples were collected along one of the planned treatment trajectories. 3–7 samples were used for histopathological evaluation and molecular genetic analysis, and 4–9 samples were collected for chlorin e6 concentration studies. The diagnosis of glioblastoma was morphologically verified in all patients.

Fluorescence intensity was analyzed in all patients. Almost all patients had high chlorin e6 fluorescence before irradiation, which also showed high chlorin e6 concentration in the extracted tissue, in parts of the tumor. The mean chlorin e6 concentrations measured along the biopsy trajectories ranged from 1.5 to 3.1 μM. The strongest chlorin e6 fluorescence intensity was found in patient 1, which was consistent with the chlorin e6 extraction values in the biopsy tissue, which were also among the highest among all patients. Slight chlorin e6 fluorescence was found in one patient, although one tissue sample showed a high chlorin e6 concentration. This tumor was characterized by an extensive area of necrosis.

Spectral measurements performed before and after iPDT showed high chlorin e6 fluorescence before irradiation and very low chlorin e6 fluorescence after irradiation, indicating significant photobleaching.

Postoperative MRI image analysis

Postoperative MRI performed within 24 h after iPDT showed minimal (3 patients (42.9%)) or no (4 patients (57.1%)) contrast enhancement in the iPDT treated area, at a distance of about 15 mm from the irradiation center.

Various pre-processing techniques were applied before image analysis. First, MRI data recorded at different time points were positionally aligned with each other. This was done automatically using the Gamma Multivox 2D/3D AWP software package, followed by manual checks and adjustments. All images, settings and segmentations were reviewed by experienced neuroradiologists. Figure 5 shows as an example the regions of interest in one patient, such as the tumor volume (consisting of the contrast enhancement area in T1 mode and the necrosis area), the perifocal edema area, the expected iPDT effect area and the area of changes after iPDT. The PDT effect area appeared after the PDT session.

Segmented volumes were rounded to the nearest 3 mm, since higher accuracy was not meaningful based on the physical resolution of the image. The necrosis-to-tumor ratio (NTR) was calculated for each case before treatment by dividing the necrosis volume by the tumor volume, according to Henker C. et al. [19].

Thus, the volume of tissue exposed to phototoxic effects from laser radiation was determined based on postoperative MRI data. The average calculated size of the phototoxic effect from one diffuser fiber was 3.1 × 2.7 × 2.8 cm. The average total target volume of involved tumor tissue from one diffuser was 3.57 ± 0.32 cm^3.

Immediate results

Transient clinical deterioration was recorded in 2 patients (28.6%), which was mainly due to increased perifocal edema and/or some hemorrhagic imbibition in the irradiation zone in the early postoperative period. However, these changes were not associated with direct traumatic effects due to the individual trajectory of the laser tip and tumor vessels. These patients showed an increase in neurological deficit in the early postoperative period (an increase in hemiparesis from 4 points to 2

points in one patient and the appearance of dysarthria and dysphasia in the second patient). Only one patient with hemiparesis showed an increase in neurological deficit after surgery, which persisted for more than 5 weeks. However, the symptoms significantly regressed within 5 weeks after iPDT even without hormonal therapy, which was avoided in order not to interfere with the possible immunological effects of PDT. Moreover, the development of postoperative complications did not depend on the volume of the tumor.

Adverse reactions associated with the use of photoditazine according to the CTCAE criteria were not detected in patients, which can be explained by the small group of patients.

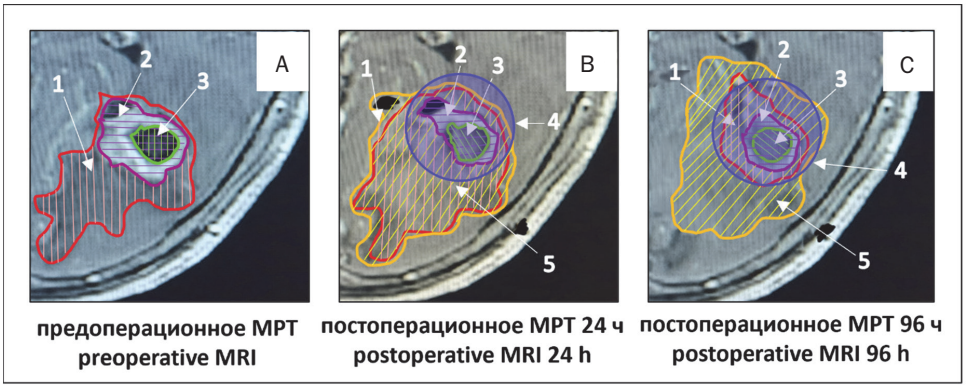

Рис. 5. Оценка МРТ до и после иФДТ, показанная в качестве примера у одного пациента. Сегментированные объемы, обозначенные цветовыми наложениями на изображениях МРТ (Т1-режим) (1 – зона перифокального отека (красная), 2+3 – объем опухоли с усилением контраста в Т1-режиме (2 – солидный компонент (фиолетовый), 3 – зона некроза (зеленый)), 4 – предполагаемая зона воздействия от иФДТ (синий), 5 – зона изменений по данным МРТ после иФДТ (желтый)).
Fig. 5. MRI evaluation before and after iPDT, shown as an example in one patient. Segmented volumes indicated by color overlays on MRI images (T1-weighted) (1 – area of perifocal edema (red), 2+3 – tumor volume with contrast enhancement in T1-weighted (2 – solid volume (purple), 3 – necrosis volume (green)), 4 – estimated area of iPDT effect (blue), 5 – area of changes according to MRI data after iPDT (yellow)).

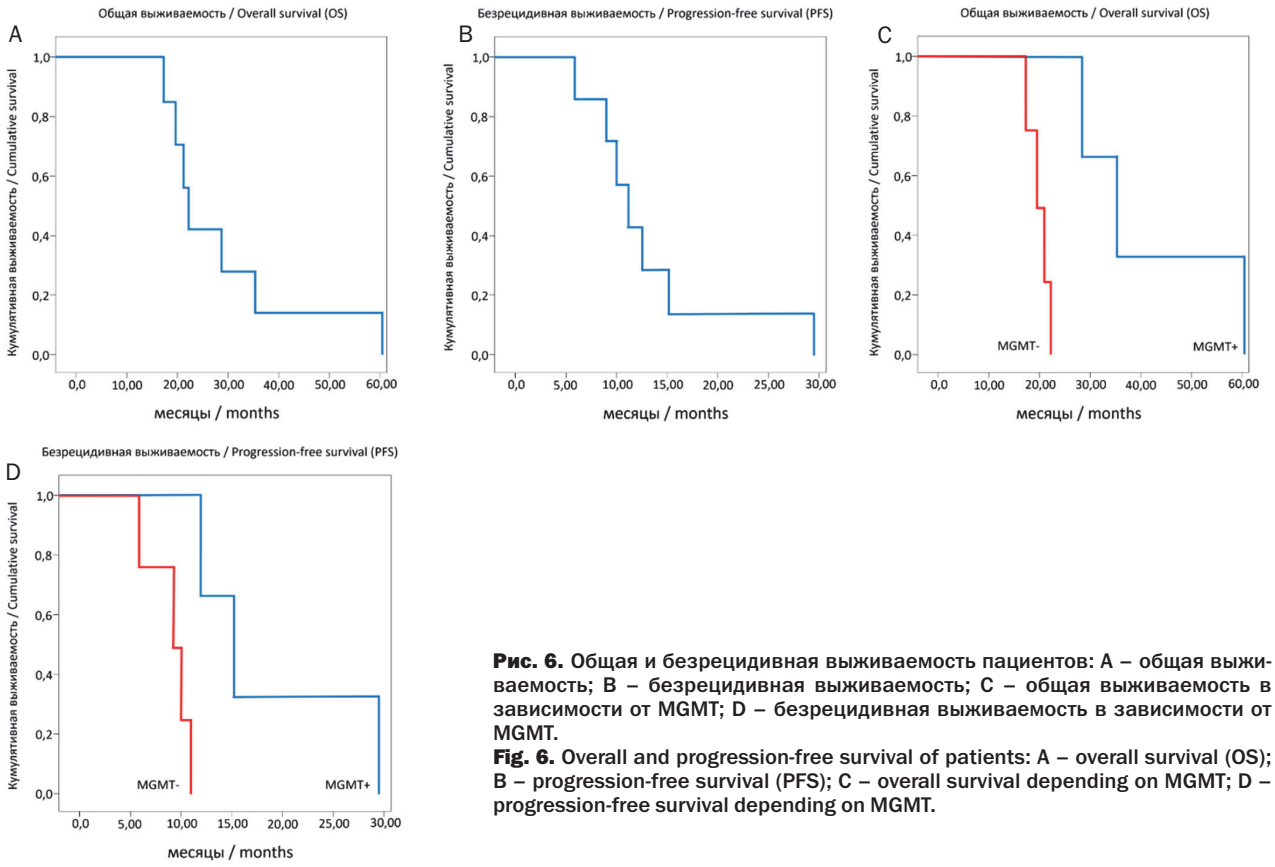

Рис. 6. Общая и безрецидивная выживаемость пациентов: A – общая выживаемость; B – безрецидивная выживаемость; C – общая выживаемость в зависимости от MGMT; D – безрецидивная выживаемость в зависимости от MGMT.
Fig. 6. Overall and progression-free survival of patients: A – overall survival (OS); B – progression-free survival (PFS); C – overall survival depending on MGMT; D – progression-free survival depending on MGMT.

Remote results

Catamnesis was monitored in all patients. The duration of observation after iPDT was up to 61 months. The cause of death was tumor progression. The median overall survival from the first diagnosis of malignant glioma to death was 28.3 months. The median relapse-free survival was 13.1 months. The median time between the first diagnosis and the course of iPDT was 10.8 months.

MGMT status played a significant role in the outcome of patients with iPDT. Patients with MGMT promoter methylation survived longer than those with unmethylated MGMT by a median of 22.1 months (based on median overall survival) and remained progression-free for an additional 9.3 months (based on median relapse-free survival) (Fig. 6C,D). The median overall survival for patients with MGMT promoter methylation was 41.3 months, while for patients with unmethylated MGMT it was 18.6 months ($p<0.005$). The median relapse-free survival was 18.6 months for patients with MGMT promoter methylation and 9.3 months for patients with unmethylated MGMT ($p<0.005$). This is usually explained by a higher sensitivity of tumor cells to adjuvant chemotherapy with temozolomide. In cases of relapsed glioblastoma treated with iPDT, no survival advantage was found for the methylated MGMT promoter compared to the unmethylated MGMT promoter. This may be due to higher resistance of the tumors of these patients to chemotherapy due to inhibition of apoptosis or upregulation of genes causing multidrug resistance.

Clinical example

Patient K., 45 years old, first relapse of glioblastoma after surgical treatment, 60 Gy RT course, temozolomide chemotherapy. iPDT with chlorin e6 was performed with assessment of photosensitizer accumulation in tumor tissue during surgery and assessment of fluorescence intensity according to spectroscopy data. MRI images with gadolinium contrast enhancement in T1 mode before and 24 hours after surgery and 3 months after surgery are presented below (Fig. 7).

Discussion

Glioblastoma is the most difficult to treat of all primary brain tumors. Factors determining the prognosis of this disease include such factors as age and working capacity status before treatment, the volume of tumor resection during surgery, the volume of postoperative radiation therapy and chemotherapy, and molecular genetic factors of the tumor [1, 2, 7, 9, 14, 29, 41]. The extremely low median survival time in patients with glioblastoma indicates that there is currently no effective treatment for this category of patients. To improve the

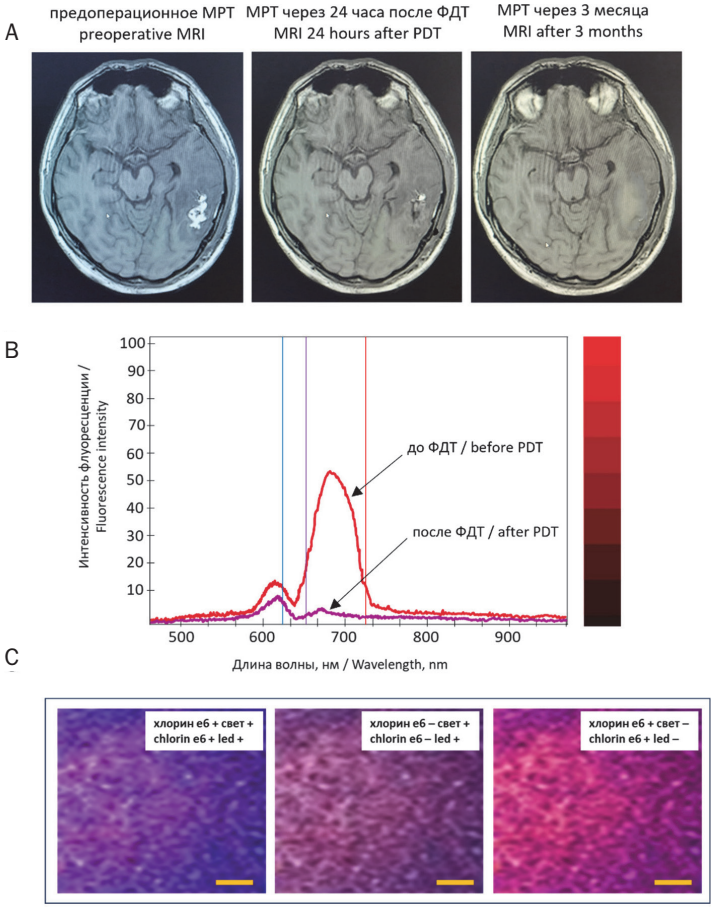

Рис. 7. Клинический пример пациент: А – МРТ головного мозга 1,5 Тесла с контрастным усилением гадолинием (перед операцией, через 24 ч после операции и через 3 мес после операции) аксиальные срезы; В – спектральный анализ флуоресценции в области целевой опухолевой ткани (до ФДТ, и после ФДТ в дозе 180 Дж/см^3); С – биопсийный материл опухоли полученный *in vivo* до иФДТ был быстро обработан, зафиксирован в 4% параформальдегиде, залит в парафин, нарезан на микротоме и подвергнут окрашиванию гематоксилином-эозином (H&E); масштабная линейка 50 мкм. Представленные изображения выполнены в 3 режимах: в режиме обычного света и под источником синего цвета (позволяющего видеть флуоресценцию хлорина е6 в ткани опухоли); в режиме только обычного света, без источника синего света; в режиме отсутствия обычного освещения, но в режиме синего цвета позволяющего видеть флуоресценцию хлорина е6.

Fig. 7. Clinical example of a patient: A – MRI of the brain 1.5 Tesla with contrast enhancement with gadolinium (before surgery, 24 hours after surgery, and 3 months after surgery) axial sections; B – spectral analysis of fluorescence in the area of the target tumor tissue (before PDT, and after PDT at a dose of 180 J/cm^3); C – tumor biopsy material obtained *in vivo* before iPDT was rapidly processed, fixed in 4% paraformaldehyde, embedded in paraffin, cut on a microtome and stained with hematoxylin and eosin (H&E); scale bar 50 μm. The presented images were obtained in 3 modes: in normal light mode and under a blue light source (allowing to see chlorin e6 fluorescence in the tumor tissue); in normal light only mode, without a blue light source; in the absence of normal lighting, but in the blue light mode allowing one to see the fluorescence of chlorin e6.

prospects for patients with glioblastoma, it is necessary to provide a larger range of treatment methods against this malignant tumor in the future [2, 9, 11, 18].

According to the literature, 90–95% of all glioblastomas recur within 2 cm of the primary tumor margin. The remaining 5–10% of recurrences beyond this 2-cm margin can be called distant recurrences. The high rate of local recurrences may be due to insufficient local eradication of tumor cells. One explanation may be that the tumor margins visible on conventional MRI do not include tumor cells disseminated into the surrounding tissues of the perifocal zone [5, 9, 19, 28, 33, 38].

At the present time, the first step of treatment is to perform the safest possible resection in order to remove as much of the tumor as possible and to avoid the development of neurological deficit. PDT is one of the methods studied in recent decades, which allows increasing the radicality of the surgical intervention, with a minimal risk of complications, and has recently been increasingly used in neurosurgical practice. The effect of PDT is based on the destruction of tumor cells through a complex mechanism of direct cellular damage caused by singlet oxygen generated by the excitation of the photosensitizer accumulated inside the tumor cells, as well as indirect effects such as damage to the intima in microvessels inside the tumor, embolic mechanisms caused by blood stagnation due to spasm of arterioles, and inflammatory reactions of immune cells [6, 8, 9, 11, 17, 25].

The current issues related to iPDT that remain at the present time are: selection of a light diffuser with suitable geometry for the application of optimal photostimulation of tumor tissue; determination of the optimal number of diffusers for introduction into the tumor in order to maximize the therapeutic effect while minimizing the harm associated with the introduction of the diffuser through normal brain tissue; the correct choice of tumors of suitable size, anatomical location and geometry for greater safety and effectiveness of iPDT [12, 14, 19, 27, 29, 35, 38].

Another problem with iPDT is the uniform delivery of photostimulation to achieve adequate energy flux to the maximum tumor volume without causing thermal damage to normal brain tissue. Model experiments studying light delivery have determined the optimal geometry of light guides for iPDT. Cylindrical light diffusers have a larger emitting surface area with a lower energy flux velocity at the tissue/light emitter interface than flat split fibers [27]. Thus, light delivery through a cylindrical diffuser improves photon distribution with reduced sensitivity to local tissue absorption variability, thereby distributing the radiation over a larger tissue volume than flat split fibers. However, the light flux falls faster from a flat fiber, which is useful when treating a tumor in close proximity to functionally significant areas of the brain. Thus, the light diffuser geometry as well as the total number of diffusers required to safely treat the tumor are factors that should be considered preoperatively to achieve optimal iPDT [33, 38, 42].

The dose of light delivered during iPDT is another important factor in this technique. The applied dosimetric model should take into account the type of photosensitizer. At the same time, to achieve the maximum therapeutic effect of iPDT, it is necessary to calculate the flow rate to achieve maximum photobleaching of the photosensitizer in the tissue (more than ≥95%). Thus, in the case of iPDT with 5-aminolevulinic acid (5-ALA), modeling shows that maximum photobleaching is achieved at a distance of about 4 mm from the surface of the light diffuser emitting a power of 200 mW/cm^2 for 1 h. Based on the expected volume of tissue affected by photoirradiation, the optimal interfiber distance of photodiffusers in iPDT should be about 10 mm, and the maximum photostimulation power should not exceed 200 mW/cm^2, since the threshold value at which the risk of tissue temperature increasing above 48°C (the threshold at which thermal side effects become a factor) increases significantly [4, 30].

Software for optimizing iPDT delivery has been developed over several decades [16]. One of the approaches uses co-registration of contrast-enhanced magnetic resonance imaging and positron emission tomography with stereotactic computed tomography images to provide virtual trajectory planning and positioning of light scatterers within the tumor [30]. The goal is to virtually plan the implantation of the optimal number of light scatterers to ablate the tumor without damaging adjacent vasculature or traversing functionally important brain areas.

In this study, we explored the potential of iPDT as part of a combination treatment for glioblastoma to motivate scientists and clinicians to further study this promising therapeutic option. iPDT is applied by stereotactically inserting a fiber optic cable into the tumor and delivering a photoemitter (laser light source) to the tumor tissue after pre-injection of a photosensitizer into the patient. The use of iPDT is similar to laser interstitial thermal therapy (LITT) for the treatment of glioblastoma, as both are minimally invasive stereotactic methods, but iPDT has the additional advantage of selectively targeting tumor cells [6, 8, 9, 11, 17, 28, 37, 39].

Analyzing the data of the research results, as well as data from available literary sources reporting on the use of iPDT as one of the methods in the treatment of glioblastoma, it is quite difficult to conduct a direct meaningful comparison of them, due to the pronounced heterogeneity of the treatment groups in different studies. The results of using the iPDT technique in patients with malignant gliomas depending on the year of work, the type of photosensitizer and the PDT parameters of some studies are presented in Table 3.

In our cohort of patients treated with iPDT, 5 of 7 patients had distant recurrence (outside the site of iPDT).

Таблица 3
Результаты использования и ФДТ у пациентов со злокачественными глиомами у разных авторов

Table 3
Results of the use of iPDT in patients with malignant gliomas by different authors

Авто Author	Год Year	Количество пациентов Number of patients	Гистология Histology	Фотосенсибилизатор Photosensitizer (PS)	Способ введения ФС Method of administration of PS	Время от введения ФС до операции Time from PS administration to surgery	Доза ФС, мг/кг Dose of PS, mg/kg	Длина волны, нм Wavelength, nm	Доза облучения, Дж/см^3 Radiation dose, J/cm^3	Медиана общей выживаемости, мес Median overall survival (OS), months	Медиана выживаемости без прогрессирования, мес Median progression-free survival (PFS), months
Muller P.J. [35]	1990	40	22 ГБМ 18 АА 22 GBM 18 AA	Гематопорфирин Hematoporphyrin	внутривенно intravenously	18 – 24	2 – 5	630	8 – 175	8,5 (6,5 – 17,1)	нет данных n/a
Powers S.K. [45]	1991	6	1 ГБМ 1 ГС 4 АА 1 GBM 1 GS 4 AA	Гематопорфирин Hematoporphyrin	внутривенно intravenously	24	2	630	400	0,5 – 11	нет данных n/a
Origata-mo T.S. [37]	1993	15	8 ГБМ 6 АА 1 ОА 8 GBM 6 AA 1 OA	Гематопорфирин Hematoporphyrin	внутривенно intravenously	48 – 72	2	630	50	8 – 16	нет данных n/a
Kostron H. [46]	1996	50	ГБМ GBM	Гематопорфирин Hematoporphyrin	внутривенно intravenously	24 – 72	2,5	630	15 – 260	10 ГР 19 ГП 10 GR 19 GP	13
Muller P.J. [9]	1996	20	11 ГБМ 9 АА 11 GBM 9 AA	Гематопорфирин Hematoporphyrin	внутривенно intravenously	12 – 36	2	630	15 – 110	9,2 ГБМ 12 АА 9,2 GBM 12 AA	нет данных n/a
Krishna-murthy S. [43]	2000	17	12 ГБМ 5 АА 12 GBM 5 AA	Гематопорфирин Hematoporphyrin	внутривенно intravenously	24 – 72	2	630	1500 – 5900	16,4 АА 3,8 ГБМ 16,4 AA 3,8 GBM	нет данных n/a
Stummer W. [33]	2007	1	ГБМ GBM	5-АЛК 5-ALA	перорально per os	24	20	633	1200	нет данных n/a	нет данных n/a
Beck T.J. [30]	2007	10	ГБМ GBM	5-АЛК 5-ALA	перорально per os	1	20	633	939 – 2304	15	нет данных n/a
Kaneko S. [44]	2008	20	16 ГБМ 4 АА 16 GBM 4 AA	Гематопорфирин Hematoporphyrin	внутривенно intravenously	24 – 48	2	630	180	20,5	нет данных n/a
Kaneko S. [44]	2011	26	18 ГБМ 6 АА 18 GBM 6 AA	Гематопорфирин Hematoporphyrin	внутривенно intravenously	24 – 48	2	630	180	15	нет данных n/a
Johans-son A. [16]	2013	5	ГБМ GBM	5-АЛК 5-ALA	перорально per os	5 – 8	20 – 30	635	720	3 и 9 (2), >29 (3)	>29 (3)
Schwartz C. [29]	2015	15	ГБМ GBM	5-АЛК 5-ALA	перорально per os	нет данных n/a	20 – 30	633	12960	34 – 37	16
Lietke S. [6]	2021	44	37 ГБМ 7 АА 37 GBM 7 AA	5-АЛК 5-ALA	перорально per os	3 – 5	20	635	5760 – 17 388	39,7	13

Quach S. [41]	2023	16	ГБМ GBM	5-АЛК 5-ALA	перорально per os	3	20	635	969 – 5760	28	16,4
Rafaelyan A.A. [26]	2023	10	7 ГБМ 3 АА 7 GBM 3 AA	5-АЛК 5-ALA	перорально per os	4	20	635	234 – 104	36,3	16,3
Rynda A.	2025	7	7 ГБМ 7 GBM	хлорин е6 chlorin e6	внутривенно intravenously	2	1	662	180	28,3	13,1

*ГБМ – глиобластома, ГС – глиосаркома, АА – анапластическая астроцитома, ОА – анапластическая олигодендроглиома, GP – первичная глиобластома, GR – рецидивная глиообластома.
*GBM – glioblastoma, GS – gliosarcoma, AA – anaplastic astrocytoma, OA – anaplastic oligodendroglioma, GP – primary glioblastoma, GR – recurrent glioblastoma.

According to the above criterion, it can be concluded that there is a lower proportion of local recurrences after iPDT compared with other treatments. However, no correlation was found between the distance of recurrence from the primary tumor and any other parameter evaluated. In our study, the median overall survival from the first diagnosis of malignant glioma to death was 28.3 months. The median recurrence-free survival was 13.1 months. Moreover, MGMT status played a significant role in the treatment outcomes of patients with iPDT.

Conclusion

In this study, we evaluated neuroimaging data, patient characteristics, and tumor molecular biological and cytogenetic data, which were collected and evaluated retrospectively. A thorough preoperative planning of the iPDT session was performed, taking into account multiple physical and biological parameters, using dedicated software. The MRI images obtained after iPDT were analyzed. In order to identify potential survival-related factors, various available parameters were examined for correlation with survival data. We also aimed to explore the potential of iPDT, and to motivate further research on this important topic and lay the foundation for future studies.

In conclusion, it should be noted that iPDT shows promising results regarding overall and relapse-free survival in the structure of complex treatment of patients with glioblastoma. At the same time, technical and clinical issues related to the small number of patients in the existing studies remain, which should be resolved in the future to determine the tactics of using iPDT and to develop a standard for the use of this technique in the treatment of malignant tumors of the central nervous system.

In the future, iPDT can also be combined with other treatment methods in order to be able to affect as many tumor cells as possible, with the initiation of a wide range of tissue and cellular processes that can help in the fight against this invasive tumor malignancy. To improve the control of tumor growth at a distance, a combination with immunotherapy or sonodynamic therapy may be of interest.

Interstitial PDT of gliomas remains a challenging procedure due to the limited depth of light penetration into the brain tissue, complex planning and implantation of the irradiator, and potential risk of clinical deterioration, especially after treatment in functionally important brain areas. However, iPDT may be a promising treatment option in a population of patients with a high risk of postoperative neurological deficit. It does not interfere with, but rather may complement, other treatment options for this disease, such as repeat radiotherapy and chemotherapy. iPDT remains a potential option for deep-seated gliomas in patients with high surgical risk and in case of tumor recurrence. Hospital stay with iPDT is significantly shorter, which reduces the cost of hospitalization. Patients treated with iPDT may receive adjuvant treatment more quickly than patients with standard craniotomy. These data strongly support further studies in controlled prospective settings.

REFERENCES

1. Louis D.N., Perry A., Wesseling P. The 2021 WHO Classification of Tumors of the Central Nervous System: a summary. *Neuro Oncol*, 2021, Vol.23(8), pp. 1231-1251. doi: 10.1093/neuonc/noab106.
2. Ostrom Q.T., Cioffi G., Waite K., et al. CBTRUS Statistical Report: primary Brain and Other Central Nervous System Tumors Diagnosed in the United States in 2014-2018. *Neuro Oncol*, 2021, Vol.23, pp. III1–III105. doi: 10.1093/NEUONC/NOAB200
3. Rynda A.Yu., Olyushin V.E., Rostovtsev D.M., et al. Intraoperative photodynamic therapy in complex treatment of malignant gliomas. *Zhurnal Voprosy Neirokhirurgii Imeni N.N. Burdenko*, 2023, Vol. 87(1), pp.25-34. (In Russian) doi:10.17116/neiro20238701125
4. Stepp H., Stummer W. 5-ALA in the management of malignant glioma. *Lasers Surg Med*, 2018, Vol.50, pp.399-419. doi: 10.1002/lsm.22933
5. Rynda A.Yu., Olyushin V.E., Rostovtsev D.M., et al. Intraoperative fluorescence control with chlorin E6 in resection of glial brain tumors. *Zhurnal Voprosy Neirokhirurgii Imeni N.N. Burdenko*, 2021, Vol.85(4), pp. 20-28. (In Russian). doi:10.17116/neiro20218504120

ЛИТЕРАТУРА

1. Louis D.N., Perry A., Wesseling P. The 2021 WHO Classification of Tumors of the Central Nervous System: a summary // Neuro Oncol. – 2021. – Vol. 23(8). – P. 1231-1251. doi: 10.1093/neuonc/noab106.
2. Ostrom Q.T., Cioffi G., Waite K. et al. CBTRUS Statistical Report: primary Brain and Other Central Nervous System Tumors Diagnosed in the United States in 2014-2018 // Neuro Oncol. – 2021. – Vol. 23. – P. III1–III105. doi: 10.1093/NEUONC/NOAB200
3. Рында А.Ю., Олюшин В.Е., Ростовцев Д.М. и соавт. Применение интраоперационной фотодинамической терапии в структуре комплексного лечения злокачественных глиом // Журнал «Вопросы нейрохирургии» имени Н.Н. Бурденко – 2023. – Т. 87, №1. – С. 25-34. doi: 10.17116/neiro20238701125
4. Stepp H., Stummer W. 5-ALA in the management of malignant glioma // Lasers Surg Med. – 2018. – Vol. 50. – P. 399-419. doi: 10.1002/lsm.22933
5. Рында А.Ю., Олюшин В.Е., Ростовцев Д.М. и соавт. Результаты использования интраоперационного флюоресцентного контроля с хлорином Е6 при резекции глиальных опухолей головного мозга // Журнал «Вопросы нейрохирургии» имени Н.Н. Бурденко. – 2021. – Т. 85, №.4. – С. 20-28. doi: 10.17116/neiro20218504120.

6. Lietke S., Schmutzer M., Schwartz C. Interstitial Photodynamic Therapy Using 5-ALA for Malignant Glioma Recurrences. *Cancers (Basel)*, 2021, Vol.13(8), pp.1767. doi: 10.3390/cancers13081767
7. Rynda A.Y., Rostovthev D.M., Zabrodskaya Y.M. et al. Immunotherapy with autologous dendritic cells in the complex treatment of malignant gliomas – results. *J. Neurooncol*, 2024, Vol.166, pp.309-319. doi: 10.1007/s11060-023-04559-1
8. Foglar M., Aumiller M., Quach S., et al. Interstitial photodynamic therapy of glioblastoma: An MRI-based follow-up analysis. Photodiagnosis and Photodynamic Therapy., 2024, Vol.46, pp.104117. doi: 10.1016/j.pdpdt.2024.104117
9. Muller P.J., Wilson B.C. Photodynamic Therapy for Malignant Newly Diagnosed Supratentorial Gliomas. *J. Clin. Laser Med. Sur*, 1996, Vol.14, pp.263-270. doi: 10.1089/clm.1996.14.263
10. Rynda A.Y., Olyushin, V., Rostovtsev D. Immunotherapy With Autological Dendritic Cells in the Structure of Complex Treatment of Gliomas. *Neurosurgery*, 2024, vol.70 (Suppl.1), pp. 196. doi: 10.1227/neu.0000000000002809_1244
11. Foglar M., Aumiller M., Bochmann K. Interstitial Photodynamic Therapy of Glioblastomas: A Long-Term Follow-up Analysis of Survival and Volumetric MRI Data. *Cancers (Basel)*, 2023, Vol.15 (9), pp.2603. doi: 10.3390/cancers15092603
12. Romanishkin I.D., Savelieva T.A., Ospanov A. Comparison of optical-spectral characteristics of glioblastoma at intraoperative diagnosis and ex vivo optical biopsy. *Biomedical Photonics*, 2024, Vol.13(4), pp.4-12. doi:10.24931/2413-9432-2024-13-4-4-12
13. Rynda A.Yu., Rostovtsev D.M., Olyushin V.E. et al. Therapeutic pathomorphosis in malignant glioma tissues after photodynamic therapy with chlorin e6 (reports of two clinical cases). *Biomedical Photonics*, 2020, Vol.9(2), pp. 45-54. doi: 10.24931/2413-9432-2020-9-2-45-54
14. Ospanov A., Romanishkin I., Savelieva T., et al. Optical Differentiation of Brain Tumors Based on Raman Spectroscopy and Cluster Analysis Methods. *Int. J. Mol. Sci*, 2023, Vol.24, pp.14432. doi:10.3390/ijms241914432
15. Rynda A.Yu., Olyushin V.E., Rostovtsev D.M., et al. Comparative analysis of 5-ALA and chlorin E6 fluorescence-guided navigation in malignant glioma surgery. Pirogov Russian Journal of Surgery = Khirurgiya. *Zurnal im. N.I. Pirogova*, 2022, Vol.1, pp.5-14. (In Russian) doi: 10.17116/hirurgia20220115
16. Johansson A., Faber F., Kniebühler G., et al. Protoporphyrin IX fluorescence and photobleaching during interstitial photodynamic therapy of malignant gliomas for early treatment prognosis. *Laser Surg. Med*, 2013, Vol.45, pp.225-234. doi:10.1002/lsm.22126.
17. Savelieva T.A., Romanishkin I.D., Ospanov A., et al. Machine learning methods for spectrally-resolved imaging analysis in neuro-oncology. *Biomedical Photonics*, 2024, Vol.13(4), pp.40-54. doi: 10.24931/2413-9432-2024-13-4-40-54
18. Rynda A.Yu., Zabrodskaya Yu.M., Olyushin V.E., et al. Morphological evaluation of the effectiveness of fluorescence navigation with chlorin e6 in surgery for malignant gliomas. *Arkhiv Patologii*, 2021, Vol.83(5), pp.13-20. (In Russian) doi: 10.17116/patol20218305113
19. Henker C., Hiepel M.C., Kriesen T., et al. Volumetric assessment of glioblastoma and its predictive value for survival. *Acta Neurochir*, 2019, Vol.161, pp.1723-1732. doi: 10.1007/s00701-019-03966-6
20. Rynda A.Yu., Rostovtsev D.M., Olyushin V.E. Fluorescence-Guided Resection of Glioma – literature review. *Russian Neurosurgical Journal named after professor A.L. Polenov*, 2018, vol.X (1), pp.97-110. (In Russian)
21. Tzerkovsky D.A., Maslakov E.A., Bagrintsev D.A., Semak I.A., Protopovich Y.L., Chizh A.G., Tatur A.A., Fomenkov I.S., Stupak D.S. The role of photodynamic therapy in the treatment of primary, recurrent and metastatic malignant brain tumors. *Biomedical Photonics*, 2018, Vol.7(2), pp.37-49. (in Russian). doi: 10.24931/2413-9432-2018-7-2-37-49.
22. Rynda A.Yu., Olyushin V.E., Rostovtsev D.M., et al. Fluorescent diagnostics with chlorin e6 in surgery of low-grade glioma. *Biomedical Photonics*, 2021, Vol. 10(4), pp. 35-43 (in Russian). doi: 10.24931/2413-9432-2021-10-4-35-43
23. Kostron H., Hochleitner B.W., Obwegeser A., Seiwald M. Clinical and experimental results of photodynamic therapy in neurosurgery., 1994, pp.126-128. doi:10.1117/12.203437.
24. Potapov A.A., Chobulov S.A., Nikitin P.V., et al. Intraoperative vascular fluorescence in cerebral glioblastomas and vascular histological features. *Burdenko's Journal of Neurosurgery*, 2019, Vol.83(6), pp.21-34. (in Russian). doi: 10.17116/neiro20198306121
25. Rynda A.Yu., Rostovtsev D.M., Olyushin V.E., Zabrodskaya Yu.M. Fluorescence-guided resection of glioma using «photoditazin». *Grekov's Bulletin of Surgery*, 2017, Vol.176(5), pp.10-15. (In Russian). doi: 10.24884/0042-4625-2017-176-5-10-15
26. Rafaelian A., Martynov B., Chemodakova K., et al. Photodynamic interstitial stereotactic therapy for recurrent malignant glioma.

6. Lietke S., Schmutzer M., Schwartz C. Interstitial Photodynamic Therapy Using 5-ALA for Malignant Glioma Recurrences // Cancers (Basel). – 2021. – Vol.13(8). – P.1767. doi: 10.3390/cancers13081767
7. Rynda A.Y., Rostovthev D.M., Zabrodskaya Y.M. et al. Immunotherapy with autologous dendritic cells in the complex treatment of malignant gliomas – results // J. Neurooncol. – 2024. – Vol.166. – P. 309-319. doi: 10.1007/s11060-023-04559-1
8. Foglar M., Aumiller M., Quach S., et al. Interstitial photodynamic therapy of glioblastoma: An MRI-based follow-up analysis // Photodiagnosis and Photodynamic Therapy. – 2024. – Vol. 46. – P.104117. doi: 10.1016/j.pdpdt.2024.104117
9. Muller P.J., Wilson B.C. Photodynamic Therapy for Malignant Newly Diagnosed Supratentorial Gliomas // J. Clin. Laser Med. Sur. – 1996. – Vol.14. – P.263-270. doi: 10.1089/clm.1996.14.263
10. Rynda A.Y., Olyushin, V., Rostovtsev D. Immunotherapy With Autological Dendritic Cells in the Structure of Complex Treatment of Gliomas // Neurosurgery. – 2024. – Vol.70 (Suppl. 1). – P. 196. doi: 10.1227/neu.0000000000002809_1244
11. Foglar M., Aumiller M., Bochmann K. Interstitial Photodynamic Therapy of Glioblastomas: A Long-Term Follow-up Analysis of Survival and Volumetric MRI Data // Cancers (Basel). – 2023. – Vol. 15, (9). – P. 2603. doi: 10.3390/cancers15092603
12. Романишкин И.Д., Савельева Т.А., Оспанов А. и др. Сравнение оптико-спектральных характеристик глиобластомы при интраоперационной диагностике и оптической биопсии ex vivo // Biomedical Photonics. – 2024. – Т.13, №4. – С. 4-12. doi:10.24931/2413-9432-2024-13-4-4-12
13. Рында А.Ю., Ростовцев Д.М., Олюшин В.Е., Забродская Ю.М. Лечебный патоморфоз в тканях злокачественной глиомы после фотодинамической терапии с хлорином е6 (сообщение о двух клинических случаях) // Biomedical Photonics. – 2020. – Т. 9, №2. – С. 45-54. doi: 10.24931/2413-9432-2020-9-2-45-54
14. Ospanov A., Romanishkin I., Savelieva T., et al. Optical Differentiation of Brain Tumors Based on Raman Spectroscopy and Cluster Analysis Methods // Int. J. Mol. Sci. – 2023. – Vol. 24. – P. 14432. doi:10.3390/ijms241914432
15. Рында А.Ю., Олюшин В.Е., Ростовцев Д.М. и соавт. Сравнительный анализ флуоресцентной навигации в хирургии злокачественных глиом с использованием 5-АЛА и хлорина Е6 // Хирургия. Журнал им. Н.И. Пирогова. – 2022. – №1. – С. 5-14. doi: 10.17116/hirurgia20220115
16. Johansson A., Faber F., Kniebühler G., et al. Protoporphyrin IX fluorescence and photobleaching during interstitial photodynamic therapy of malignant gliomas for early treatment prognosis // Laser Surg. Med. – 2013. – Vol.45. – P.225-234. doi:10.1002/lsm.22126.
17. Савельева Т.А., Романишкин И.Д., Оспанов А. и др. Методы машинного обучения для анализа спектрально-разрешенных изображений в нейроонкологии. // Biomedical Photonics. – 2024. – Т.13, №4. – С. 40-54. doi:10.24931/2413-9432-2024-13-4-40-54
18. Рында А.Ю., Забродская Ю.М., Олюшин В.Е. и соавт. Морфологическая оценка эффективности флуоресцентной навигации с хлорином е6 в хирургии злокачественных глиом // Архив патологии. – 2021. – Т. 83, №5. – С.13-20. doi: 10.17116/patol20218305113
19. Henker C., Hiepel M.C., Kriesen T., et al. Volumetric assessment of glioblastoma and its predictive value for survival // Acta Neurochir. – 2019. – Vol.161. – P.1723-1732. doi: 10.1007/s00701-019-03966-6
20. Рында А.Ю., Ростовцев Д.М., Олюшин В.Е. Флуоресцентно-контролируемая резекция астроцитарных опухолей головного мозга – обзор литературы. // Российский нейрохирургический журнал имени профессора А.Л. Поленова. – 2018. – Т. X, №1. – С. 97-110.
21. Церковский Д.А., Маслаков Е.А., Багринцев Д.А., и др. Роль фотодинамической терапии в лечении первичных, рецидивных и метастатических злокачественных опухолей головного мозга // Biomedical Photonics. – 2018. – Т. 7, № 2. – С. 37-49. doi: 10.24931/2413–9432–2018–7–2–37–49
22. Рында А.Ю., Олюшин В.Е., Ростовцев Д.М. и соавт. Флуоресцентная диагностика с хлорином е6 в хирургии глиом низкой степени злокачественности // Biomedical Photonics. – 2021. – Т. 10, № 4. – С. 35-43. doi: 10.24931/2413–9432–2021–10-4-35-43
23. Kostron H., Hochleitner B.W., Obwegeser A., Seiwald M. Clinical and experimental results of photodynamic therapy in neurosurgery. – 1994. – P. 126-128. doi:10.1117/12.203437.
24. Потапов А.А., Чобулов С.А., Никитин П.В. и соавт. Интраоперационная флуоресценция сосудов в структуре глиобластом головного мозга и их гистологическая характеристика // Журнал «Вопросы нейрохирургии» имени Н.Н. Бурденко. – 2019. – Т.83, №6. – С.21-34. doi: 10.17116/neiro20198306121
25. Рында А.Ю., Ростовцев Д.М., Олюшин В.Е., Забродская Ю.М. Флюоресцентно-контролируемая резекция глиальных опухолей с «Фотодитазином» // Вестник хирургии имени И.И. Грекова. – 2017. – Т.176, №5. – С.10-15. doi: 10.24884/0042-4625-2017-176-5-10-15

Asian J Oncol, 2023, Vol.9, pp.14. doi:10.25259/ASJO-2022-69-(433)
27. Baran T.M., Foster T.H. Comparison of flat cleaved and cylindrical diffusing fibers as treatment sources for interstitial photodynamic therapy. *Med Phys*, 2014, Vol. 41, pp. 1-8. doi: 10.1118/1.4862078
28. Rynda A., Olyushin V., Rostovtsev D. Fluorescence navigation in glioma surgery using 5 ALA and chlorin E6. *Neuro-Oncology*, 2021, Vol. 23 (Suppl. 2), pp. ii25. doi: 10.1093/neuonc/noab180.086
29. Schwartz C., Rühm A., Tonn J.-C., Kreth S., Kreth F.-W. SURG-25 Interstitial photodynamic therapy of de-novo glioblastoma multiforme who iv. *Neuro-Oncol*, 2015, vol.17, pp. v219-v220. doi: 10.1093/neuonc/nov235.25
30. Beck T.J., Kreth F.W., Beyer W., et al. Interstitial photodynamic therapy of nonresectable malignant glioma recurrences using 5-aminolevulinic acid induced protoporphyrin IX. *Laser Surg. Med*, 2007, Vol.39, pp.386-393. doi:10.1002/lsm.20507.
31. Romanishkin I.D., Savelieva T.A., Ospanov A., et al. Classification of intracranial tumors based on optical-spectral analysis. *Biomedical Photonics*, 2023, Vol.12(3), pp.4-10. doi; 10.24931/2413-9432-2023-12-3-4-10
32. Rynda A.Yu., Olyushin V.E., Rostovtsev D.M., et al. Patients with long-term survival in malignant gliomas after photodynamic therapy. *S.S. Korsakov Journal of Neurology and Psychiatry*, 2024, Vol.124(6), pp.54-61. (In Russian). doi: 10.17116/jnevro202412406154
33. Stummer W., Beck T., Beyer W., et al. Long-sustaining response in a patient with non-resectable, distant recurrence of glioblastoma multiforme treated by interstitial photodynamic therapy using 5-ALA: case report. *J. Neuro-Oncol*, 2007, Vol.87, pp.103-109. doi:10.1007/s11060-007-9497-x
34. Rafaelian A.A., Martynov B.V., Chemodakova K.A. Stereotactic Photodynamic Therapy of Recurrent Malignant Gliomas. *Sovrem Tekhnologii Med*, 2024, Vol.16(2), pp.58-65. doi: 10.17691/stm2024.16.2.06
35. Muller P.J., Wilson B.C. Photodynamic therapy of malignant brain tumours. *Can. J. Neurol. Sci*, 1990, Vol.17 (2), pp.193-198. doi: 10.1017/s0317167100030444.
36. Rynda A.Yu., Olyushin V.E., Rostovtsev D.M., Zabrodskaya Yu.M., Papayan G.V. Results of microsurgical resection of glioblastomas under endoscopic and fluorescent control. *Biomedical Photonics*, 2024, Vol.13(3), pp.20-30. doi: 10.24931/2413-9432-2024-13-3-20-30
37. Origitano T.C., Reichman O.H. Photodynamic Therapy for Intracranial Neoplasms. *Neurosurgery*, 1993, vol. 32, pp. 587-596. doi:10.1227/00006123-199304000-00015.
38. Rynda A.Y., Olyushin V.E., Rostovtsev D.M. et al. Patients with Long-Term Survival in Malignant Gliomas after Photodynamic Therapy. *Neurosci Behav Physi*, 2024, Vol. 54, pp. 1215-1221. doi:10.1007/s11055-024-01717-4
39. Savelieva T., Romanishkin I. Ospanov A. Machine Learning and Artificial Intelligence Systems Based on the Optical Spectral Analysis in Neuro-Oncology. *Photonics*, 2025, vol.12(1), pp.37. doi: 10.3390/photonics12010037
40. Olyushin V.E., Kukanov K.K., Nechaeva A.S., Sklyar S.S., Vershinin A.E., Dikonenko M.V., Golikova A.S., Mansurov A.S., Safarov B.I., Rynda A.Y., Papayan G.V. Photodynamic therapy in neurooncology. *Biomedical Photonics*, 2023, Vol.12(3), pp.25-35. doi: 10.24931/2413-9432-2023-12-3-25-35
41. Quach S., Schwartz C., Aumiller M. et al. Interstitial photodynamic therapy for newly diagnosed glioblastoma. *J. Neurooncol*, 2023, Vol.162, pp.217-223. doi:10.1007/s11060-023-04284-9
42. Rafaelyan A.A., Alekseev D.E., Martynov B.V., et al. Stereotactic photodynamic therapy for recurrent glioblastoma. Case report and literature review. *Burdenko's Journal of Neurosurgery*, 2020, Vol.84(5), pp.81-88. (In Russian). doi: 10.17116/neiro20208405181
43. Krishnamurthy S., Powers S.K., Witmer P., Brown T. Optimal light dose for interstitial photodynamic therapy in treatment for malignant brain tumors. *Laser Surg. Med*, 2000, Vol.27, pp. 224-234. doi:10.1002/1096-9101(2000)27:3<224:aid-lsm4>3.0.co;2-#
44. Kaneko S. 悪性グリオーマに対する光線力学療法. *Nippon Laser Igakkaishi*, 2011, Vol. 32, pp.131-138. doi:10.2530/jslsm.32.131.
45. Powers S.K., Cush S.S., Walstad D.L., Kwock L. Stereotactic intratumoral photodynamic therapy for recurrent malignant brain tumors. *Neurosurgery*, 1991, Vol.29, pp. 688. doi:10.1097/00006123-199111000-00008.
46. Kostron H., Obwegeser A., Jakober R. Photodynamic therapy in neurosurgery: a review. *J. Photochem. Photobiol. B*, 1996, Vol.36(2), pp.157-168. doi: 10.1016/s1011-1344(96)07364-2
47. Ramakrishnan D., Reppert M., Krycia M. Evolution and implementation of radiographic response criteria in neuro-oncology. *Neuro-Oncology Advances*, 2023, Vol.5 (1), pp. vdad118. doi:10.1093/noajnl/vdad118
48. National Institutes of Health Common Terminology Criteria for Adverse Events (CTCAE); National Cancer Institute: Bethesda, MD, USA, 2017.

26. Rafaelian A., Martynov B., Chemodakova K., et al. Photodynamic interstitial stereotactic therapy for recurrent malignant glioma // Asian J Oncol. – 2023. – Vol.9. – P.14. doi:10.25259/ASJO-2022-69-(433)
27. Baran T.M., Foster T.H. Comparison of flat cleaved and cylindrical diffusing fibers as treatment sources for interstitial photodynamic therapy // Med Phys. – 2014. – Vol. 41. – P. 1-8. doi: 10.1118/1.4862078
28. Rynda A., Olyushin V., Rostovtsev D. Fluorescence navigation in glioma surgery using 5 ALA and chlorin E6. // Neuro-Oncology. – 2021. – Vol. 23 (Suppl. 2). – P. ii25. doi: 10.1093/neuonc/noab180.086
29. Schwartz C., Rühm A., Tonn J.-C., Kreth S., Kreth F.-W. SURG-25 Interstitial photodynamic therapy of de-novo glioblastoma multiforme who iv // Neuro-Oncol. – 2015. – Vol.17. – P. v219-v220. doi: 10.1093/neuonc/nov235.25
30. Beck T.J., Kreth F.W., Beyer W., et al. Interstitial photodynamic therapy of nonresectable malignant glioma recurrences using 5-aminolevulinic acid induced protoporphyrin IX // Laser Surg. Med. – 2007. – Vol.39. – P.386-393. doi:10.1002/lsm.20507.
31. Романишкин И.Д., Савельева Т.А., Оспанов А., и др. Классификация внутричерепных опухолей на основе оптико-спектрального анализа // Biomedical Photonics. – 2023. – Т.12, №3. – С. 4-10. doi: 10.24931/2413-9432-2023-12-3-4-10
32. Рында А.Ю., Олюшин В.Е., Ростовцев Д.М. и соавт. Пациенты с длительной выживаемостью при злокачественных глиомах после фотодинамической терапии // Журнал неврологии и психиатрии им. С.С. Корсакова. – 2024. – Т. 124, №6. – С. 54-61. doi: 10.17116/jnevro202412406154
33. Stummer W., Beck T., Beyer W., et al. Long-sustaining response in a patient with non-resectable, distant recurrence of glioblastoma multiforme treated by interstitial photodynamic therapy using 5-ALA: case report // J. Neuro-Oncol. – 2007. – Vol.87. – P. 103-109. doi:10.1007/s11060-007-9497-x
34. Рафаелян А.А., Мартынов Б.В., Чемодакова К.А., и др. Стереотаксическая фотодинамическая терапия рецидивных злокачественных глиом // Современные технологии в медицине. – 2024. – Т.16, №2. – С.58-67. doi: 10.17691/stm2024.16.2.06
35. Muller P.J., Wilson B.C. Photodynamic therapy of malignant brain tumours // Can. J. Neurol. Sci. – 1990. –Vol.17(2). – P.193-198. doi: 10.1017/s0317167100030444.
36. Рында А.Ю., Олюшин Д.М., Ростовцев Д.М., Забродская Ю.М., Папаян Г.В. Результаты микрохирургической резекции глиобластом под эндоскопическим и флуоресцентным контролем // Biomedical Photonics. – 2024. – Vol. 13(3). – P. 20-30. doi: 10.24931/2413-9432-2024-13-3-20-30
37. Origitano T.C., Reichman O.H. Photodynamic Therapy for Intracranial Neoplasms // Neurosurgery. – 1993. – Vol. 32. – P. 587-596. doi:10.1227/00006123-199304000-00015.
38. Rynda A.Y., Olyushin V.E., Rostovtsev D.M. et al. Patients with Long-Term Survival in Malignant Gliomas after Photodynamic Therapy // Neurosci Behav Physi. – 2024. – Vol. 54. – P. 1215-1221. doi: 10.1007/s11055-024-01717-4
39. Savelieva T., Romanishkin I. Ospanov A. Machine Learning and Artificial Intelligence Systems Based on the Optical Spectral Analysis in Neuro-Oncology // Photonics. – 2025. – Vol.12(1). – P.37. doi: 10.3390/photonics12010037
40. Олюшин В.Е., Куканов К.К., Нечаева А.С., и др. Фотодинамическая терапия в нейроонкологии // Biomedical Photonics. – 2023. – Vol.12(3). – P.25-35. doi: 10.24931/2413-9432-2023-12-3-25-35
41. Quach S., Schwartz C., Aumiller M. et al. Interstitial photodynamic therapy for newly diagnosed glioblastoma // J. Neurooncol. – 2023. – Vol.162. – P.217-223. doi:10.1007/s11060-023-04284-9
42. Рафаелян А.А., Алексеев Д.Е., Мартынов Б.В., и др. Стереотаксическая фотодинамическая терапия в лечении рецидива глиобластомы. Случай из практики и обзор литературы // Журнал «Вопросы нейрохирургии» имени Н.Н. Бурденко. – 2020. – Vol. 84(5). – P.81-88. doi: 10.17116/neiro20208405181
43. Krishnamurthy S., Powers S.K., Witmer P., Brown T. Optimal light dose for interstitial photodynamic therapy in treatment for malignant brain tumors. // Laser Surg. Med. – 2000. – Vol.27. – P. 224-234. doi:10.1002/1096-9101(2000)27:3<224:aid-lsm4>3.0.co;2-#
44. Kaneko S. 悪性グリオーマに対する光線力学療法 // Nippon Laser Igakkaishi. – 2011. – Vol. 32. – P.131-138. doi:10.2530/jslsm.32.131.
45. Powers S.K., Cush S.S., Walstad D.L., Kwock L. Stereotactic intratumoral photodynamic therapy for recurrent malignant brain tumors // Neurosurgery. – 1991. – Vol.29. – P. 688. doi:10.1097/00006123-199111000-00008.
46. Kostron H., Obwegeser A., Jakober R. Photodynamic therapy in neurosurgery: a review // J. Photochem. Photobiol. B. – 1996. – Vol.36(2). – P.157-168. doi: 10.1016/s1011-1344(96)07364-2
47. Ramakrishnan D., Reppert M., Krycia M. Evolution and implementation of radiographic response criteria in neuro-oncology // Neuro-Oncology Advances. – 2023. – Vol.5 (1). – P. vdad118. doi:10.1093/noajnl/vdad118
48. National Institutes of Health Common Terminology Criteria for Adverse Events (CTCAE); National Cancer Institute: Bethesda, MD, USA. – 2017.

ORIGINAL ARTICLES

PULSED WIDE-SPECTRAL PHOTOTHERAPY OF SOFT TISSUE GUNSHOT WOUNDS

Bagrov V.V.[1], Bobin A.N.[2], Bobylev V.A.[2], Volodin L.Y.[1], Davydov D.V.[2,3], Kamrukov A.S.[1], Kondratiev A.V.[1], Nesterova M.V.[2], Pecherskaya M.S.[2], Fateev A.V.[2], Shchedrina M.A.[2], Esaulenko N.B.[2]

[1]Bauman Moscow State Technical University (National Research University), Moscow, Russia
[2]Main Military Clinical Hospital named after Academician N.N. Burdenko of the Ministry of Defense of the Russian Federation, Moscow, Russia
[3]Patrice Lumumba Peoples' Friendship University of Russia, Moscow, Russia

Abstract

A new method has been proposed for the treatment of gunshot wounds complicated by nosocomial microflora. The method is based on the treatment of wounds with high-intensity pulsed optical radiation of a continuous spectrum in the wavelength range from 200 to 1100 nm. A pulsed xenon lamp is used as a radiation source. The effect of high-intensity pulsed wide-spectrum optical radiation and low-intensity continuous UV radiation with a maximum at a wavelength of 272 nm and a half-width of the spectrum of 12 nm on the course of the wound process in a gunshot injury was compared. It has been shown that the effect of such radiation on tissues with signs of purulent-inflammatory process provides an antibacterial effect and stimulates tissue regeneration. At the same time, high-intensity wide-spectral optical radiation has a more pronounced anti-inflammatory effect and contributes to the earlier development of tissue regeneration compared with low-intensity narrow-spectrum UV radiation. However, the use of high-intensity optical radiation requires an individual dosage for each phase of the wound process.

Keywords: pulsed wide-spectrum phototherapy, gunshot wound, optical radiation, antibacterial effect, tissue regeneration

Contacts: Kamrukov A.S., e-mail: kamrukov@bmstu.ru

For citations: Bagrov V.V., Bobin A.N., Bobylev V.A., Volodin L.Y., Davydov D.V., Kamrukov A.S., Kondratiev A.V., Nesterova M.V., Pecherskaya M.S., Fateev A.V., Shchedrina M.A., Esaulenko N.B. Pulsed wide-spectral phototherapy of soft tissue gunshot wouds, *Biomedical Photonics*, 2025, vol. 14, no. 1, pp. 20–28. doi: 10.24931/2413–9432–2025–14–1–20–28

ИМПУЛЬСНАЯ ШИРОКОСПЕКТРАЛЬНАЯ ФОТОТЕРАПИЯ ОГНЕСТРЕЛЬНЫХ РАН МЯГКИХ ТКАНЕЙ

В.В. Багров[1], А.Н. Бобин[2], В.А. Бобылев[2], Л.Ю. Володин[1], Д.В. Давыдов[2,3], А.С. Камруков[1], А.В. Кондратьев[1], М.В. Нестерова[2], М.С. Печерская[2], А.В. Фатеев[2], М.А. Щедрина[2], Н.Б. Эсауленко[2]

[1]Московский государственный технический университет имени Н.Э. Баумана (национальный исследовательский университет), Москва, Россия
[2]Главный военный клинический госпиталь имени академика Н.Н. Бурденко Министерства обороны Российской Федерации, Москва, Россия
[3]Российский университет дружбы народов им. Патриса Лумумбы, Москва, Россия

Резюме

Предложен новый метод для лечения огнестрельных ран, осложненных контаминацией нозокомиальной микрофлорой. Метод основан на обработке ран высокоинтенсивным импульсным оптическим излучением сплошного спектра в диапазоне длин волн от 200 до 1100 нм. В качестве источника излучения используется импульсная ксеноновая лампа. Проведено сравнение влияния на течение раневого процесса при огнестрельной травме высокоинтенсивного импульсного широкоспектрального оптического излучения и низкоинтенсивного непрерывного УФ излучения с максимумом на длине волны 272 нм и полушириной спектра 12 нм. Показано, что воздействие таких излучений на ткани с признаками гнойно-воспалительного процесса обеспечивает антибактериальный эффект и стимулирует регенерацию тканей. При этом высокоинтенсивное широкоспектральное оптическое излучение обладает более выраженным противовоспалительным действием и способствует более раннему развитию регенерации тканей по сравнению с низкоинтенсивным УФ излучением узкого спектра. Однако применение высокоинтенсивного оптического излучения требует индивидуальной дозировки для каждой фазы раневого процесса.

Ключевые слова: импульсная широкоспектральная фототерапия, огнестрельная рана, оптическое излучение, антибактериальный эффект, регенерация тканей.

Контакты: Камруков А.С., e-mail: kamrukov@bmstu.ru

Для цитирования: В.В. Багров, А.Н. Бобин, В.А. Бобылев, Л.Ю. Володин, Д.В. Давыдов, А.С. Камруков, А.В. Кондратьев, М.В. Нестерова, М.С. Печерская, А.В. Фатеев, М.А. Щедрина, Н.Б. Эсауленко. Импульсная широкоспектральная фототерапия огнестрельных ран мягких тканей // Biomedical Photonics. – 2025. – Т. 14, № 1. – С. 20–28. doi: 10.24931/2413–9432–2025–14–1–20–28

Introduction

In modern medicine, one of the issues that remains extremely relevant is the search for methods that increase the effectiveness of local treatment of wounds of various etiologies [1, 2]. This problem has acquired particular significance in connection with the increase in the number of military conflicts and terrorist attacks [3, 4, 5]. In case of gunshot injury, complex pathomorphological processes occur in the body [6]. Polyorganic structural disorders and functional changes resulting from tissue damage and metabolic imbalance combined with inevitable bacterial contamination of gunshot wounds create conditions that increase the incidence of infectious complications in wounded patients by 5-6 times compared with surgical patients [7, 8, 9, 10].

One of the causes of complications due to gunshot wounds are pathogens of nosocomial infections (*S.aureus, P.aeruginosa, E.coli, Klebsiella spp., etc.*), the etiological significance of which has increased significantly in recent years [8]. A distinctive feature of hospital microflora is polyresistance to antibacterial drugs and increased virulence of opportunistic pathogens with relatively low pathogenicity (for example, *Acinetobacter spp.*) against the background of reduced reactivity of the body and inhibition of the reparative regeneration process [6].

In these conditions, it is rational to use technologies that allow simultaneous action on various pathogenetic links of the wound process. For this purpose, various methods of local wound treatment have been proposed: chemical, biological, physical and reconstructive-plastic [11].

Active study and development of physical methods of influencing wounds, in particular, optical radiation of various spectral ranges [12, 13], are due to the prospect of their use for targeted regulation of wound process phases. The experimental data available today indicate high efficiency of the biocidal action of high-intensity pulsed optical radiation of a wide spectrum [14, 15, 16, 17]. However, the issue of its effect on reparative tissue regeneration in the area of a gunshot wound is currently insufficiently studied, which complicates the development of new approaches to the treatment of acquired infected defects of soft tissues.

The aim of this work was to study the efficiency of high-intensity pulsed optical radiation of a continuous spectrum in the wavelength range of 200-1100 nm as a new physical factor on the course of the wound process in the treatment of gunshot infected defects of soft tissues and its comparison with the wound healing effect of continuous low-intensity UV radiation.

Materials and methods

Characteristics of the research object

The object of the study were 30 sexually mature male Wistar rats weighing 390±10 g. The animals were kept under standard vivarium conditions in individual cages with free access to food and water. The experiments were conducted in accordance with international and national legislation on compliance with the principles of humane treatment of animals. Permission to conduct the study was obtained from the Independent Ethics Committee of the Burdenko Main Military Clinical Hospital of the Ministry of Defense of the Russian Federation.

Anesthetic support

All manipulations with animals were performed under general anesthesia. The main anesthetic used was Zoletil®100 (VIRBAC, France) (5 mg/kg of animal weight), approved for use in the Russian Federation.

Modeling of an infected gunshot wound

The development and creation of a model of gunshot injury were implemented in the conditions of shooting range of the 111th Main State Center for Forensic and Criminalistic Examinations of the Ministry of Defense of the Russian Federation.

After induction into anesthesia, fixation of the animal in a specially designed device (Fig. 1) and topographic marking

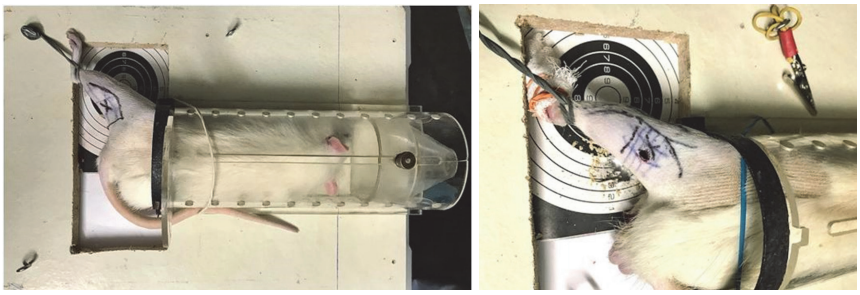

Рис. 1. Формирование модели огнестрельного ранения.
Fig. 1. Formation of a model of a gunshot wound.

Таблица
Распределение животных по группам в зависимости от характера воздействия на сформированную огнестрельную рану

Table
The distribution of animals into groups depending on the nature of the impact on the formed gunshot wound

Группы животных Groups of animals	Вид воздействия на раневую поверхность Type of impact on the wound surface	Количество животных Number of animals
I	Огнестрельная рана (группа I) Gunshot wound (group I)	6
II	Инфицированная огнестрельная рана (контрольная группа II) An infected gunshot wound (control group II)	8
III	Инфицированная огнестрельная рана + высокоинтенсивное импульсное оптическое излучение широкого спектра (аппарат «Зарница-А»). **Параметры облучения:** спектральный диапазон – Δλ=200-1100 нм; энергетическая доза облучения – 1,5 Дж/см^2; доза в УФ-С диапазоне (Δλ=200-280 нм) – 0,15 Дж/см^2; импульсная облученность раны ~200 Вт/см^2; режим воздействия – импульсно-периодический. Infected gunshot wound + high-intensity pulsed optical radiation of a wide spectrum (Zarnitsa-A device) **Irradiation parameters:** spectral range – Δλ=200-1100 nm; energy dose of radiation – 1.5 J/cm^2; the dose in the UV-C range (Δλ=200-280 nm) – 0.15 J/cm^2; the pulse irradiation of the wound ~200 W/cm^2; the exposure mode – pulse-periodic.	8
IV	Инфицированная огнестрельная рана + низкоинтенсивное непрерывное УФ излучение узкого спектра (аппарат «Зарница-Д») **Параметры облучения:** спектральный диапазон λ=272±6 нм; энергетическая доза облучения – 0,29 Дж/см^2; доза в УФ-С диапазоне – 0,23 Дж/см^2; облученность раны ~4 мВт/см^2; режим воздействия – непрерывный. Infected gunshot wound + low-intensity continuous narrow-spectrum UV radiation (Zarnitsa-D device) **Irradiation parameters:** spectral range – λ=272±6 nm; the energy dose of radiation – 0.29 J/cm^2; the dose in the UV-C range – 0.23 J/cm^2; the irradiation of the wound ~4 mW/cm^2; the exposure mode – continuous.	8
	Всего лабораторных животных: Total laboratory animals:	30

of the main anatomical structures located in the area of the back of the left thigh on the skin, each animal received one penetrating gunshot bullet wound. The weapon used was a small-caliber rifle CZ 452-2E ZKM (made in the Czech Republic) with Standard cartridges of 22 caliber (bullet with a diameter of 5.66 mm and a weight of 2.6 g). The rifle was placed in a specialized fixing machine for small arms. The shot was fired from a distance of 1.0 m. The muzzle velocity of the bullet was 320 m/sec; kinetic energy – 133 J.

Depending on the nature of the subsequent impact on the gunshot wound, all animals were divided into four groups (table). In three groups of animals (groups II, III and IV), 2 hours after the gunshot wound, the wounds were infected once with a suspension of *Klebsiella pneumoniae* and *Acinetobacter baumannii* bacteria. In group I, the gunshot wound was not artificially infected.

Equipment for experiments on remote exposure of wounds to optical radiation

Prototypes of phototherapeutic devices of two types were used in the study[1]:

- a high-intensity pulsed optical irradiation device "Zarnitsa-A" based on a pulsed xenon lamp generating continuous spectrum radiation in the wavelength range from 200 to 1100 nm [15, 16];
- a LED device "Zarnitsa-D" providing irradiation of wounds with low-intensity continuous UV radiation of a narrow spectrum with a spectral band width of 12 nm and a maximum at a wavelength of 272 nm [18] (this device can be considered a modern analogue

[1] The Zarnitsa-A and Zarnitsa-D devices were developed and manufactured at the Research Institute of Power Engineering of the Bauman Moscow State Technical University.

of traditional medical devices based on low-pressure mercury lamps).

The Zarnitsa-A device uses a compact pulsed xenon lamp PPF2-5/60 (manufactured by Rider LLC, Russia) with an internal diameter of the quartz shell of 5 mm and an interelectrode gap length of 60 mm, the initial xenon pressure in the lamp is 400 mm Hg. The lamp shell is made of high-quality quartz glass with transmission in the UV region at wavelengths of λ = 210-400 nm of more than 80%. The lamp is mounted on the axis of a conical aluminized reflector with an output quartz window with a light diameter of 50 mm. The average electric power of the lamp is 100 W at a pulse repetition rate of 5 Hz and their duration of ~ 20 μs.

The wound surface was irradiated daily for 21 days, starting from the first day after infection. Before irradiation, the wound was cleaned of necrotic tissue, fibrin and dried.

Irradiation parameters

The Zarnitsa-A device was used to treat gunshot wounds at a distance of 10 cm from the irradiator to the wound surface with a wound irradiation duration of 60 s. The total dose of UV-C radiation (Δλ = 200-280 nm) per irradiation cycle (60 s) was 0.15 J/cm^2; in the integral radiation spectrum (Δλ = 200-1100 nm) ~1.5 J/cm^2 (in the center of the light spot); the diameter of the irradiation zone (light spot) at the half-intensity level was 5 cm. The density of the pulsed power of optical radiation on the object (irradiance) was ~200 W/cm^2.

When irradiating gunshot wounds with the Zarnitsa-D device, the distance from the irradiator to the wound surface was 2 cm; duration of the procedure (1 cycle) of wound irradiation was 72 s; total dose of UV radiation (Δλ= 272±6 nm) per 1 irradiation cycle was 0.29 J/cm^2 (UV-C dose – 0.23 J/cm2), diameter of the irradiation zone (spot) – 5 cm. Radiation power density on the object was about 4 mW/cm^2.

The work with the devices was carried out using UV-protective glasses for the researcher and a protective screen for the eyes of the animals.

Research methods

Clinical studies

Clinical monitoring of the somatic condition of the animals was carried out daily for up to 21 days: the body weight of the animals was measured, the pain component was assessed. Regionally, the course of the wound process was assessed based on clinical markers of inflammation (the degree of hyperemia and tissue edema, the amount and nature of wound discharge), as well as the dynamics of wound healing using photography and video filming.

The presence and severity of pain syndrome in the wound area were determined by changes in the eating behavior of the animals: in case of no changes in the volume of food consumed, it was assumed that pain symptomatology was absent (0 points), and in case of refusal of food, the severity of pain was significant (3 points).

A scoring system was also used to assess the severity of hyperemia and tissue edema: 0 points – pale pink color / no edema; 1 point – mild hyperemia / minor edema; 2 points – moderate hyperemia / moderate edema; 3 points – severe hyperemia/pronounced edema.

Microbiological studies were performed at the Center for Clinical Laboratory Diagnostics of the Federal State Budgetary Institution "N.N. Burdenko Main Military Clinical Hospital" of the Ministry of Defense of the Russian Federation.

In preparation for the described cycle of experiments with a gunshot wound, we preliminarily conducted *in vitro* microbiological studies on the bactericidal properties of the types of optical radiation used – broad-spectrum high-intensity pulsed ("Zarnitsa-A") and narrow-band low-intensity continuous ("Zarnitsa-D"). Six clinically significant strains of microorganisms obtained from the biomaterial of patients were selected as objects of research, including gram-negative strains: *Klebsiella pneumoniae, Escherichia coli, Proteus mirabilis, Acinetobacter baumanii* and gram-positive strains: *Staphylococcus epidermidis, Enterococcus faecalis*. The studies showed a higher bactericidal efficiency of high-intensity pulsed radiation, but did not reveal a significant difference in the photoresistance of the studied types of bacterial microflora to the applied optical radiation. The results of these studies were partially published in [15, 16, 18]. In this regard, two clinical polyresistant strains isolated from the biomaterial of patients in the surgical departments of the hospital and related to gram-negative ESKAPE pathogens were selected as representative exogenous sources of contamination of gunshot wounds: *A.baumanii* and *K.pneumoniae*.

The daily culture of microorganisms was diluted with saline to a concentration of 10^8 CFU/ml, which corresponded to an optical density of 0.5 according to the McFarland turbidity standard for each microorganism. Turbidity was measured using a BD Phoenix Spec nephelometer (Becton Dickinson@Company, USA).

Wound infection in animals of groups II, III and IV was carried out by dropwise introduction of 0.1 ml of a suspension of a mixed bacterial culture of *A.baumanii* and *K.pneumoniae* into the area of the wound channel entrance, which ensured contamination of the wound with ~5.10^6 cells of each microorganism. In group I, the gunshot wound was not artificially infected.

On days 1, 3, 7, 10, 15 and 21 from the moment of gunshot injury and wound infection, microbiological studies of wound discharge with a quantitative determination of each strain of microorganism were performed in all animals.

Pathomorphological studies were conducted in the Department of Pathological Anatomy of the Burdenko Main Military Clinical Hospital of the Russian Ministry of Defense. A 0.5×1.0 cm^2 soft tissue fragment was taken from the entry wound site of a gunshot wound for pathomorphological studies in all experimental groups on days 1, 3, 7, 10, 15, and 21 after injury and infection. A standard protocol was used to process the obtained biological material. Samples were prepared using a Leica ASP6025S automatic

vacuum histological processor (Leica Biosystems, USA). All preparations were stained with hematoxylin and eosin. Histological micropreparations were examined at 10x, 20x, and 40x magnification using a Leica DM3000 direct light laboratory microscope (Germany).

Microscopic preparations were scanned on an Aperio AT2 scanning device (manufacturer Leica, USA) at a magnification of 20^x. For morphological analysis, microphotographs were prepared from scanned slides in the Aperio ImageScope (12.3.3) program (developer Leica, USA).

Results

Somatic condition assessment

Starting from day 3 to day 15 of observation, a decrease in body weight was noted in all laboratory animals in all groups (Fig. 2). The greatest loss of body weight (15.7%) was recorded in animals of group III; the smallest (5%) was noted in groups I and IV. After day 15, most animals in all groups gained weight, reaching the initial indicators by day 21.

Pain syndrome assessment

Gunshot injury was accompanied by pain syndrome, the intensity of which in animals in all groups was greatest on the 3rd day after the start of the experiment (1.13±0.2 points in group I, 2.5±0.16 points in group II, 1.92±0.24 points in group III, 1.58±0.2 points in group IV).

During the entire subsequent observation period, a gradual decrease in the intensity of the pain syndrome was recorded, and the average pain intensity values in points in animals of group II were always higher than in animals of groups III and IV, which indicates that broad-spectrum optical and short-wave UV irradiation reduce pain syndrome in the case of infected wounds.

Evaluation of the degree of tissue hyperemia and edema

In all groups, the maximum degrees of tissue hyperemia/edema developed by the 3rd day of observation, with the most pronounced ones occurring in animals of groups II and III (Fig. 3).

By the 10th day, the color of the perifocal tissues and the degree of edema in the laboratory animals of group I returned to normal values, in the other groups the severity of hyperemia/edema gradually decreased, remaining to the greatest extent in the group with an infected gunshot wound (group II). On the 15th day, hyperemia and edema were noted only in the group with an infected gunshot wound (group II).

The purulent-hemorrhagic nature of the wound discharge persisted for up to 7 days in all groups. Starting from the 7th day, in laboratory animals in groups I, III and IV, the nature of the wound discharge was serous-hemorrhagic.

Thus, the greatest severity and duration of the inflammatory process in the area of the gunshot wound were observed in the experimental animals of group II (infected gunshot wound). Exposure to high-intensity continuous-spectrum optical radiation (group III) and low-intensity continuous narrow-spectrum UV radiation (group IV) reduced the duration and activity of the inflammatory process in an infected wound, bringing the dynamics of the wound process closer to the nature of the course in an uninfected wound (group I).

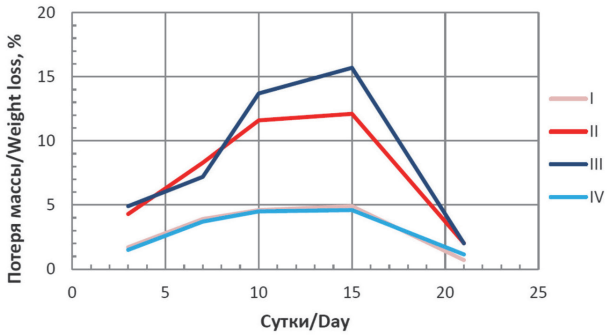

Рис. 2. Динамика уменьшения массы тела лабораторных животных в ходе эксперимента (римские цифры соответствуют номерам экспериментальных групп животных).
Fig. 2. Dynamics of decrease in body weight of laboratory animals during the experiment (Roman numerals correspond to the numbers of experimental groups of animals).

Results of microbiological studies

In experimental groups III and IV, where the corresponding types of optical radiation exposure to the wound surface were applied, there was no growth of *K.pneumonia* and *A.baumannii* strains, starting from the first day. In group II, the growth of the declared pathogenic strains (K.pneumonia and A.baumannii) persisted for up to 17 days with a gradual decrease in concentration to 10^3 CFU/ml by the specified time.

Analysis of the results of microbiological examination of wound discharge in animals with a gunshot infected wound demonstrated a stable bactericidal effect of high-intensity optical radiation of the continuous spectrum of the Zarnitsa-A device and low-intensity continuous UV radiation of the narrow spectrum of the Zarnitsa-D LED device on gram-negative bacteria *K.pneumoniae* and *A.baumannii*. This effect was expressed throughout the study.

Results of morphological studies

The dynamics of the wound process at the cellular and tissue levels was studied by microscopic examination of the material obtained as a result of a lifetime biopsy of soft tissues from the zone of the gunshot defect in animals of all experimental groups. A brief description of the results obtained is given below.

Fig. 4 shows micropreparations of the animal wound on the 3rd day of treatment.

In the wound injuries of animals of groups I and II on the third day, the prevalence of necrobiotic changes remained the same as on the first day, namely: cellular detritus with diffusely expressed dense segmented nuclear infiltration, a large number of neutrophilic leukocytes (75-80%) in a state of degeneration and destruction (in the form of karyopyknosis and karyorrhexis, cytolysis). The remaining 20-25% of the cellular composition is represented by

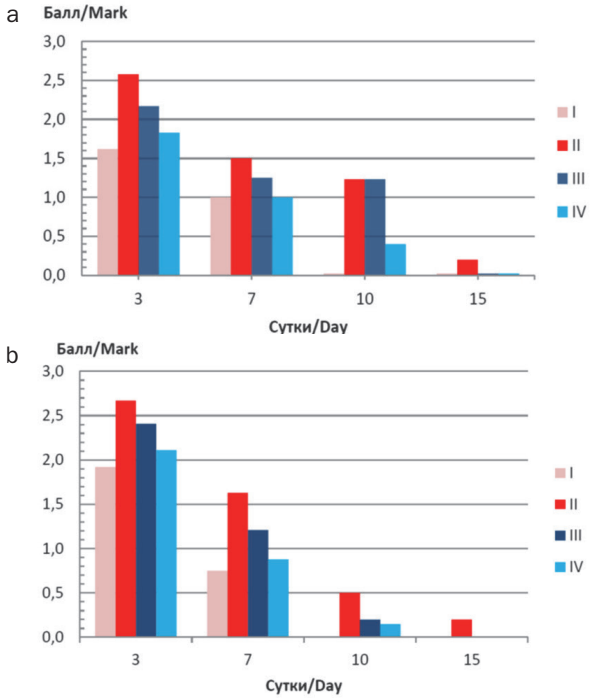

Рис. 3. Динамика развития гиперемии (а) и отека (б) у лабораторных животных в ходе эксперимента (римские цифры соответствуют номерам экспериментальных групп животных)
Fig. 3. Dynamics of hyperemia (a) and edema (б) in laboratory animals during the experiment (Roman numerals correspond to the numbers of experimental groups of animals)

lymphocytes, monocytes and individual macrophages and polyblasts. In general, the nature of changes in soft tissues in these groups on the third day of observation corresponded to the first phase of the wound process and did not have significant morphological and morphometric differences in intergroup comparison.

In group III of animals, against the background of a decrease in morphological markers of inflammation, cases of formation of immature granulation tissue were noted. Enhanced angiogenesis with proliferation of vascular endothelium was observed (in different rats from 19 to 26 vessels per 1 mm^2). In the structure of the cellular composition, a decrease in the content of neutrophilic leukocytes to 65-50% and an increase in the number of macrophages were observed.

In group IV, all laboratory animals in biopsy specimens still showed a predominance of necrobiotic changes, namely: cellular detritus with pronounced dense segmented nuclear infiltration and a large number of neutrophilic leukocytes (70-60%). However, the severity of the inflammatory process decreased.

By the seventh day, animals of group I showed signs of transition of the wound process to the regeneration phase and decreased severity of inflammation, as evidenced by changes in the cellular composition: a 1.6-2.5-fold decrease (compared to the first three days) in the number of neutrophilic leukocytes, an increase in the number of regeneration predictors: macrophages, mast cells, fibroblast proliferation, increased angiogenesis (in different rats from 9 to 16 vessels per 1 mm^2), as well as the development of immature granulation tissue.

In animals of group II, a pronounced inflammatory process persisted: the predominant elements of the cellular composition were neutrophilic leukocytes (70-80%); angiogenesis was poorly developed, fibrin thrombi persisted in some vessels.

In animals of groups III and IV, regression of inflammatory reactions and activation of reparative regeneration due to external exposure to optical radiation were clearly observed. Formation of mature granulation tissue was clearly visible in biopsies. Formation of vertically located vessels with endothelial proliferation was observed (from 10 to 15 per 1 mm^2). In the structure of the cellular composition, tissue undifferentiated polyblasts, fibroblasts, lymphocytes, as well as macrophages and mast cells predominated (70-80%). The content of neutrophilic leukocytes was 20-30%, which indicates a significant decrease in the severity of the inflammatory process, mainly in group III (Zarnitsa-A device). In general, the nature of changes in soft tissues in groups III and IV corresponded to the second phase of the wound process – the regeneration phase.

On the 10th day, the majority of laboratory animals in three of the four experimental groups – I, III and IV – showed a morphological picture reflecting the progression of regeneration in the area of the gunshot wound.

In all animals in groups III and IV, whose wounds were irradiated with optical radiation, the biopsy specimens clearly showed the formation of mature granulation tissue, the formation of vertically located vessels with endothelial proliferation (from 10 to 12 per 1 mm^2); stroma with signs of

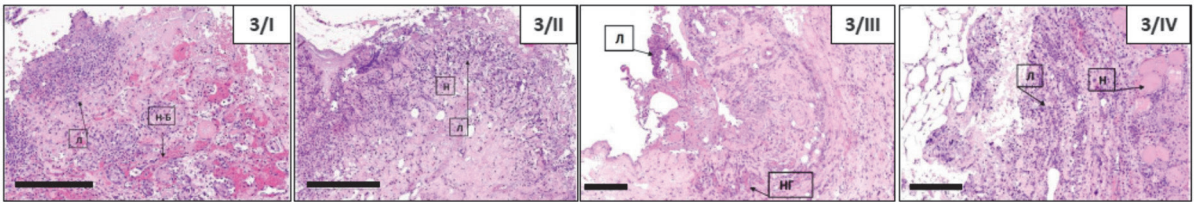

Рис. 4. Микропрепараты раны животных на 3-й день лечения (3/I – 1-я группа; 3/II – II-я группа; 3/III – III-я группа; 3/IV – IV-я группа): Л – сегментоядерные лейкоциты; Н – некроз мягких тканей; Н-Б – некроз мягких тканей с кровоизлиянием; НГ – незрелая грануляционная ткань, развитие ангиогенеза с очаговой пролиферацией эндотелия. Масштабная метка – 200 мкм; окраска – гематоксилин-эозин.
Fig. 4. Micro-preparations of animal wounds on the 3rd day of treatment (3/I – 1st group; 3/II – II group; 3/III – III group; 3/IV – IV group): Л – segmented leukocytes; Н – necrosis of soft tissues; Н-Б – necrosis of soft tissues with hemorrhage; НГ – immature granulation tissue, development of angiogenesis with focal proliferation of the endothelium. The scale label is 200 microns; the color is hematoxylin-eosin.

fibrosis. In the structure of the cellular composition, fibroblasts, macrophages and mast cells predominated (75-80%). The content of neutrophilic leukocytes was 20-25%, indicating an insignificant severity of the inflammatory process.

In group II of animals, a pronounced inflammatory process persisted by the 10th day. There were no trends towards activation of the connective tissue regeneration process in the area of the infected gunshot wound. In all the biopsies examined from the area of the gunshot wound, immature granulation tissue with a predominance of neutrophilic leukocytes in the structure of the cellular composition was determined. Angiogenesis was poorly developed, fibrin thrombi were noted.

On the 15th day, the positive dynamics of the wound healing process in Group I was generally maintained, in particular, a partial transition from the regeneration phase to the phase of scar reorganization (reparation) and epithelialization (phase III of the wound process) was noted.

In Group II, positive dynamics were also noted compared to the previous morphological picture: five animals showed pronounced activity of the tissue regeneration process in the area of the gunshot infected wound. Morphologically, granulation tissue formation was observed in biopsies, the number of vessels decreased (up to 15 per 1 mm^2), the vessels took a vertical position, and the endothelium showed signs of proliferation. In the structure of the cellular composition, the content of neutrophilic leukocytes was 35-45%. However, in the other three animals of the group, regeneration was less pronounced: immature granulation tissue, active angiogenesis (the number of vessels up to 25 per 1 mm^2), and stroma with minimal signs of collagenization were determined. The cellular composition is represented by 50-60% neutrophilic leukocytes.

In group III, all examined biopsies showed the presence of mature granulation tissue, vertically oriented vessels, and endothelium with signs of proliferation. Angiogenesis activity was reduced: the number of vessels was up to 10 per 1 mm^2. The stroma was compacted with collagenization. However, compared to the previous morphological picture, in this group, on the 15th day, a slowdown in the rate of tissue regeneration with an increase in the activity of the inflammatory process was observed. In the structure of the cellular composition, the content of neutrophilic leukocytes increased from 20-25% to 40-50%; the remaining 50-60% of cells are represented by tissue undifferentiated polyblasts, fibroblasts, lymphocytes, as well as macrophages and mast cells.

Unlike group III, laboratory animals of group IV did not show any increase in the activity of the inflammatory process and maintained a stable sequence of early interphase transition in the dynamics of the wound process, namely, the transition from the regeneration phase to the scar reorganization and epithelialization phase. In the cellular composition, the proportion of neutrophilic leukocytes was 20-30%, tissue undifferentiated polyblasts, fibroblasts, lymphocytes, as well as macrophages and mast cells formed 70-80%. Formation of mature granulation tissue was clearly visible in the wound. Angiogenesis activity was reduced: the number of vessels was up to 10 per 1 mm^2. The vessels were located vertically, the endothelium showed signs of proliferation.

Fig. 5 shows micropreparations of the animal wound on the 21st day of treatment.

When analyzing the dynamics of the wound process on the 21st day, it was noted that in groups I and IV, the wound process entered the phase of scar reorganization and epithelialization in all laboratory animals. In group II, the process of transition to the third phase was not completed in most animals, but maintained positive dynamics. In the structure of the cellular composition, the content of neutrophilic leukocytes was 30-40%. In group III, no significant differences in the dynamics of the wound process were observed compared to the previous morphological picture – the rate of tissue regeneration in the wound area was slowed down against the background of the continued activity of the inflammatory process.

Discussion of the results

The conducted studies of reparative regeneration of soft tissues in the area of infected gunshot injury allow to make the following clinical conclusions.

The slowest development of the regeneration process was observed in Group II (infected gunshot wound). This is

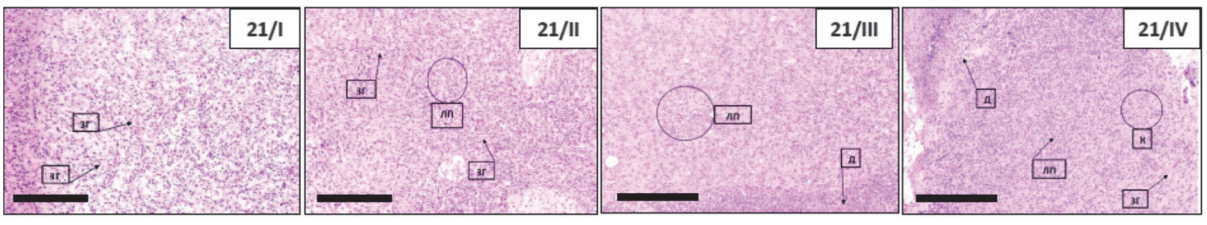

Рис. 5. Микропрепараты раны животных на 21-й день лечения (21/I – 1-я группа; 21/II – II-я группа; 21/III – III-я группа; 21/IV – IV-я группа): ЗГ – формирование зрелой грануляционной ткани с началом образования вертикально расположенных сосудов с пролиферацией эндотелия; ЛП – воспаление представлено рассеянными лейкоцитами, лимфоцитами и плазмоцитами; Д – клеточный детрит; К – пролиферация фибробластов, тучных клеток и макрофагов. Масштабная метка – 200 мкм; окраска – гематоксилин-эозин.
Fig. 5. Micro-preparations of animal wounds on the 21st day of treatment (21/I – 1st group; 21/II – II group; 21/III – III group; 21/IV – IV group): ЗГ – formation of mature granulation tissue with the onset of formation vertically located vessels with endothelial proliferation; ЛП – inflammation is represented by scattered leukocytes, lymphocytes and plasmocytes; Д – cellular detritus; К – proliferation of fibroblasts, mast cells and macrophages. The scale label is 200 microns; the color is hematoxylin-eosin.

due to the presence of long-term (up to 10 days) bacterial inflammation.

The effect of high-intensity optical radiation of a wide spectrum and low-intensity continuous UV radiation of a narrow spectrum on the tissues of infected gunshot wounds accelerates the transition between the inflammatory and regenerative phases of the wound process. Compared with Group II, the regeneration process in the area of the infected wound began 7-10 days faster, and compared with Group I (uninfected gunshot wound) – 3-5 days faster.

When analyzing the wound-healing effects of various types of optical radiation, it was found that high-intensity broad-spectrum optical radiation has a more pronounced anti-inflammatory effect in the first phase of the wound process and ensures earlier development of tissue regeneration compared to low-intensity continuous narrow-spectrum UV radiation.

However, at prolonged application (more than 10 days) high-intensity pulsed optical radiation of wide spectrum with the dosage selected in this work caused slowing down of tissue regeneration process in the area of wound damage, which should be taken into account when carrying out therapeutic procedures.

It should be noted that in the described experiments the dosage of the optical radiation used was set based on the results of previously conducted *in vitro* microbiological studies, which determined the bactericidal effectiveness of various types of optical radiation against clinically significant strains of pathogenic microorganisms [15, 16, 18]. The doses used reduced the initial level of bacterial contamination of the surface of the nutrient media by more than 6 decimal orders. Thus, the magnitude of the energy dose in these experiments was determined by the requirement to ensure a bactericidal effect in the wound. It was believed that effective suppression of bacterial flora activity is one of the main factors determining the nature of the course and duration of the wound process.

In this regard, it can be assumed that the observed effect of inhibition of regenerative histogenesis in the wound with a simultaneous increase in the activity of the inflammatory process in the case of long-term use (more than 10 days) of sufficiently high energy doses of pulsed optical irradiation is associated with an overdose of such an effect on the granulation tissues and epithelial layers that arise during regeneration. An overdose of optical radiation, and primarily its short-wave UV component (UV-C and UV-B components) is accompanied by increased concentrations of photochemical destruction products of intracellular structures (proteins, lipids, nucleic acids, etc.). These destruction products are, in fact, photoinduced antigens and should be neutralized and removed as a result of the inflammatory process. This can explain the prolonged nature of inflammation and inhibition of reparation observed in the experiments after 10 days of irradiation with the Zarnitsa-A device. Thus, the use of high-intensity pulsed irradiation for wound therapy requires strict methodological justification of the regime parameters and, first of all, the applied dose characteristics for each phase of the wound process.

Based on the results of the study, we can make a preliminary conclusion about the need for a gradual reduction in the doses of pulsed broad-spectrum optical irradiation in the phases of regeneration and reorganization of the scar (II and III phases of the wound process) to a preventive level of exposure, which is 10-20% of the initial dose, providing an anti-inflammatory (bactericidal) effect.

The experiments also showed that low-intensity UV radiation from LEDs, even at higher energy doses compared to pulsed optical radiation, has a smaller photochemical effect in biological tissues and, under the modes used in these experiments, did not cause any pronounced negative effects. Nevertheless such radiation accelerated the development of the phases of regeneration and reorganization of the scar and epithelialization.

Conclusion

The research proposes a new approach to the treatment of gunshot wounds complicated by nosocomial microflora. The essence of the method lies in the effect on the wound surface of high-intensity pulsed optical radiation of a wide spectrum, continuously covering the entire UV range (from 200 to 400 nm), visible and near infrared spectral regions. A pulsed xenon lamp is used as a radiation source, on the basis of which the Zarnitsa-A device was created. A comparison was made of the effect on the course of the wound process in gunshot trauma of high-intensity pulsed broad-spectrum optical radiation and low-intensity continuous UV radiation of a LED device emitting a narrow-band emission spectrum with a maximum at a wavelength of 272 nm and a half-width of 12 nm. It has been shown that high-intensity optical radiation of a broad spectrum has a more pronounced anti-inflammatory effect in the first phase of the wound process and ensures earlier development of tissue regeneration compared to low-intensity continuous UV radiation of a narrow spectrum. However its use requires justification of dose characteristics for each phase of the wound process.

Based on the results of the studies, it is recommended to gradually reduce the dosage of pulsed broadband optical irradiation in phases II and III of the wound process to a preventive level of exposure, which is 10-20% of the dose that provides a bactericidal effect. The results of the studies show the potential for using optical irradiation devices such as "Zarnitsa-A" and "Zarnitsa-D" for the treatment of infected gunshot wounds for the purpose of targeted action on the phases of the wound process and accelerating healing.

Funding of the work

The work was carried out with the financial support of Oniko-M LLC.

REFERENCES

1. Dai T., Vrahas M.S., Murray C.K., Hamblin M.R. Ultraviolet C irradiation: an alternative antimicrobial approach to localized infections? *Expert Rev. Anti Infect. Ther*, 2012, Vol.10(2), pp.185-195.
2. Klochkov H.D. et al. // In the collection «*Experience of medical support for troops in Afghanistan 1979-1989: Organization and volume of surgical care for the wounded*», edited by I.A. Yeryukhin, V.I. Frailkin. – M.: GVKG im. Academician N.N. Burdenko, 2002, Vol. 2, pp. 68-131.
3. Stewart S., Tunstall C., Stevenson T. Gunshot wounds in civilian practice: a review of epidemiology, pathophysiology and management. *Orthopaedics and Trauma*, 2023, Vol. 37(4), pp. 216-221. https://doi.org/10.1016/j.mporth.2023.05.002.
4. Trukhan A.P. Gunshot wounds and explosive trauma in peacetime. Features, organization and provision of surgical care (clinical and experimental research). *Dissertation of the Doctor of Medical Sciences (Military Medical Academy named after S.M. Kirov" of the Ministry of Defense of the Russian Federation, St. Petersburg*, 2022.
5. Chizh I.M. et al. // Experience of medical support for troops in internal armed conflict in the North Caucasus region of the Russian Federation in 1994-1996 and 1999-2002. *Edited by Fisuna A.Ya. (Rostov-on-Don: Rostov State Medical University of the Russian Ministry of Health*, 2014, Vol. 1, pp. 223-234.
6. Martin M.J., Eastridge B., Ruggero J.M. Combat trauma care: Lessons learned from recent combat operations. Current Therapy of Trauma and Surgical Critical Care *(Third Edition)*. Editors: Asensio J.A., Meredith J.W.,2024, Elsevier. https://doi.org/10.1016/B978-0-323-69787-3.00109-X.
7. Ataev A.R., Ataeva L.A., Ataev E.A. and others. Comprehensive treatment of wound infection in gunshot wounds and its objective criteria of effectiveness. *Practical medicine*, 2022, Vol. 20(4), pp.7-12.
8. Military field surgery: textbook. – 2nd ed., ed. and supplement / Ed. by E.K. Gumanenko. – M.: GEOTAR-Media, 2008, p.768. ISBN 978-5-9704-0911-4
9. Trishkin D.V., Kryukov E.V., Chuprina A.P. and others. Methodological recommendations for the treatment of combat surgical trauma. *Military Medical Academy named after S.M. Kirov. Saint Petersburg*, 2022, p. 373.
10. Plotnikov A.V. Infectious complications of gunshot wounds. *Thesis. LXX International Scientific and practical Conference "Actual problems of modern medicine and pharmacy", edited by* A.V. Sikorsky, O.K. Doronina. Minsk: BSMU, 2016, pp. 846-847.
11. Obolensky V.N. Modern methods of treatment of chronic wounds. *Medical Council*, 2016, Vol.10, pp.148-154.
12. Rasulov M.M., Motorina I.G., Yushkov G.G., and others. The effect of short-wave ultraviolet radiation on the healing of burn wounds (experimental study). *Issues of balneology, physiotherapy and therapeutic physical culture*, 2016, Vol.93(5), pp.38 42.
13. Motorina I.G., Rasulov M.M., Gukasov V.M., Myakinkova L.L. The effectiveness of phototherapy in the treatment of long-term non-healing wounds. *Innovation and expertise*, 2017, Vol. 2(20), pp. 225-234.
14. Arkhipov V.P., Bagrov V.V., Byalovsky Yu.Y. and others. Organization of preclinical studies of the bactericidal and wound-healing effects of the Zarya pulsed phototherapy apparatus. *Problems of social hygiene, public health and the history of medicine*, 2021, Vol. 29(5), 1156-1162. http://dx.doi.org/10.32687/0869-866X-2021-29-5 – 1156-1162
15. Bagrov V.V., Bukhtiyarov I.V., Volodin L.Y. et al. A High-Intensity Optical Irradiation Device for the Treatment of Wounds and Wound Infections. *Biomedical Engineering*, 2023, Vol. 57, pp. 77-80. https://doi.org/10.1007/s10527-023-10272-0.
16. Bagrov V.V., Bukhtiyarov I.V., Volodin L.Y. at al., Preclinical Studies of the Antimicrobial and Wound-Healing Effects of the High-Intensity Optical Irradiation «Zarnitsa-A» Apparatus. *Applied Sciences*, 2023, Vol. 13, pp. 10794. https://doi.org/10.3390/app131910794 V.13. – 10794.
17. Abduvosidov H.A., Chudnykh S.M., Egorov V.S. and others. Bactericidal efficiency of using high–intensity pulsed broadband radiation in the treatment of infected wounds // Biomedical Photonics, 2024, Vol. 13(2), pp. 26-33. https://doi.org/10.24931/2413-9432-2023-13-2-26-33
18. Bagrov V.V., Volodin L.Y., Kamrukov A.S. at al. LED device of short-wave ultraviolet irradiation. *Biomedical Engineering*, 2023. https://doi.org/10.1007/s10527-023-10307-6.

ЛИТЕРАТУРА

1. Dai T., Vrahas M.S., Murray C.K., Hamblin M.R. Ultraviolet C irradiation: an alternative antimicrobial approach to localized infections? // Expert Rev. Anti Infect. Ther. – 2012. – Vol.10(2). – P.185-195.
2. Клочков Н.Д. и др. // В сб. «Опыт медицинского обеспечения войск в Афганистане 1979-1989 гг.: Организация и объем хирургической помощи раненым», под ред. И.А. Ерюхина, В.И. Хрупкина. – М.: ГВКГ им. акад. Н. Н. Бурденко. – 2002. – Т.2, С. 68-131.
3. Stewart S., Tunstall C., Stevenson T. Gunshot wounds in civilian practice: a review of epidemiology, pathophysiology and management // Orthopaedics and Trauma. – 2023. – Vol. 37, No. 4. – C. 216-221. https://doi.org/10.1016/j.mporth.2023.05.002.
4. Трухан А.П. Огнестрельные ранения и взрывная травма мирного времени. Особенности, организация и оказание хирургической помощи (клинико-экспериментальное исследование) // Диссертация доктора медицинских наук (Военно-медицинская академия имени С.М. Кирова» Министерства обороны Российской Федерации, СПб. – 2022.
5. Чиж И.М. и др. // Опыт медицинского обеспечения войск во внутреннем вооруженном конфликте на территории Севера Кавказского региона Российской Федерации в 1994-1996 гг. и 1999-2002 гг. Под ред. Фисуна А.Я.. (Ростов-на-Дону: ГБОУ ВПО РостГМУ Минздрава России. – 2014, Т.1. – С. 223-234.
6. Martin M.J., Eastridge B., Ruggero J.M. Combat trauma care: Lessons learned from recent combat operations. Current Therapy of Trauma and Surgical Critical Care (Third Edition) // Editors: Asensio J.A., Meredith J.W. – 2024. – Elsevier. https://doi.org/10.1016/B978-0-323-69787-3.00109-X.
7. Атаев А.Р., Атаева Л.А., Атаев Э.А. и др. Комплексное лечение раневой инфекции при огнестрельных ранениях и ее объективные критерии эффективности // Практическая медицина. – 2022. – Т.20, №4. – С.7-12.
8. Военно-полевая хирургия: учебник. – 2-е изд., изм. и доп. / Под ред. Е.К. Гуманенко. – М.: ГЭОТАР-Медиа. – 2008. – С.768. ISBN 978-5-9704-0911-4
9. Тришкин Д.В., Крюков Е.В., Чуприна А.П. и др. Методические рекомендации по лечению боевой хирургической травмы // Военно-медицинская академия имени С.М. Кирова. Санкт-Петербург. – 2022. – С. 373.
10. Плотников А.В. Инфекционные осложнения огнестрельных ран // Тез. докл. LXX Международная научно-практическая конференция «Актуальные проблемы современной медицины и фармации», под ред. А.В. Сикорского, О.К. Дорониной. Минск: БГМУ. – 2016. – С. 846-847.
11. Оболенский В.Н. Современные методы лечения хронических ран // Медицинский Совет. – 2016. – №10. – С.148-154.
12. Расулов М.М., Моторина И.Г., Юшков Г.Г., и др. Влияние коротковолнового ультрафиолетового облучения на заживление ожоговых ран (экспериментальное исследование) // Вопросы курортологии, физиотерапии и лечебной физической культуры. – 2016. – Т.93, №5. – С.38-42.
13. Моторина И.Г., Расулов М.М., Гукасов В.М, Мякинькова Л.Л. Эффективность фототерапии при лечении длительно незаживающих ран //Инноватика и экспертиза. – 2017. – №. 2(20). – С. 225-234.
14. Архипов В.П., Багров В.В., Бяловский Ю.Ю. и др. Организация доклинических исследований бактерицидного и ранозаживляющего действия аппарата импульсной фототерапии "Заря" // Проблемы социальной гигиены, здравоохранения и истории медицины. – 2021. –Т. 29, №5. – 1156-1162. http://dx.doi.org/10.32687/0869-866X-2021-29-5- 1156-1162
15. Bagrov V.V., Bukhtiyarov I.V., Volodin L.Y. et al. A High-Intensity Optical Irradiation Device for the Treatment of Wounds and Wound Infections // Biomedical Engineering. – 2023. Vol. 57. – P. 77-80. https://doi.org/10.1007/s10527-023-10272-0.
16. Bagrov V.V., Bukhtiyarov I.V., Volodin L.Y. at al., Preclinical Studies of the Antimicrobial and Wound-Healing Effects of the High-Intensity Optical Irradiation «Zarnitsa-A» Apparatus // Applied Sciences. – 2023. – Vol. 13. – P. 10794. https://doi.org/10.3390/app131910794 V.13. – 10794.
17. Абдувосидов Х.А., Чудных С.М., Егоров В.С. и др. Бактерицидная эффективность использования высокоинтенсивного импульсного широкополосного облучения при лечении инфицированных ран // Biomedical Photonics. – 2024. – Vol. 13(2). – P. 26-33. https://doi.org/10.24931/2413-9432-2023-13-2-26-33
18. Bagrov V.V., Volodin L.Y., Kamrukov A.S. at al. LED device of short-wave ultraviolet irradiation // Biomedical Engineering. – 2023. https://doi.org/10.1007/s10527-023-10307-6.

A PLANIMETRIC STUDY OF EXPERIMENTALLY MODELED INFECTED WOUNDS EXPOSED TO HIGH-INTENSITY PULSED BROADBAND RADIATION

Chudnykh S.M.[1,2,3], Egorov V.S.[1,2], Abduvosidov Kh.A.[1,3,4], Snitsar A.V.[5], Chekmareva I.A.[6,7], Emaimo John A.[7]

[1]Moscow Clinical Scientific Center n.a. A.S. Loginov, Moscow, Russia
[2]Russian University of Medicine, Moscow, Russia
[3]Tver State Medical University, Tver, Russia
[4]Russian Biotechnological University, Moscow, Russia
[5]City Clinical Hospital №24 of the Moscow Department of Health, Moscow, Russia
[6]A.V. Vishnevsky National Medical Research Center of Surgery, Moscow, Russia
[7]Peoples' Friendship University of Russia, Moscow, Russia

Abstract

An experimental model of an infected wound was created in 90 Wistar rats using a mixture of cultures of *Staphylococcus aureus*, *Pseudomonas aeruginosa*, *Klebsiella pneumoniae*, and *Candida albicans*. The animals are divided into 3 groups of 30 individuals. The first group consisted of animals treated with pulsed high-intensity broadband irradiation using an experimental apparatus with a pulsed xenon lamp operating in a pulsed periodic mode with an average UV-C (200-280 nm) radiation power of 3 W, and a pulsed UV-C power of 24 kW. In the second group, traditional ultraviolet irradiation of wounds with a mercury bactericidal lamp was used for treatment, with an average UV-C (254 nm) radiation power of 1.2 W. The third group received only a local antiseptic treatment. The computer planimetry was used for monitoring the effectiveness of treatment. Parameters such as wound area, rate, and degree of epithelialization were recorded on days 1, 7, 14, and 21 of treatment. The study showed that in the first group of animals, the rate and degree of epithelialization, as well as the reduction in wound area at each control stage, were statistically significantly greater compared to the use of traditional ultraviolet irradiation and local antiseptic monotherapy. This dynamic is associated with the earlier cleansing of wounds from pathogenic microorganisms and the morphological changes that correspond to an earlier transition from the inflammatory phase to the proliferation and regeneration phases. Therefore, the local treatment of infected wounds with antiseptic agents in combination with pulsed high-intensity wideband radiation promotes the earlier epithelialization of the wounds.

Keywords: purulent wounds, infected wounds, high-intensity pulsed broadband radiation, ultraviolet radiation, regeneration, epithelialization, planimetry

Contacts: Abduvosidov Kh.A., sogdiana99@gmail.com

For citations: Chudnykh S.M., Egorov V.S., Abduvosidov Kh.A., Snitsar A.V., Chekmareva I.A., Emaimo John A. A planimetric study of experimentally modeled infected wounds exposed to high-intensity pulsed broadband radiation, *Biomedical Photonics*, 2025, vol. 14, no. 1, pp. 29–35. doi: 10.24931/2413–9432–2025–14–1–29–35

ПЛАНИМЕТРИЧЕСКОЕ ИССЛЕДОВАНИЕ ЭКСПЕРИМЕНТАЛЬНО МОДЕЛИРОВАННЫХ ИНФИЦИРОВАННЫХ РАН ПРИ ВОЗДЕЙСТВИИ ВЫСОКОИНТЕНСИВНОГО ИМПУЛЬСНОГО ШИРОКОПОЛОСНОГО ОБЛУЧЕНИЯ

С.М. Чудных[1,2,3], В.С. Егоров[1,2], Х.А. Абдувосидов[1,3,4], А.В. Сницарь[5], И.А. Чекмарева[6,7], А. Эмаимо Джон[7]

[1]Московский клинический научно-практический центр им. А.С. Логинова ДЗМ, Москва, Россия
[2]Российский университет медицины Минздрава России, Москва, Россия

[3]Тверской государственный медицинский университет Минздрава России, Тверь, Россия
[4]Российский биотехнологический университет, Москва, Россия
[5]Городская клиническая больница № 24 ДЗМ, Москва, Россия
[6]Национальный медицинский исследовательский центр хирургии им. А.В. Вишневского Минздрава России, Москва, Россия
[7]Российский университет дружбы народов имени Патриса Лумумбы, Москва, Россия

Резюме

Изучено действие широкополосного облучения на инфицированные раны. Экспериментально моделирована инфицированная рана у 90 крыс линии Wistar при помощи смеси культур *Staphylococcus aureus*, *Pseudomonas aeruginosa*, *Klebsiella pneumoniae*, *Candida albicans*. Животные были разделены на 3 группы по 30 особей. Первую группу составили животные для лечения, которых использовано импульсное высокоинтенсивное широкополосное облучение экспериментальным аппаратом с импульсной ксеноновой лампой, работающей в импульсно-периодическом режиме со средней мощностью УФ-С (200-280 нм) излучения – 3 Вт, импульсной мощностью УФ-С – 24 кВт. Во второй группе для лечения использовали традиционное ультрафиолетовое облучение ран ртутной бактерицидной лампой, со средней мощностью УФ-С (254 нм) излучения – 1,2 Вт. В третьей группе использовали только местное применение антисептика. Для контроля эффективности проводимого лечения нами использована компьютерная планиметрия. Учтены параметры площади, скорости и степени эпителизации ран в 1-й, 7-й, 14-й и 21-й дни лечения. Исследование показало, что у животных первой группы скорость и степень эпителизации и, соответственно, уменьшение площади ран на каждом этапе контроля статистически значимо больше по сравнению с использованием традиционного ультрафиолетового облучения и местной монотерапии антисептиком. Такая динамика связана с более ранним очищением ран от патогенной микробной флоры и более ранним переходом воспалительной фазы в фазу пролиферации и регенерации. Таким образом, местное лечение инфицированных ран антисептиками с комбинацией импульсного высокоинтенсивного широкополосного облучения способствует более ранней эпителизации ран.

Ключевые слова: гнойные раны, инфицированные раны, высокоинтенсивное импульсное широкополосное облучение, ультрафиолетовое облучение, регенерация, эпителизация, планиметрия.

Контакты: Абдувосидов Х.А., sogdiana99@gmail.com

Для цитирования: Чудных С.М., Егоров В.С., Абдувосидов Х.А., Сницарь А.В., Чекмарева И.А., Эмаимо Джон А. Результаты планиметрического исследования экспериментально моделированных инфицированных ран при воздействии высокоинтенсивного импульсного широкополосного облучения // Biomedical Photonics. – 2025. – Т. 14, № 1. – С. 29–35. doi: 10.24931/2413–9432–2025–14–1–29–35

Introduction

The factors of ineffective prevention and treatment of purulent complications in surgery are increasing resistance of microorganisms to antibacterial therapy, decreasing reactivity of the organism, increasing number of surgeries, their complexity, including in comorbid and elderly patients. All this determines the need to improve the existing and develop new types of prophylaxis and treatment [1,2,3].

In this regard, the works based on the effect of optical radiation on infected wounds are of considerable interest. In the scientific bases there are data on the successful application of various types of this radiation in wound infection: visible, infrared, ultraviolet radiation, as well as photodynamic therapy. The mentioned types of optical radiation have a destructive effect on *Pseudomonas bacillus* and multidrug-resistant strains (e.g., MRSA) and they also improve regenerative processes in the wound [4,5,6,7].

The biocidal effect of optical radiation is based on the presence of different spectral absorption bands in different microorganisms. The maximum destructive effect will be achieved in microorganisms whose maximum spectral sensitivity will coincide or is maximally close to the spectral line of the radiation source. The biocidal effect of UV radiation has been known for a relatively long time, as well as the fact that different parts of the UV spectrum have different biological activity. The UV-C region (from 200 to 280 nm) has the maximum biocidal effect, causing the death of various types of microorganisms - bacteria, spores and viruses. In this regard, the use of high-intensity pulsed broadband optical irradiation is of great interest. However there are very few works devoted to this method of exposure, which does not allow making reliable conclusions about the feasibility of its application, and requires further study and improvement [8,9].

The aim of the study was to evaluate the rate of wound surface reduction under high-intensity pulsed broadband irradiation of experimentally modeled infected wounds.

Materials and Methods

An experimental study with modeling of infected wound on 90 male Wistar rats was carried out. The approval of the Interuniversity Ethics Committee was obtained (extract from protocol No. 06-23 dated 15.06.23). Under aseptic conditions and general anesthesia with

the solution of xylazine and zoletil 100 in the withers area a bordering incision with removal of skin and subcutaneous tissue up to fascia was performed, after which a defect with a diameter of 20 mm was formed. Infection of soft tissues was performed with a trigger moistened in a mixture of cultures from control strains of *Staphylococcus aureus, Pseudomonas aeruginosa, Klebsiella pneumoniae, Candida albicans* in equal volumes and dilutions, containing 10^9 microbial bodies in 1 ml. The skin defect was sutured and aseptic dressing was applied. After 1 day, the wound was opened by removing the sutures. Daily all animals without exception were treated with 0.1% chlorhexidine solution. The studied animals were randomly divided into three groups of thirty animals each.

In the first, main, group of animals for wound treatment, high-intensity pulsed broadband irradiation was performed using an experimental apparatus developed by the Research Institute of Power Engineering of Bauman Moscow State Technical University. The apparatus is equipped with a pulsed xenon lamp of PPD (pulsed, pumping, direct) 5/60 type, operating in pulse-periodic mode with pulse frequency of 5 Hz and average electric power of 100 W. The average power of the lamp radiation in the UV-C range of the spectrum (200-280 nm) was 3 W, the pulse power of UV-C radiation was 24 kW. The device had three modes with irradiation cycle duration of 10 s (mode 1-50 pulses), 20 s (mode 2-100 pulses) and 40 s (mode 3-200 pulses). We selected the following method of wound treatment: in the first 5 days of treatment we used radiation mode 3 (200 pulses with irradiation cycle duration of 40 s) with irradiation distance of 5 cm from the wound; starting from the 6th day of treatment the next 5 days mode 2 was used (100 pulses with cycle duration of 20 s) at a distance of 10 cm.

In the second group of animals for the treatment of wounds traditional UV irradiation with the device UQI-01 (Ultraviolet Quartz Irradiator) "Solnyshko", UV quartz irradiator with a mercury bactericidal lamp type ACBU-7 (arc, compact, bactericidal, universal) with a power of 7 W, and UV-C with a radiation power 1.2 W - 275-180 nm were used. Irradiation was carried out daily for 10 days for 3 min at a distance of 10 cm from the wound. And in the third, control, group of animals the treatment of wounds was carried out only with the help of antiseptic by daily toileting and applying a dressing with 0.1% chlorhexidine solution to the wound.

One of the criteria of treatment efficiency was the study of wound healing parameters, which include the rate and degree of epithelialization, indicators of area reduction and direct control of wound area in different periods of treatment. All these parameters were analyzed.

To measure the wound area, ImageJ - a computer program for image analysis and editing - was used on the Windows XP platform. For this purpose, at each control stage (day 1, day 7, day 14, day 21 of treatment) we photographed the wound and saved the file in JPEG format. Then each of the JPEG files was opened in ImageJ program and wound area parameters were calculated. The rates and degrees of wound epithelialization were calculated in the periods between days of area control, and therefore time periods or intervals were identified. The first of such periods was the time interval from the beginning of treatment to the 7th day. The second period was from the 7th to the 14th day of treatment, and the third control period was from the 14th to the 21st day of treatment.

The study of wound epithelization rate was performed according to the following formula:

$$ER=S-Sn/t\ (mm^2)$$

where ER is the rate of wound epithelization per day, S is the area of the defect in the previous study, Sn is the area of the defect in the current study and t is the number of days between studies.

Analysis of the dynamics of the epithelization rate was performed using the following formula:

$$Sc=(S-Sn)x100/Sxt\ (\%)$$

where Sc is the degree of ulcer epithelization per day (in %), S is the ulcer area in the previous study, Sn is the ulcer area in this study, t is the number of days between the previous and this study.

Results

The analysis of wound epithelization rate showed that in the first 7 days of treatment against the background of cleansing in the first group of animals, to which pulsed high-intensity broadband irradiation was used in the treatment of wounds, the dynamics of epithelization rate was the highest compared to that in the animals of the second and third groups (Fig. 1). Thus, in the first group the epithelization rate in the first 7 days of treatment was 1.43 (1.29;1.71) mm/day ($p<0.0001$ in relation to the indicators of the second and third groups), while in the second and third groups it was 0.86 (0.57;0.87) mm/day ($p=0.0024$ in relation to the indicators of the third group) and 0.57 (0.57;0.71) mm/day, respectively. In the time interval between the 7th and 14th days the rates of wound epithelization in animals of the first and second groups did not differ significantly ($p=0.61$), and were equal to 0.71 (0.71;0.86) mm/day and 0.71 (0.57;0.86) mm/day, which was statistically significantly higher compared to the same indicators in animals of the third group (0.57(0.43;0.71) mm/day $p=0.004$ and $p=0.016$, respectively).

When comparing the epithelization rate within the groups (Fig. 1) between the first and second time intervals, it was revealed that the rate of wound epithelization decreased after the 7th day of treatment compared to the first 7 days of treatment in the first group of animals ($p<0.0001$). In the interval between

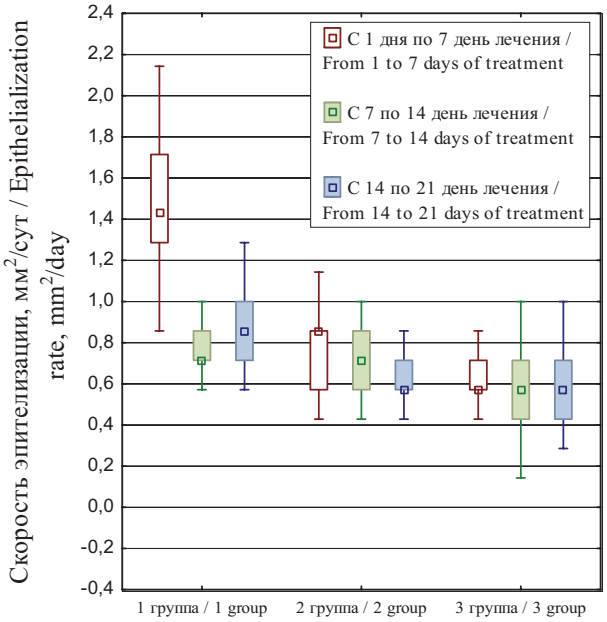

Рис. 1. Показатели скорости эпителизации ран у животных с разными видами лечения (мм/сут)
Fig. 1. Indicators of wound epithelialization rate in animals with different types of treatment (mm/day)

the 14th and 21st days of treatment the rate of wound epithelization in the first group of animals was 0.86 mm/day, which is statistically significantly higher compared to the indicators of the animals of the second and third groups ($p<0.0001$ for both groups). At the same time, in the first group, where pulsed high-intensity broadband irradiation was used during wound treatment, and in the second group, where traditional ultraviolet irradiation was used, in the period from the 14th to the 21st days of treatment the epithelization rate was significantly lower in comparison with the first control period (in the first 7 days of treatment) ($p<0.0001$ for the first group, $p=0.006$ for the second group).

During the first 7 days of treatment in animals of the first group the degree of wound epithelization was 3,97 (3,47;4,4) % per day ($p<0,0001$ in relation to the indicators of the second and third groups), in the second group it was 2,2 (1,59;2,38) % per day ($p<0,0001$ in relation to the indicators of the third group). In animals of the third group, where only antiseptic degree was used in wound treatment, epithelization was equal to 1.59 (1.5;1.88) % per day (Fig. 2).

In the period from the 7th to the 14th day the degree of wound epithelization in animals of the first group decreased in comparison with the previous period to 2.7 (2.38;3.06) % per day ($p<0.0001$). At the same time it was statistically significantly higher compared to the indicators of animals of the second and third groups ($p=0.003$ and $p<0.0001$, respectively). In animals of the second and third groups, the dynamics of the degree of epithelization did not change significantly compared to the previous control period (Fig. 1). In the control period from day 14 to day 21 an increase in the degree of wound epithelization up to 3.99 (3.43;4.55) % per day was observed in animals treated with pulsed high-intensity broadband irradiation, which was significantly higher compared to the indicators in the previous control period ($p<0.0001$) and compared to the indicators of the animals of the second and third groups ($p<0.0001$). In animals of the second and third groups, the indicators of the degree of epithelization were not significantly different from the previous control periods and compared to each other, and were equal to 2.2 (2.04;2.65) % per day and 2.04 (1.71;2.46) % per day (Fig. 2), respectively.

The study showed that during the whole period of observation the degree of wound epithelization in animals of the first group was 2.78 (2.65;2.83) % per day, which was statistically significantly higher compared to the indicators in the first and second groups ($p<0.0001$). In animals of the second group the degree of wound epithelization was equal to 1.85 (1.72;2.06) % per day ($p=0.00012$ compared to the third group), and in animals of the third group 1.58 (1.5;1.85) % per day (Fig. 2).

The area of wounds before treatment in animals of all three groups was not statistically different (Fig. 3). By the 7th day of treatment there was a statistically significant positive dynamics within each group compared to the initial indicators ($p<0.0001$ for each group). It should be noted that when comparing the wound area between the groups there was a significant difference ($p<0,0001$). In the first group of animals, where treatment was carried out by pulsed high-intensity broadband irradiation, the

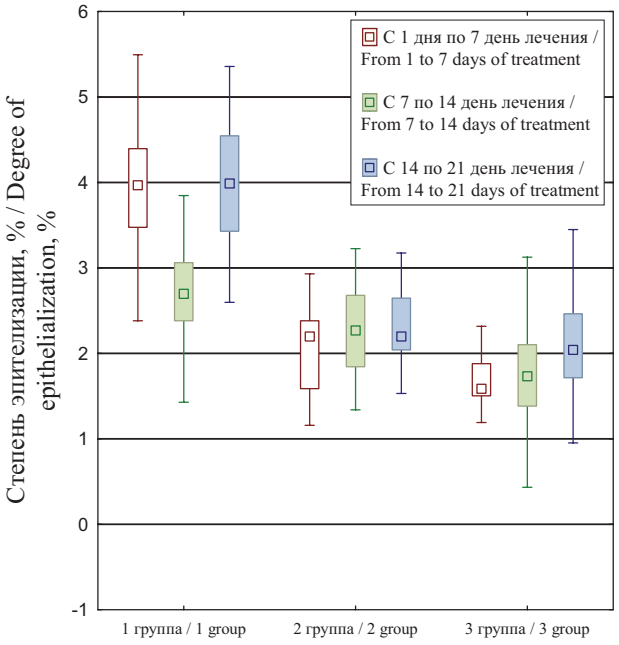

Рис. 2. Показатели степени эпителизации ран у животных с разными видами лечения (%).
Fig. 2. Indicators of the degree of epithelialization of wounds in animals with different types of treatment (%).

wound area decreased by 10 (9;12) mm², and was equal to 27 (26,28) mm² (p<0,0001 in relation to the indicators of the second and third groups). And in the third group, the area was 33 (32;34) mm², decreasing by 4 (4;5) mm².

By day 14 of treatment, the wound area in all groups of animals was statistically significantly smaller compared to day 7 of control (p<0.0001). In the first group of animals the wound area decreased compared to day 7 of the control by 6 (4;6) mm² and was equal to 22 (21;23) mm²; in the second group it decrease by 5 (4;6) mm² and amounted to 27 (26;28) mm²; and in the third group the wound decreased by 4 (4;5) mm², reaching 29 (28;30) mm². At this point in the study, there was a statistically significant difference in wound area between the groups.

The wound area on day 21 of treatment within each group was statistically significantly smaller compared to the previous day's control. In group one, the wound surface area was 15 (15;16) mm² (p<0.0001 compared to the rates in groups one and two), while in group two it was 22 (21;24) mm² (p<0.0001 compared to the rates in group three), and in group three it was 24 (23;26) mm².

Further analysis showed that in the first group of animals, where pulsed high-intensity irradiation was applied to treat infected wounds, complete epithelization of wounds was achieved within 37 (36;38) days (Fig. 4), which was statistically significantly less compared to the group where conventional UV irradiation was performed (p<0.0001) and to the group using only antiseptic (p<0.0001). In the second group of animals, we observed complete epithelialization of wounds by the 48th (47;49) day of treatment, which was significantly less (p<0.0001) compared to the third group, where complete epithelialization was achieved by the 61st (59;61) day.

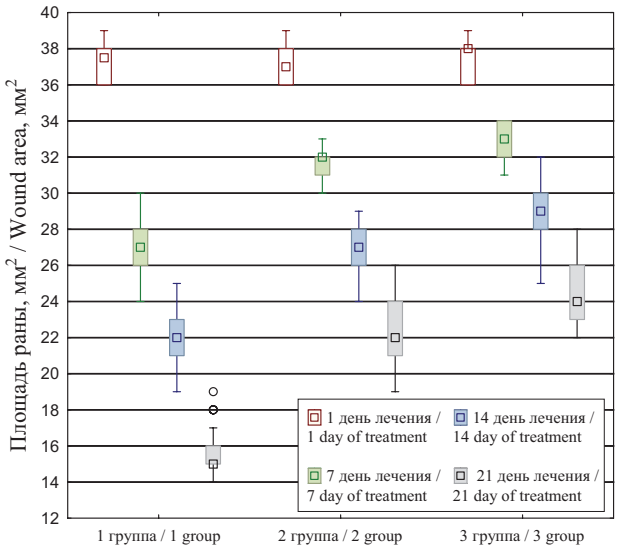

Рис. 3. Динамика площади ран у животных с разными методами лечения.
Fig. 3. Dynamics of wound area in animals with different treatment methods.

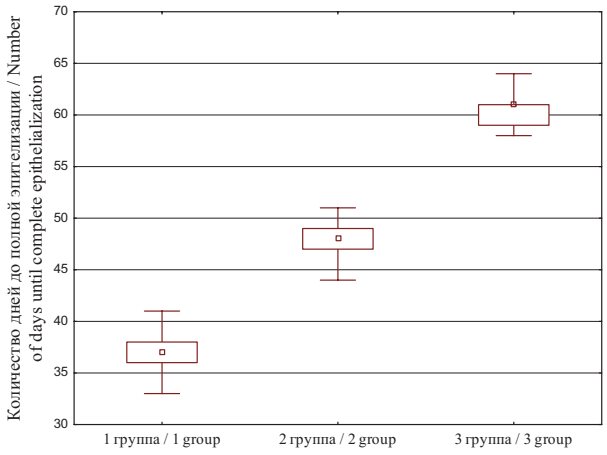

Рис. 4. Сроки полной эпителизации инфицированных ран у животных трех групп с различными методами лечения.
Fig. 4. The timing of complete epithelialization of infected wounds in animals of three groups with different treatment methods.

Discussion

In modern scientific literature there are a sufficient number of studies devoted to the treatment of wounds, including infected ones. According to Ashja Zadeh M.A. *et al*., the area of experimentally infected wounds in rats with diabetes when using the extract of Crocus Pallasii Subsp. Haussknechtii Boiss leaves by the 21st day of treatment is reduced by more than three times compared to classical treatment methods. At the same time, the authors claim bactericidal effectiveness when using this extract [10]. There is also evidence that the combined use of local antiseptic polyhexanide and exposure of the wound surface to erbium laser in chronic purulent wounds contributes to significant cleansing, decontamination and, consequently, earlier epithelization of wounds [11]. Another method of exogenous physical treatment of infected wounds is cryotherapy. Thus, according to some authors, irrigation of the wound surface with liquid nitrogen, both monotherapy and in combination with local application of antiseptics, as well as in combination with antibacterial therapy, leads to a rapid decrease in signs of inflammation, activates the processes of granulation and epithelialization [12].

To assess the effectiveness of wound treatment in modern surgery, numerous methods of control are used, including bacterial, cytologic, morphologic, which includes both light microscopy, immunohistochemical methods and electron microscopy, as well as morphometry and other control methods. One of the most used criteria for analyzing the results of wound treatment, including infected wounds, is planimetry, a method of dynamic control of the wound area. With the development of computer technology in modern practical surgery, doctors use electronic programs and mobile applications for planimetry [13]. There is data on

the use of computer planimetry, which allows to analyze different parameters of the wound surface, such as the area, the presence of necrosis in the wound, fibrin plaque, the appearance of granulation and epithelization, which makes it possible to determine the choice of further treatment, compare and evaluate different approaches and methods of local therapy [14].

We modeled an experimentally infected wound using a mixture of cultures of *Staphylococcus aureus, Pseudomonas aeruginosa, Klebsiella pneumoniae, Candida albicans*. The animals were divided into three groups depending on the type of treatment. The first group consisted of animals for the treatment of which a combination of pulsed high-intensity broadband irradiation and local application of antiseptic was used. In the second group a combination of traditional ultraviolet irradiation of wounds was used with local application of antiseptic. In the third group only local application of antiseptic was used. To control the effectiveness of treatment computerized planimetry was applied. At each stage of the control photofixation of the wound was carried out, subsequently the photo file in JPEG format was entered into the ImageJ program and counting of the wound area was performed. The planimetric study showed that in animals that were treated with pulsed high-intensity broadband irradiation for the treatment of infected wounds, the rate and degree of epithelialization and, accordingly, the reduction in the area of wounds at each stage of control were statistically significantly greater compared to the use of traditional ultraviolet irradiation and local antiseptic monotherapy. Such dynamics is associated with earlier clearing of wounds from pathogenic microbial flora [15] and morphologic picture [16, 17], i.e. earlier transition of the inflammatory phase to the phase of proliferation and regeneration.

Conclusion

Local treatment of infected wounds with antiseptics and combination of pulsed high-intensity broadband irradiation promotes earlier epithelization of wounds.

REFERENCES

1. Amaral A.L., Aoki A., Andrade S.A. Could light be a broad-spectrum antimicrobial? // *Evid Based Dent*, 2024, Vol. 25(l4)? pp. 192-193. doi:10.1038/s41432-024-01042-2
2. Alcolea J.M., Hernández E., Martínez-Carpio P.A., et al. Treatment of Chronic Lower Extremity Ulcers with A New Er: Yag Laser Technology. *Laser Ther*. – 2017. – Vol. 26(3). – P. 211-222. doi:10.5978/islsm.17-OR-17
3. Aleksandrowicz H., Owczarczyk-Saczonek A., Placek W. Venous Leg Ulcers: Advanced Therapies and New Technologies. *Biomedicines*, 2021, Vol. 96(11), pp. 1569. doi:10.3390/biomedicines9111569
4. Gupta A., Avci P., Dai T., Huang Y.Y., Hamblin M.R. Ultraviolet Radiation in Wound Care: Sterilization and Stimulation. *Adv Wound Care (New Rochelle)*, 2013, Vol. 2(8). – pp. 422-437. doi:10.1089/wound.2012.0366;
5. Wang D., Kuzma M.L., Tan X., et al. Phototherapy and optical waveguides for the treatment of infection. *Adv Drug Deliv Rev*, 2021, Vol. 179, pp. 114036. doi:10.1016/j.addr.2021.114036;
6. Chepurnaya J.L., Melkonyan G.G., Gul'muradova N.T., Sorokin A.A. The effect of photodynamic therapy on the wound process dynamics in patients with purulent hand diseases. *Biomedical Photonics*, 2021, Vol. 10(2), pp. 4-17. https://doi.org/10.24931/2413-9432-2021-10-2-4-17
7. Soltan H.H., Afifi A., Mahmoud A., Refaat M., Al Balah O.F. Влияние наночастиц серебра и низкоинтенсивного лазера на иммунный ответ и заживление кожных ран мышей-альбиносов. *Biomedical Photonics*, 2024, Vol. 13(1), pp. 16-27.
8. https://doi.org/10.24931/2413-9432-2023-13-1-16-27;
9. Arkhipov V.P., Bagrov V.V., Byalovsky Yu.Y. and others. Organization of preclinical studies of the bactericidal and wound-healing effects of the Zarya pulsed phototherapeutic apparatus. *Problems of social hygiene, public health and the history of medicine*, 2021, Vol. 29(5), pp.1156-1162. DOI 10.32687/0869-866X-2021-29-5-1156-1162.
10. Davydov A.I., Lipatov D.V., Kamrukov A.S. and others. The use of pulsed high-intensity optical irradiation and exogenous nitrogen monoxide in the complex treatment of patients with purulent inflammation of the uterine appendages. *Issues of gynecology, obstetrics and perinatology,* 2007, Vol. 6(1), pp. 14-17.
11. Ashja Zadeh M.A., Ebrahimi M., Salarian A.A., Abtahi S.R., Jahandideh A. Evaluation of Beneficial Influence of Local Appli-

ЛИТЕРАТУРА

1. Amaral A.L., Aoki A., Andrade S.A. Could light be a broad-spectrum antimicrobial? // Evid Based Dent. – 2024. – Vol. 25(l4). – P. 192-193. doi:10.1038/s41432-024-01042-2
2. Alcolea J.M., Hernández E., Martínez-Carpio P.A., et al. Treatment of Chronic Lower Extremity Ulcers with A New Er: Yag Laser Technology // Laser Ther. – 2017. – Vol. 26(3). – P. 211-222. doi:10.5978/islsm.17-OR-17
3. Aleksandrowicz H., Owczarczyk-Saczonek A., Placek W. Venous Leg Ulcers: Advanced Therapies and New Technologies // Biomedicines. – 2021. – Vol. 96(11). – P. 1569. doi:10.3390/biomedicines9111569
4. Gupta A., Avci P., Dai T., Huang Y.Y., Hamblin M.R. Ultraviolet Radiation in Wound Care: Sterilization and Stimulation // Adv Wound Care (New Rochelle). – 2013. – Vol. 2(8). – P. 422-437. doi:10.1089/wound.2012.0366;
5. Wang D., Kuzma M.L., Tan X., et al. Phototherapy and optical waveguides for the treatment of infection // Adv Drug Deliv Rev. – 2021. – 179. – P. 114036. doi:10.1016/j.addr.2021.114036;
6. Chepurnaya J.L., Melkonyan G.G., Gul'muradova N.T., Sorokin A.A. The effect of photodynamic therapy on the wound process dynamics in patients with purulent hand diseases // Biomedical Photonics. – 2021. - Vol. 10(2). – P. 4-17. https://doi.org/10.24931/2413-9432-2021-10-2-4-17
7. Soltan H.H., Afifi A., Mahmoud A., Refaat M., Al Balah O.F. Влияние наночастиц серебра и низкоинтенсивного лазера на иммунный ответ и заживление кожных ран мышей-альбиносов // Biomedical Photonics. – 2024. – Vol. 13(1). – P. 16-27.
8. https://doi.org/10.24931/2413-9432-2023-13-1-16-27;
9. Архипов В.П., Багров В.В., Бяловский Ю.Ю. и др. Организация доклинических исследований бактерицидного и ранозаживляющего действия импульсного фототерапевтического аппарата «Заря» // Проблемы социальной гигиены, здравоохранения и истории медицины. – 2021. - Т. 29, №5. – С. 1156-1162. DOI 10.32687/0869-866X-2021-29-5-1156-1162.
10. Давыдов А.И., Липатов Д.В., Камруков А.С. и др. Использование импульсного высокоинтенсивного оптического облучения и экзогенного монооксида азота в комплексном лечении больных гнойным воспалением придатков матки // Вопросы гинекологии, акушерства и перинатологии. – 2007. – Т. 6, № 1. – С. 14-17.
11. Ashja Zadeh M.A., Ebrahimi M., Salarian A.A., Abtahi S.R., Jahandideh A. Evaluation of Beneficial Influence of Local Application

cation of Crocus Pallasii Subsp. Haussknechtii Boiss. Extract on Healing of Full Thickness Excisional Infected Wounds in Diabetic Rats. *Bull Emerg Trauma*, 2020, Vol. 8(3), pp. 169-178. doi:10.30476/BEAT.2020.82567

12. Zaitsev A.E., Asanov O.N., Chekmareva I.A. Analysis of the effectiveness of an erbium laser in the treatment of trophic purulent wounds in an experiment. *Medical Bulletin of the North Caucasus*, 2023, Vol. 18(4), pp. 394-397. DOI – https://doi.org/10.14300/mnnc.2023.18093
13. Pavlov A.V., Maskin S.S., Igolkina L.A. Acceleration of healing of experimentally modeled purulent wounds under local cryotherapy. *Science of the young (Eruditio Juvenium)*, 2022, Vol. 10(4), pp. 391-400. https://doi.org/10.23888/HMJ2022104391-400 .
14. Bokov D.A., Mikhailov N.O., Laptieva A.Yu., Goryushkina E.S. Modern methods of measuring the area of the wound surface and their comparison with each other. *Youth Innovation Bulletin*, 2023, Vol. 12(2), pp. 14-16.
15. Ivanov G.G., Yarosh V.N., Balashov I.A. Determination of the size and structural elements of the RAS based on computer planimetry. Photoprotocol in assessing the course of the wound process. Wounds and wound infections. B.M. Kostyuchenko Journal, 2023, Vol. 10(1), pp. 38-44. https://doi.org/10.25199/2408-9613-2023-10-1-38-44
16. Abduvosidov Kh.A., Chudnykh S.M., Egorov V.S., Filimonov A.Yu., Korolyova I.A., Kamrukov A.S., Bagrov V.V., Kondrat'ev A.V. Bactericidal effectiveness of high-intensity pulsed broadband irradiation in treating infected wounds. *Biomedical Photonics*, 2024, Vol.13(2), pp. 26-33. https://doi.org/10.24931/2413-9432-2023-13-2-26-33
17. Egorov V.S., Filimonov A.Yu., Chudnykh S.M., Abduvosidov Kh.A., Chekmareva I.A., Paklina O.V., Baranchugova L.M., Kondrat'ev A.V. Morphological evaluation of the effectiveness of treating infected wounds with high-intensity pulsed broadband irradiation. *Biomedical Photonics*, 2024, Vol. 13(3), pp. 31-41. https://doi.org/10.24931/2413-9432-2024-13-3-31-41
18. Egorov V.S., Filimonov A.Yu., Chudnykh S.M., Spiryakina E.V., Abduvosidov Kh.A. Experimental substantiation of the use of high–intensity pulsed broadband radiation in the treatment of infected wounds. *Kazan Medical Journal*, 2025, Vol. 106(1), pp.79-87. doi:https://doi.org/10.17816/KMJ634565

of Crocus Pallasii Subsp. Haussknechtii Boiss. Extract on Healing of Full Thickness Excisional Infected Wounds in Diabetic Rats // Bull Emerg Trauma. – 2020. – T. 8(3). – P. 169-178. doi:10.30476/BEAT.2020.82567

12. Зайцев А.Е., Асанов О.Н., Чекмарёва И.А. Анализ эффективности эрбиевого лазера при лечении трофических гнойных ран в эксперименте. Медицинский вестник Северного Кавказа. – 2023. – Т. 18, №4. – С. 394-397. DOI – https://doi.org/10.14300/mnnc.2023.18093
13. Павлов А.В., Маскин С.С., Иголкина Л.А. Ускорение заживления экспериментально моделированных гнойных ран при локальном криовоздействии // Наука молодых (Eruditio Juvenium). – 2022. – Т. 10, № 4. – С. 391-400. https://doi.org/10.23888/HMJ2022104391-400.
14. Боков Д.А., Михайлов Н.О., Лаптиёва А.Ю., Горюшкина Е.С. Современные способы измерения площади раневой поверхности и их сравнение между собой // Молодежный инновационный вестник. – 2023. – Т. 12, №2. – С. 14-16.
15. Иванов Г.Г., Ярош В.Н., Балашов И.А. Определение размеров и структурных элементов ран на основе компьютерной планиметрии. Фотопротокол в оценке течения раневого процесса // Раны и раневые инфекции. Журнал имени проф. Б.М. Костючёнка. – 2023. – Т. 10, №1. – С. 38-44. https://doi.org/10.25199/2408-9613-2023-10-1-38-44
16. Abduvosidov Kh.A., Chudnykh S.M., Egorov V.S., Filimonov A.Yu., Korolyova I.A., Kamrukov A.S., Bagrov V.V., Kondrat'ev A.V. Bactericidal effectiveness of high-intensity pulsed broadband irradiation in treating infected wounds // Biomedical Photonics. – 2024. – Vol. 13(2). – P. 26-33. https://doi.org/10.24931/2413-9432-2023-13-2-26-33
17. Egorov V.S., Filimonov A.Yu., Chudnykh S.M., Abduvosidov Kh.A., Chekmareva I.A., Paklina O.V., Baranchugova L.M., Kondrat'ev A.V. Morphological evaluation of the effectiveness of treating infected wounds with high-intensity pulsed broadband irradiation // Biomedical Photonics. – 2024. – Vol. 13(3). – P. 31-41. https://doi.org/10.24931/2413-9432-2024-13-3-31-41
18. Егоров В.С., Филимонов А.Ю., Чудных С.М., Спирякина Е.В., Абдувосидов Х.А. Экспериментальное обоснование использования высокоинтенсивного импульсного широкополосного облучения в лечении инфицированных ран // Казанский медицинский журнал. – 2025. – Т. 106, №1. – С.79-87. doi:https://doi.org/10.17816/KMJ634565

ORIGINAL ARTICLES

DUAL-WAVELENGTH FLUORESCENCE STUDY OF *IN VIVO* ACCUMULATION AND FORMATION OF 5-ALA-INDUCED PORPHYRINS

Zavedeeva V.E.[1], Efendiev K.T.[2,3], Kustov D.M.[2], Loschenova L.Yu.[4], Loschenov V.B.[2,3]
[1]Sorbonne University, Faculty of Science and Engineering, Paris, France
[2]Prokhorov General Physics Institute of the Russian Academy of Sciences, Moscow, Russia
[3]National Research Nuclear University «MEPhI», Moscow, Russia
[4]BIOSPEC Ltd., Moscow, Russia

Abstract

This article discusses the processes of 5-aminolevulinic acid (5-ALA) metabolism, as well as the accumulation and photobleaching of protoporphyrin IX (PpIX) during photodynamic therapy (PDT) of benign skin tumors using the application method of introducing a 20% 5-ALA solution. The exposure time of the drug was 4 h. The study included two patients, one with dermatofibroma and one with congenital melanocytic nevus. Spectral fluorescence study was performed by fluorescence excitation using lasers at wavelengths of 405 and 632.8 nm. Fluorescence of normal and pathological tissues was recorded in the range of 350-800 nm at λ_{exc}=405 nm and in the range of 600-750 nm at λ_{exc}=632.8 nm. The dynamics of PpIX accumulation was studied. In the superficial tissue layers (at λ_{exc}=405 nm), the maximum accumulation of PpIX was recorded 3 h after the 5-ALA administration. In deeper tissue layers (at λ_{exc}=632.8 nm), the PpIX accumulation increased during 4 h of observation. After PDT with laser radiation with a wavelength of 635 nm, photobleaching of PpIX and the formation of its chlorin-type photoproducts with a fluorescence maximum in the range of 670–700 nm were observed. It was not possible to establish the presence of uroporphyrins I and III and/or coproporphyrin I, which could indicate a disturbance in the mitochondrial metabolism of necrotic cells. The obtained results expand the possibilities of spectral-fluorescent diagnostics and can contribute to increasing the effectiveness of 5-ALA-PDT of tumors.

Key words: spectral fluorescence diagnostics, photodynamic therapy, 5-aminolevulinic acid, porphyrins, protoporphyrin IX, chlorin-type photoproducts, fluorescence spectra.

Contacts: Zavedeeva V.E., e-mail: vezavedeeva@gmail.com

For citations: Zavedeeva V.E., Efendiev K.T., Kustov D.M., Loschenova L.Yu., Loschenov V.B. Dual-wavelength fluorescence study of *in vivo* accumulation and formation of 5-ALA-induced porphyrins, *Biomedical Photonics*, 2025, vol. 14, no. 1, pp. 36–46. doi: 10.24931/2413–9432–2025–14–1–36–46

ДВУХВОЛНОВОЕ ФЛУОРЕСЦЕНТНОЕ ИССЛЕДОВАНИЕ *IN VIVO* НАКОПЛЕНИЯ И ОБРАЗОВАНИЯ 5-АЛК-ИНДУЦИРОВАННЫХ ПОРФИРИНОВ

В.Е. Заведеева[1], К.Т. Эфендиев[2,3], Д.М. Кустов[2], Л.Ю. Лощенова[4], В.Б. Лощенов[2,3]
[1]Университет Сорбонна, Факультет науки и инженерии, Париж, Франция
[2]Институт общей физики им. А.М. Прохорова РАН, Москва, Россия
[3]Национальный исследовательский ядерный университет «МИФИ», Москва, Россия
[4]ООО «БИОСПЕК», Москва, Россия

Резюме

В данной статье рассмотрены процессы метаболизма 5-аминолевулиновой кислоты (5-АЛК), а также накопления и фотообесцвечивания протопорфирина IX (ПпIX) в процессе фотодинамической терапии (ФДТ) доброкачественных опухолей кожи с применением аппликационного способа введения 20%-го раствора 5-АЛК. Время экспозиции препарата составило 4 ч. В исследовании участвовали два пациента с дерматофибромой и врожденным меланоцитарным невусом. Спектрально-флуоресцентное исследование проводили с возбуждением флуоресценции лазерами на длинах волн 405 и 632,8 нм. Флуоресценцию нормальной и патологически измененной ткани регистрировали в диапазоне 350–800 нм при $\lambda_{воз}$=405 нм и в диапазоне 600–750 нм при $\lambda_{воз}$=632,8 нм. Исследована динамика накопления ПпIX. В поверхностных слоях тканей (при $\lambda_{воз}$=405 нм) максимум накопления ПпIX регистрировали спустя 3 ч после введения 5-АЛК. В более глубоких слоях тканей (при $\lambda_{воз}$=632,8 нм) накопление ПпIX увеличивалось в течение 4 ч наблюдения. После ФДТ

лазерным излучением с длиной волны 635 нм наблюдали фотообесцвечивание PpIX и образование его фотопродуктов хлоринового типа, с максимумом флуоресценции в диапазоне 670–700 нм. Установить наличие уропорфиринов I и III и/или копропорфирина I, которые могли бы свидетельствовать о нарушении митохондриального метаболизма некротических клеток, не удалось. Полученные результаты расширяют возможности спектрально-флуоресцентной диагностики и могут способствовать повышению эффективности 5-АЛК-ФДТ опухолей.

Ключевые слова: спектрально-флуоресцентная диагностика, фотодинамическая терапия, 5-аминолевулиновая кислота, порфирины, протопорфирин IX, фотопродукты хлоринового типа, спектры флюоресценции.

Контакты: Заведеева В.Е., e-mail: vezavedeeva@gmail.com

Для цитирования: Заведеева В.Е., Эфендиев К.Т., Кустов Д.М., Лощенова Л.Ю., Лощенов В.Б. Двухволновое флуоресцентное исследование *in vivo* накопления и образования 5-алк-индуцированных порфиринов // Biomedical Photonics. – 2025. – Т. 14, № 1. – С. 36–46. doi: 10.24931/2413–9432–2025–14–1–36–46

Introduction

Fluorescence diagnostics and photodynamic therapy (PDT) using 5-aminolevulinic acid (5-ALA) are widely used in leading clinics around the world to treat various oncological and non-oncological diseases. PDT includes two key steps: administration of a photosensitizer (PS) which has the ability to selectively accumulate in tumor tissues and cells, and then exposure of the sensitized tissues to light of a specific wavelength. It is optimal if the wavelength corresponds to one of the PS absorption peaks, which triggers the process of generation of reactive oxygen species, mainly singlet oxygen (Fig. 1).

The transfer of molecular oxygen from the triplet state to the singlet state is facilitated by the energy transfer from the PS in the excited triplet state. When the PS absorbs laser radiation, the molecule passes into an excited state, which can exist in either singlet or triplet configuration. The PS molecule in the singlet state quickly passes back to the ground state, accompanied by the emission of light quanta (fluorescence) or is converted into kinetic thermal energy of the reaction products. In contrast, the PS in the triplet state has a longer lifetime, which increases the probability of energy transfer to nearby (within 0–20 nm) oxygen molecules, thereby transferring them to the singlet state. According to [1], 5-ALA has two metabolic pathways. The first pathway leads to the formation of photodynamically active protoporphyrin IX (PpIX). The second pathway leads to the formation of fluorescent uroporphyrin I, which either does not have photodynamic activity or exhibits it to an insignificant degree (Fig. 2).

It is especially important that 5-ALA metabolism in necrotic tissues has been shown to occur via an alternative pathway [1]. In cells that have undergone apoptosis under the influence of PDT, metabolic disturbances are also observed, which indicates the possibility of switching the metabolism of irradiated cells to an alternative pathway. Furthermore, it has been demonstrated that the intensity of the PpIX accumulation process diminishes with laser irradiation when light exposure occurs prior to reaching maximum accumulation [1]. This phenomenon can likely

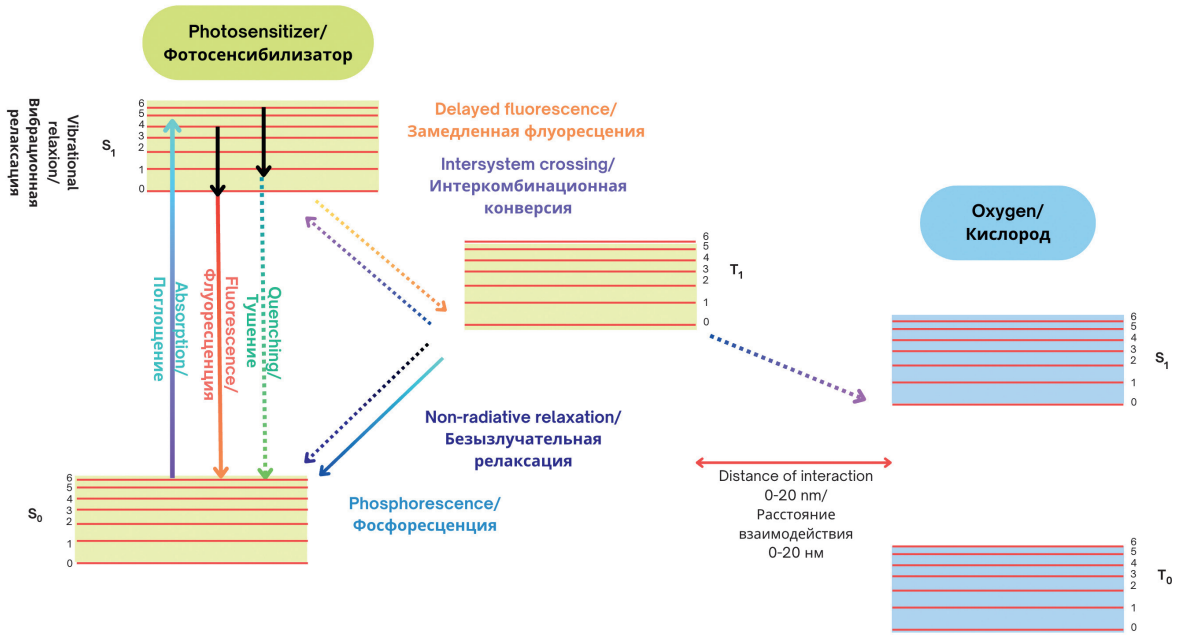

Рис. 1. Схема образования возбужденного (синглетного) состояния кислорода в процессе ФДТ.
Fig. 1. Scheme of formation of the excited (singlet) oxygen state in the PDT process.

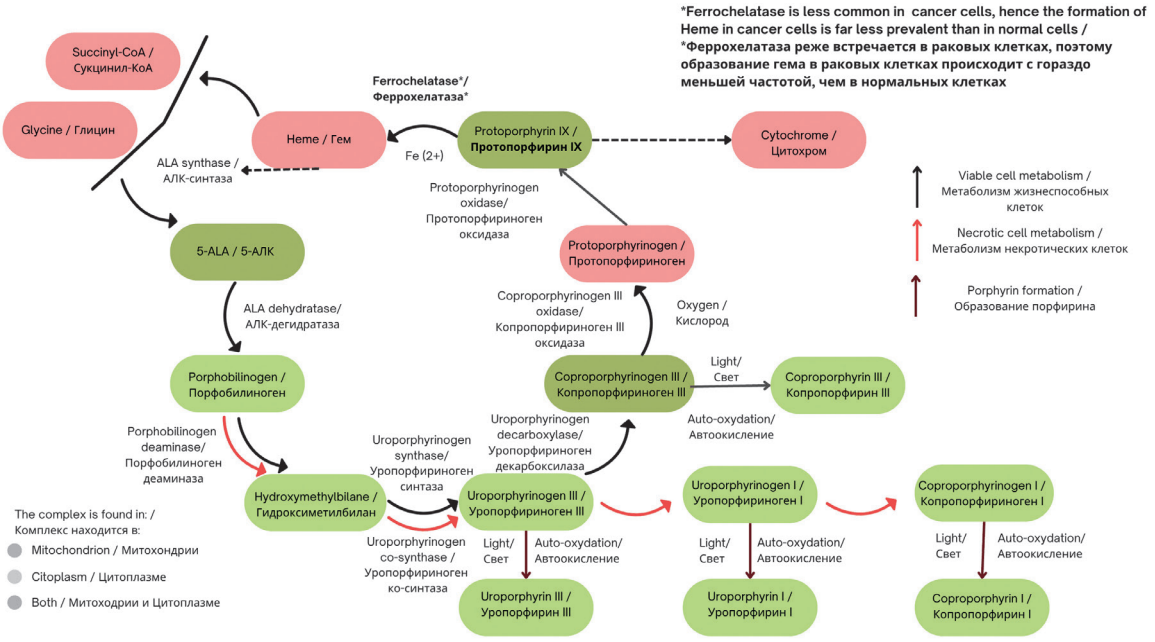

Рис. 2. Схема метаболических путей 5-АЛК в нормальных, раковых и некротических клетках.
Fig. 2. Scheme of metabolic pathways in normal, cancerous and necrotic cells.

be attributed to the requirement of molecular oxygen for the conversion of coproporphyrinogen III to PpIX. It can be hypothesized that premature irradiation limits the access of molecular oxygen to coproporphyrinogen III, since it leads to the activation of molecular oxygen to its singlet state, which, in turn, prevents the formation of PpIX.

Therefore, two competing mechanisms can be identified: one that reduces photodynamic activity and the other one that increases it. The isolation of the spectra of the products of natural metabolism of 5-ALA and its photochemical transformation *in vivo* is a methodologically complex process. This complexity arises from the substantial overlap between the absorption and fluorescence spectra of these compounds. The current state of technical capabilities precludes the simultaneous excitation of several wavelengths corresponding to the absorption of various porphyrin derivatives of 5-ALA, as well as the effective separation of the recorded spectra.

In order to solve this problem, it is necessary to have precise knowledge of the absorption and fluorescence spectra of the porphyrins under study in the biological tissues under study. In this case, the focus is on porphyrins such as uroporphyrin I, uroporphyrin III, coproporphyrin I, coproporphyrin III and PpIX. However, the spectra of these fluorophores are most often reported for acidic, alkaline, or other media that do not correspond to the physiological conditions of the human body. Fig. 3–4 illustrate the absorption and fluorescence spectra of uroporphyrins I and III, coproporphyrin I, and PpIX in various media [2, 3].

Table 1 shows the characteristic fluorescence and absorption maxima of coproporphyrin I, uroporphyrin I, uroporphyrin III and PpIX [2, 3].

Таблица 1.
Сравнительная таблица пиков флуоресценции и поглощения копропорфирина I, уропорфирина I, уропорфирина III и ПпIX [2,3]

Table 1.
Comparative table of fluorescence and absorption peaks of coproporphyrin I, uroporphyrin I, uroporphyrin III and PpX [2,3]

Porphyrin Порфирин	Максимум поглощения, нм Absorption maximum, nm					Максимум флуоресценции, нм Fluorescence maximum, nm		
	1	2	3	4	5	1	2	3
КП I CP I	375	389	503	537	559	609	614	677
УП I UP I	406	552	592	-	-	-	-	-
УП III UP III	398	502	538	560	612	-	618	681
Пп IX Pp IX	408	506	542	577	631	-	633	722

КП I – копропорфирин I, УП I – уропорфирин I, УП III – уропорфирин III, ПпIX – протопорфирин IX
CP I – coproporphyrin I, UP I – uroporphyrin I, UP III – uroporphyrin III, Pp IX – protoporphyrin IX

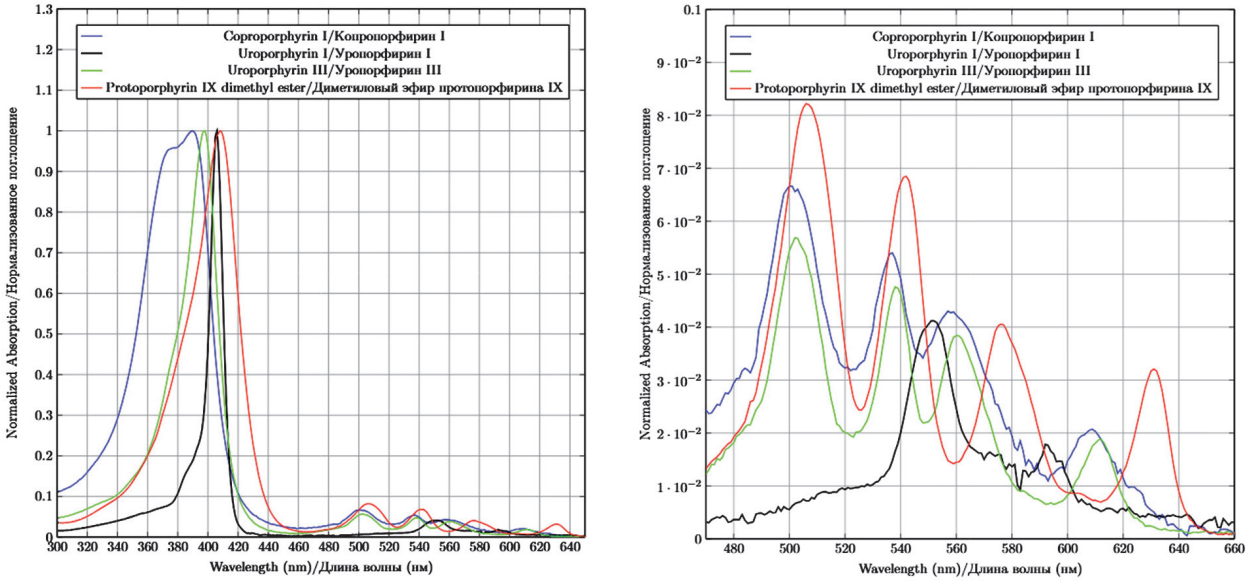

Рис. 3. Спектры поглощения 5-АЛК-индуцированных порфиринов: раствора КП I в 0,1 М калийно-фосфатного буфера, раствора УП I в 1,0 М растворе соляной кислоты, раствора УП III в 0,1 М растворе калийно-фосфатного буфера и раствора ПпIX диметил эстера в хлороформе [2, 3].
Fig. 3. Absorption spectra of 5-ALA-induced porphyrins: a solution of coproporphyrin I in 0.1 M potassium phosphate buffer, a solution of uroporphyrin I in 1.0 M hydrochloric acid, a solution of uroporphyrin III in 0.1 M potassium phosphate buffer, and a solution of PpIX dimethyl ester in chloroform [2, 3].

The purpose of this study is to characterize the absorption and fluorescence spectra of 5-ALA-induced porphyrins for subsequent use in spectral separation. In addition, to investigate the formation of PpIX photoproducts - chemical compounds formed as a result of photochemical reactions during PDT.

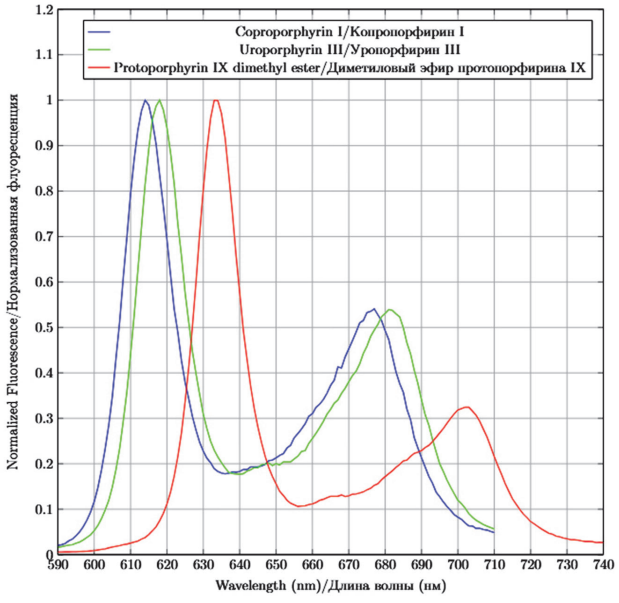

Рис. 4. Спектры флуоресценции 5-АЛК индуцированных порфиринов: раствора КП I в 0,1 М калийно-фосфатного буфера, раствора УП III в 0,1 М калийно-фосфатного буфера и раствора ПпIX диметил эстера в растворе метанола [2, 3].
Fig. 4. Fluorescence spectra of 5-ALA-induced porphyrins: a solution of coproporphyrin I in 0.1 M potassium phosphate buffer, a solution of uroporphyrin III in 0.1 M potassium phosphate buffer, and a solution of PpIX dimethyl ester in methanol solution [2, 3].

Differences in the fluorescence lifetime of uroporphyrin I, coproporphyrin III, PpIX and its photoproducts open up the possibility of differentiating the metabolic pathways of 5-ALA. From a practical point of view, this is especially important, since such differentiation of spectra can allow the presence of necrotic tissue in the irradiated area to be detected even before the start of PDT.

Monitoring of PpIX concentration and its photobleaching in different parts of the irradiated tissue is of greatest interest, as it can help to detect initiated processes of necrotic or apoptotic cell death. If in certain parts of the tissue the concentration of PpIX is lower than in the actively proliferating part of the tumor, and the fluorescence intensity does not decrease after irradiation, it may indicate partial necrotization of the tissue or lack of oxygen access caused by stenosis or obstruction of blood vessels.

Materials and methods

Patients

This study included two clinical cases of benign skin tumors – dermatofibroma and congenital melanocytic nevus. Both patients underwent spectral fluorescence diagnostics to assess the accumulation of 5-ALA-induced porphyrins before and after PDT. The dynamics of accumulation and the intensity of photobleaching of PpIX in different tissue layers were also studied. The main parameters of the patients involved in the study are presented in Table 2.

Fig. 5 shows images of patients' tumors with indication of the areas where spectral fluorescence diagnostics was performed.

Таблица 2
Основные параметры пациентов
Table 2
Main parameters of patients

Параметр Parameter	Пациент 1 Patient 1	Пациент 2 Patient 2
Диагноз Diagnosis	Дерматофиброма Dermatofibroma	Врожденный меланоцитарный невус Congenital melanocytic nevus
Пол Gender	женский female	женский female
Возраст Age	56 лет 56 years	35 лет 35 years

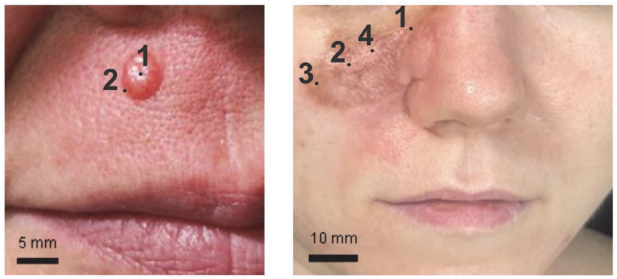

a b

Рис. 5. Опухоли с указанием зон, где проводили флуоресцентные исследования: a – пациент с дерматофибромой (зона 1 – центральная область опухоли; зона 2 – периферия опухоли); b – пациент с врожденным меланоцитарным невусом (зоны 1–3 – области с повышенным содержанием меланоцитов; зона 4 – область свободная от меланоцитов).
Fig. 5. Tumors with indication of the zones where fluorescence studies were performed: a – patient with dermatofibroma (zone 1 – central area of the tumor; zone 2 – tumor periphery); b – patient with congenital melanocytic nevus (zones 1–3 – areas with increased content of melanocytes; zone 4 – area free of melanocytes).

The study included several stages, one of them being spectral-fluorescent studies of the accumulation and photobleaching of PpIX (Fig. 6).

For 24 h after the administration of 5-ALA, patients strictly observed the light regime (excluding exposure to direct sunlight, watching television programs, etc.). All procedures were carried out in accordance with the recommendations of the Helsinki Declaration of the World Medical Association.

Photosensitizer

A 20% aqueous solution of 5-ALA prepared immediately before use was utilized for the spectral-fluorescent study. The administration was carried out by the application method: a sterile gauze napkin was soaked in the solution and applied to the area of the pathological focus. Before applying the preparation, the skin was cleaned with distilled water.

To prevent evaporation of the 5-ALA solution and improve its penetration, the treated area was covered with cling film. During the entire observation period of 5-ALA-induced PpIX accumulation (up to 4 h), the patient was in a darkened room to minimize exposure to external light.

Spectral fluorescence diagnostics

Laser electron-spectral unit LESA-01-BIOSPEC (BIOSPEC Ltd., Moscow) was used for spectral-fluorescence study. Tissue fluorescence was excited by laser irradiation with wavelengths of 405 and 632.8 nm. Excitation with wavelength in blue and red spectral bands was performed in order to study the distribution of PpIX in superficial and deeper tissue layers [4]. When the fluorescence was excited at 405 nm wavelength, the spectral signal was recorded in the range of 350-800 nm. While excited at 632.8 nm wavelength, the spectral signal was recorded in the range of 600-750 nm, respectively. Both bands included diffusely scattered laser emission signal and tissue fluorescence in the red region of the spectrum.

Spectral fluorescence imaging of normal skin and neoplasm skin was performed before PS injection to determine endogenous tissue fluorescence. The cheek skin was chosen as a reference in measurements. Tissue fluorescence spectra were also recorded 1, 2, 3, and 4 hours after 5-ALA application, before the start of PDT. Spectral fluorescence imaging was performed again after PDT.

Photodynamic therapy

Both continuous and pulsed irradiation modes were used for PDT. The laser LFT-02-BIOSPEC (BIOSPEC Ltd., Moscow) with a 635 nm wavelength and the maximum output power of 1.5 W was used in continuous irradiation mode. Laser radiation delivery was carried out through a quartz optical fiber with a polymer shell with a total

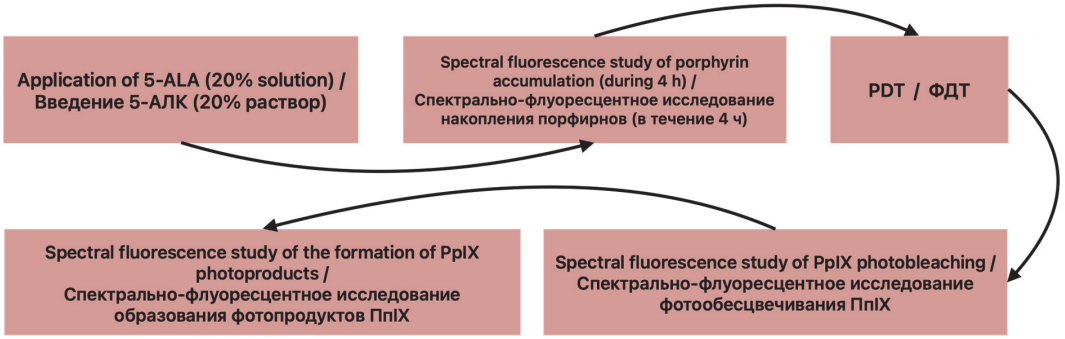

Рис. 6. Общая схема проведения исследования.
Fig. 6. General scheme of the study.

diameter of 600 μm. Output power of laser emission was varied in the range of 400-1200 mW.

Skin neoplasms were continuously irradiated with a wavelength 635 nm and a power density of 380-440 mW/cm^2. The energy dose was 95-100 J/cm^2. Laser irradiation was stopped when the pain effect increased. A significant increase in pain symptoms exceeding the pain threshold was recorded 10-20 sec after the beginning of continuous irradiation. After this, laser irradiation in pulse mode was performed. Pulsed irradiation of pathologic tissues with PpIX accumulation contributes to the pain reduction of patients in the light exposure area [5]. To minimize the impact on the surrounding healthy tissues, a medical dressing with a 10 mm hole diameter was applied to the pathological tissues area before pulse irradiation. A pulse system based on a ring xenon gas discharge lamp (BIOSPEC Ltd., Moscow) was used for pulsed PDT treatment. Patients received 10-12 pulses sequentially with an average energy density of 1 J/cm^2 and a total energy dose of 10-12 J/cm^2. Applying the pulse mode allowed to reduce pain in patients during PDT of tissues with PpIX accumulation.

Results and discussion

The spectral fluorescence study was performed with fluorescence excitation at wavelengths of 405 and 632.8 nm. This approach allowed the diagnosis of both superficial and deeper tissue layers [6]. Fig. 7 shows the spectral data of PpIX accumulation under fluorescence excitation at wavelengths λ_{exc} = 405 nm and λ_{exc} = 632.8 nm. The recorded data include diffusely scattered laser irradiation and fluorescence of tissue from a patient with a dermatofibroma: central region and tumor periphery.

When fluorescence was excited at λ_{exc} = 405 nm, two intense peaks were recorded at 625-670 nm and 700-740 nm. A fluorescence peak in the 690-740 nm wavelength region was observed by irradiation at λ_{exc} = 632.8 nm. Fig. 8 shows the integral fluorescence intensities distribution in the indicated spectral ranges.

The results show that during the 4-hour observation period after the application of 5-ALA, an increase in the accumulation of PpIX was observed both in the superficial (Fig. 8a, b) and in the deeper (Fig. 8c) tissue layers. PDT was performed in the zones of PpIX accumulation. After PDT, a new fluorescence peak was registered in the wavelength range of 670-700 nm under laser excitation at a wavelength of 405 nm (Fig. 9).

Earlier in [7] it was shown that laser irradiation with a wavelength of 635 nm and an energy dose of 43 J/cm^2 of human adenocarcinoma cells leads to the formation of photodynamically active PpIX photoproducts. These photoproducts that fluoresce with a minor short-wavelength shift, are characterized as a mixture of chlorin-type photoproducts [7]. The main photoproduct in the mixture is photoprotoporphyrin: two chlorin-type hydroxyaldehyde isomers that exhibit fluorescence in the wavelength range of 670-690 nm.

Chlorin-type photoproducts differ from PpIX by the presence of an absorption band in the 450 nm region and an intense fluorescence peak in the 650-700 nm wavelength range. The property of PpIX photoproducts

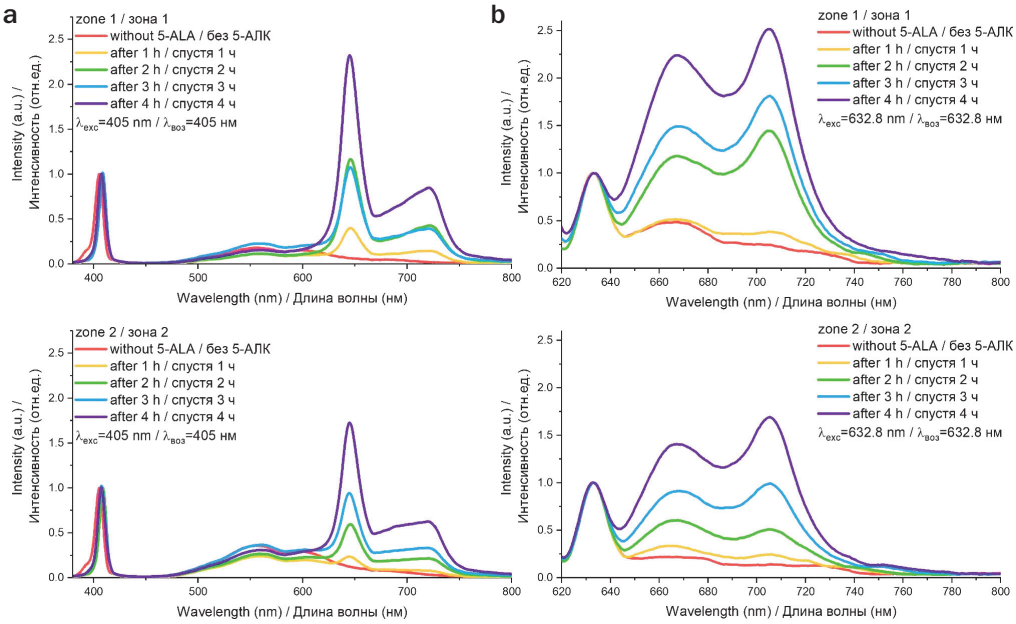

Рис. 7. Спектральные данные, включающие диффузно рассеянное лазерное излучение и флуоресценцию в центральной области (зона 1) и периферии (зона 2) дерматофибромы в различные временные точки после введения 5-АЛК: (a) при $\lambda_{воз}$=405 нм; (b) при $\lambda_{воз}$=632,8 нм. Спектры нормированы на максимальное значение интенсивности диффузно рассеянного лазерного излучения.
Fig. 7. Spectral data including diffusely scattered laser radiation and fluorescence in the central area (zone 1) and periphery (zone 2) of dermatofibroma at different time points after 5-ALA administration: (a) at λ_{exc}=405 nm; (b) at λ_{exc}=632.8 nm. The spectra were normalized to the maximum intensity of diffusely scattered laser radiation.

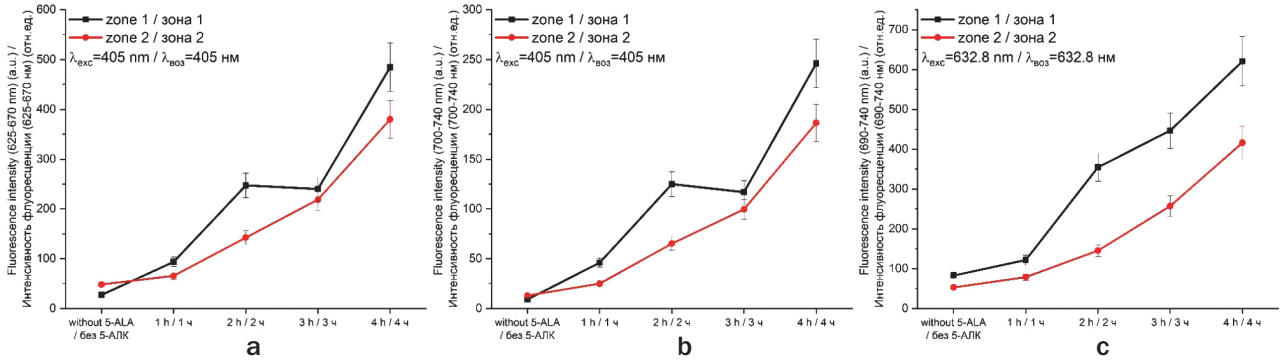

Рис. 8. Распределение интегральных интенсивностей флуоресценции в центральной области (зона 1) и периферии (зона 2) дерматофибромы: a – в диапазоне 625-670 нм; b – в диапазоне 700-740 нм; c – в диапазоне 690-740 нм.
Fig. 8. Distribution of integrated fluorescence intensities in the central region (zone 1) and periphery (zone 2) of dermatofibroma: a – in the range of 625-670 nm; b – in the range of 700-740 nm; c – in the range of 690-740 nm.

is sometimes used to improve the efficiency and contrast of 5-ALA fluorescence navigation [8]. Exposure to 635 nm laser excitation leads to a decrease in the PpIX fluorescence intensity and is followed by the formation of a new fluorescence peak at 675 nm [8].

An increase in tissue fluorescence intensity in the 670-700 nm wavelength range was also recorded in both central and peripheral regions of dermatofibroma, indicating the presence of chlorin-type photoproducts in tissue after PDT. PpIX photoproducts have photodynamic activity and can be used in 5-ALA-PDT. The quantum yield of singlet oxygen of photoprotoporphyrin is 0.69 [9].

To evaluate the contribution of photoproduct fluorescence to the recorded signal, the photoprotoporphyrin fluorescence index was calculated as the ratio of the integral fluorescence intensities in the 670-700 nm wavelength range to the integral intensity in the 625-670 nm wavelength range (Fig. 10).

Currently, scattered data are available on the dynamics of 5-ALA-induced PpIX accumulation. The maximal accumulation time of PpIX may vary depending on the route of administration of 5-ALA as well as the tumor type. The most common 5-ALA-PDT of skin tumors is performed by topical (local) drug administration in the form of gel or aqueous solution. This route of administration demonstrates a more rapid PpIX accumulation in tissues compared to oral and inhalation administration of 5-ALA [10]. The PpIX maximum accumulation in skin tumors is observed by 3.5-6

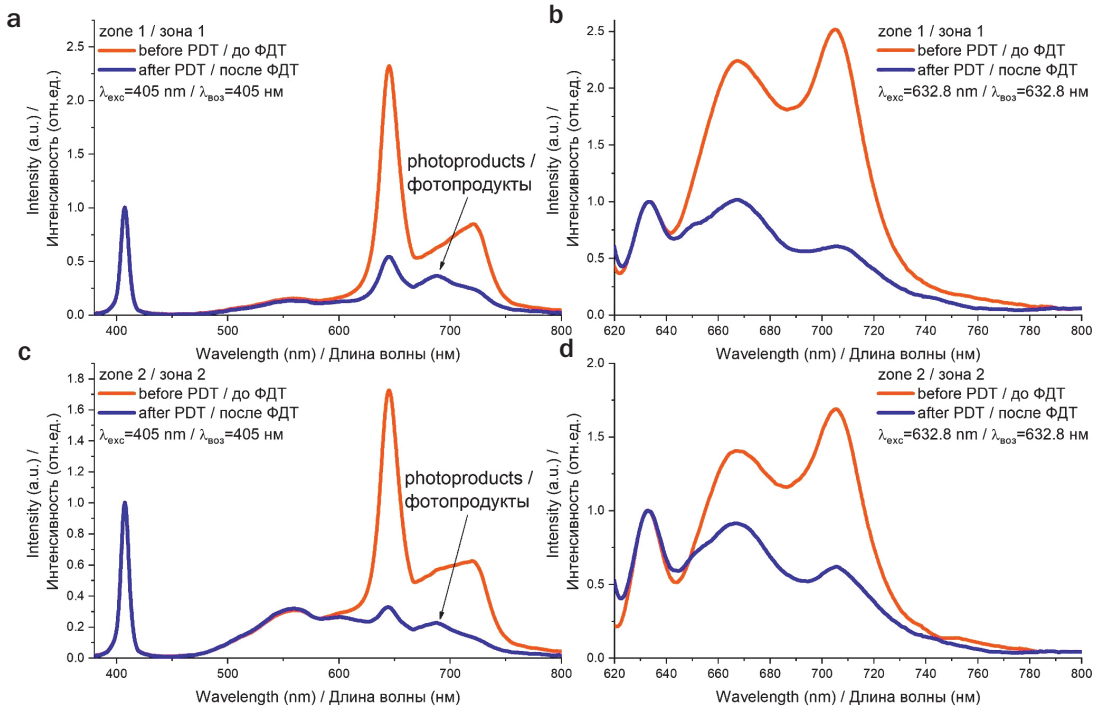

Рис. 9. Результаты спектрально-флуоресцентной диагностики в центральной области (зона 1) и периферии (зона 2) дерматофибромы: a – до ФДТ (спустя 4 ч после введения 5-АЛК); b – после ФДТ.
Fig. 9. Results of spectral fluorescence diagnostics in the central area (zone 1) and periphery (zone 2) of dermatofibroma: a – before PDT (4 hours after 5-ALA administration); b – after PDT.

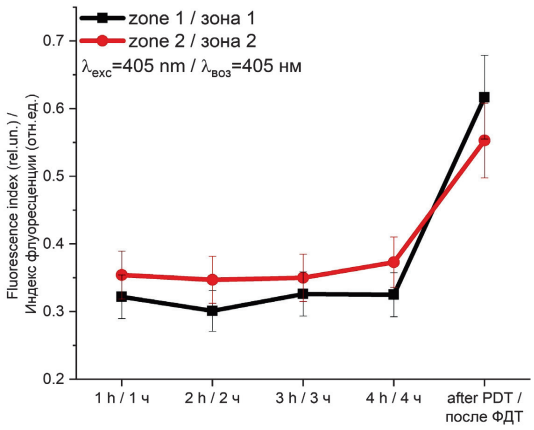

Рис. 10. Изменение флуоресценции фотопродуктов хлоринового типа в процессе накопления 5-АЛК-индуцированного ПпIX и после проведения ФДТ дерматофибромы (λ=635 нм, плотность мощности 380 мВт/см^2, доза энергии 100 Дж/см^2).
Fig. 10. Changes in the fluorescence of chlorin-type photoproducts during the accumulation of 5-ALA-induced PpIX and after PDT (λ=635 nm, power density 380 mW/cm^2, energy dose 100 J/cm^2).

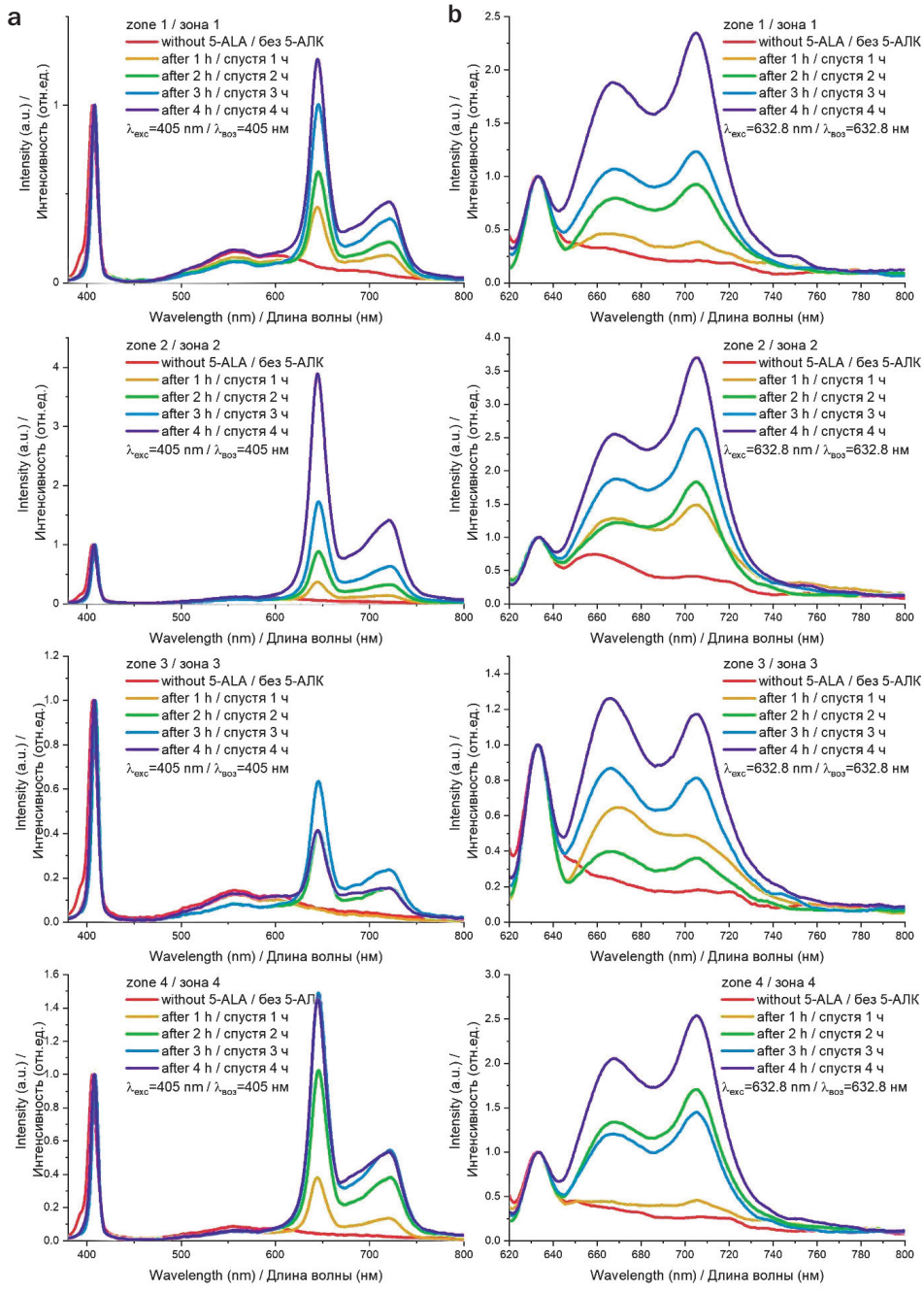

Рис. 11. Спектральные данные, включающие диффузно рассеянное лазерное излучение и флуоресценцию тканей меланоцитарного невуса в зонах с повышенным содержанием меланоцитов (зоны 1-3) и в зоне, относительно свободной от меланоцитов (зона 4): a – при $\lambda_{воз}$=405 нм; b – при $\lambda_{воз}$=632,8 нм. Спектры нормированы на максимальное значение интенсивности диффузно рассеянного лазерного излучения.
Fig. 11. Spectral data including diffusely scattered laser radiation and fluorescence of melanocytic nevus tissues in areas with an increased content of melanocytes (zones 1-3) and in an area relatively free of melanocytes (zone 4): a – at λ=405 nm; b – at λ=632.8 nm.

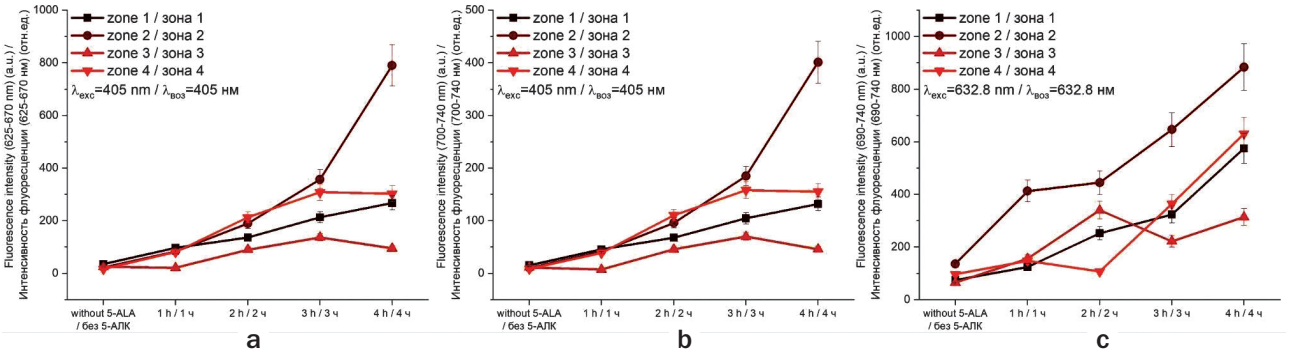

Рис. 12. Распределение интегральных интенсивностей флуоресценции тканей меланоцитарного невуса в зонах с повышенным содержанием меланоцитов (зоны 1-3) и в зоне, относительно свободной от меланоцитов (зона 4): a – в диапазоне 625-670 нм; b – в диапазоне 700-740 нм; c – в диапазоне 690-740 нм.

Fig. 12. Distribution of integrated fluorescence intensities of melanocytic nevus tissues in areas with an increased content of melanocytes (zones 1-3) and in an area relatively free of melanocytes (zone 4): a – in the range of 625-670 nm; b – in the range of 700-740 nm; c – in the range of 690-740 nm.

h after application of 5-ALA [11]. For example, in squamous cell cancer with local injection of a 20% solution of 5-ALA, peak accumulation was recorded after 4 h, whereas in basal cell cancer it was recorded 6 h after administration [11].

In case of the patient with congenital melanocytic nevus, intensive PpIX accumulation was registered as early as 1 h after 5-ALA application, both in the areas with increased melanocyte content (zones 1-3) and in the area relatively free of melanocytes (zone 4) (Fig. 11).

The spectra were normalized to the maximum value of the intensity of diffusely scattered laser radiation.

As in the case of the dermatofibroma patient, two intense peaks were recorded at λ_{exc} = 405 nm in the wavelength range of 625-670 nm and 700-740 nm. A

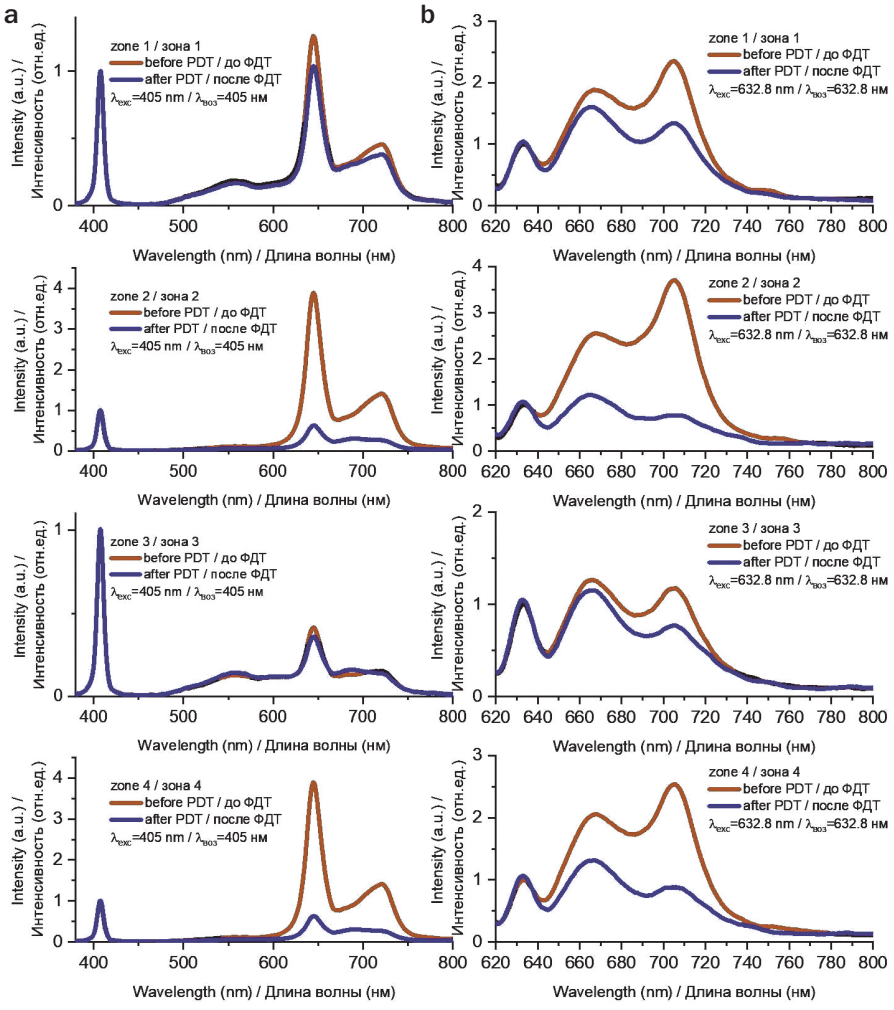

Рис. 13. Результаты спектрально-флуоресцентной диагностики меланоцитарного невуса в зонах с повышенным содержанием меланоцитов (зоны 1-3) и в зоне, относительно свободной от меланоцитов (зона 4): a – до ФДТ (спустя 4 ч после введения 5-АЛК); b – после ФДТ.

Fig. 13. Results of spectral fluorescence diagnostics of melanocytic nevus in areas with an increased content of melanocytes (zones 1-3) and in an area relatively free of melanocytes (zone 4): a – before PDT (4 h after 5-ALA administration); b – after PDT.

fluorescence peak in the region of 690-740 nm was observed at λ_{exc} = 632.8 nm. Fig. 12 shows the distribution of integrated fluorescence intensities in the indicated ranges.

In comparison to dermatofibroma tissues, the results showed that in the superficial tissue layers (at λ_{exc} = 405 nm) of the investigated zones 3 and 4, the PpIX maximum accumulation was observed 3 h after 5-ALA application (Fig. 12a,b). The 5-ALA-induced PpIX accumulation continued to increase 4 h after injection (Fig. 12c) in deeper tissue layers (at λ_{exc}=632,8 nm). PDT was performed in all areas. Photobleaching of PpIX was observed in both superficial and deeper tissue layers as a result (Fig.13).

Photoprotoporphyrin formation was observed in all investigated areas of melanocytic nevus after PDT (Fig. 14). There was no correlation between the intensity of photoprotoporphyrin formation and the intensity of PpIX accumulation (Fig. 12, 14).

PpIX photoproducts are of great interest and offer new opportunities for high-contrast fluorescence imaging using 5-ALA [8]. PpIX photoproducts can easily move in the intracellular space due to their greater water solubility compared to PpIX [12], and be less sensitive to the singlet oxygen generated by PpIX [13]. Despite the lower singlet oxygen generation efficiency compared to PpiX, PpIX photoproducts can potentially be used for PDT [7, 14]. In summary, PpIX photoproducts can expand the fluorescence diagnostic capabilities and improve the efficiency of PDT, which requires further research for their practical application.

Conclusion

The dynamics of PpIX accumulation in superficial and deep dermatofibroma layers and congenital melanocytic nevus with fluorescence excitation at wavelengths 405 and 632.8 nm with administration of a 20% 5-ALA solution was studied. PpIX accumulation in dermatofibroma tissues continued to increase during 4 h of observation in both superficial and deep tissue layers, in the central and the peripheral regions of the tumor. In comparison to melanocytic nevus tissues, maximum PpIX accumulation in superficial layers was reached after 3 h, while in deep layers an increase in PpIX accumulation within 4 h was observed. It is found that in the process of tumor PDT by laser excitation with a 635 nm wavelength, chlorin-type photoproducts characterized by intense fluorescence in the range of 670-700 nm are formed.

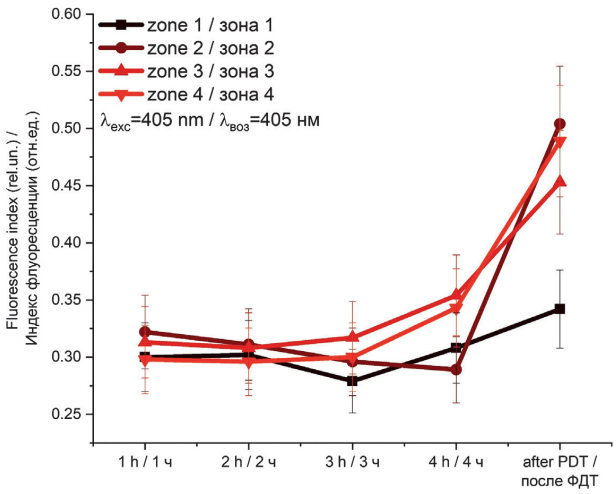

Рис. 14. Изменение флуоресценции фотопродуктов хлоринового типа в процессе накопления 5-АЛК-индуцированного ПпIX и после проведения ФДТ меланоцитарного невуса (λ=635 нм, плотность мощности 380 мВт/см², доза энергии 100 Дж/см²).

Fig. 14. Changes in fluorescence of chlorin-type photoproducts during the accumulation of 5-ALA-induced PpIX and after PDT of melanocytic nevus (λ=635 nm, power density 380 mW/cm², energy dose 100 J/cm²).

REFERENCES

1. Beika M., Harada Y., Minamikawa T., Yamaoka Y., Koizumi N., Murayama Y., Konishi H., Shiozaki A., Fujiwara H., Otsuji E., Takamatsu T. and Tanaka H. Accumulation of Uroporphyrin I in Necrotic Tissues of Squamous Cell Carcinoma after Administration of 5-Aminolevulinic Acid. *International Journal of Molecular Sciences*, 2021, Vol. 22(18), pp. 10121. https://doi.org/10.3390/ijms221810121
2. Du H., Amy Fuh R., Li J., Corkan L.A. and S. Lindsey J. PhotochemCAD: A computer-aided design and research tool in photochemistry. *Photochemistry and Photobiology*, 1998, Vol. 68, pp.141-142. https://doi.org/10.1111/j.1751-1097.1998.tb02480.x
3. Dixon J. M., Taniguchi M. and S. Lindsey J. PhotochemCAD 2. A refined program with accompanying spectral databases for photochemical calculations. *Photochemistry and Photobiology*, 2004, Vol. 81, pp. 212-213. https://doi.org/10.1111/j.1751-1097.2005.tb01544.x
4. Khilov, Aleksandr Vladimirovich, et al. "Analytical model of fluorescence intensity for the estimation of fluorophore localisation in biotissue with dual-wavelength fluorescence imaging." *Quantum Electronics,* 2021, Vol. 51(2), pp. 95. DOI 10.1070/QEL17503

ЛИТЕРАТУРА

1. Beika M., Harada Y., Minamikawa T., Yamaoka Y., Koizumi N., Murayama Y., Konishi H., Shiozaki A., Fujiwara H., Otsuji E., Takamatsu T. and Tanaka H. Accumulation of Uroporphyrin I in Necrotic Tissues of Squamous Cell Carcinoma after Administration of 5-Aminolevulinic Acid // International Journal of Molecular Sciences. – 2021. – Vol. 22(18).– P. 10121. https://doi.org/10.3390/ijms221810121
2. Du H., Amy Fuh R., Li J., Corkan L.A. and S. Lindsey J. PhotochemCAD: A computer-aided design and research tool in photochemistry // Photochemistry and Photobiology. – 1998. – Vol. 68. – P.141-142. https://doi.org/10.1111/j.1751-1097.1998.tb02480.x
3. Dixon J. M., Taniguchi M. and S. Lindsey J. PhotochemCAD 2. A refined program with accompanying spectral databases for photochemical calculations // Photochemistry and Photobiology. – 2004. – Vol. 81. – P.212-213. https://doi.org/10.1111/j.1751-1097.2005.tb01544.x
4. Khilov, Aleksandr Vladimirovich, et al. "Analytical model of fluorescence intensity for the estimation of fluorophore localisation in biotissue with dual-wavelength fluorescence imaging." // Quantum Electronics. – 2021. – Vol. 51(2). – P. 95. DOI 10.1070/QEL17503

5. Efendiev K., Alekseeva P.M., Bikmukhametova I.R., Piterskova L.S., Orudzhova K.F., Agabekova U.D., Slovokhodov E.K. and Loschenov V.B. Comparative investigation of 5-aminolevulinic acid and hexyl aminolevulinate-mediated photodynamic diagnostics and therapy of cervical dysplasia and vulvar leukoplakia. *Laser Physics Letters*, 2021, Vol. 18(6), pp. 065601. DOI 10.1088/1612-202X/abf5cf
6. Kirillin, M., Khilov, A., Kurakina, D., Orlova, A., Perekatova, V., Shishkova, V., ... & Sergeeva, E. (2021). Dual-wavelength fluorescence monitoring of photodynamic therapy: from analytical models to clinical studies. *Cancers*, 13(22), pp. 5807. https://doi.org/10.3390/cancers13225807
7. Bagdonas S., Ma L.W., Iani V., Rotomskis R., Juzenas P. and Moan J. Phototransformations of 5-Aminolevulinic Acid–induced Protoporphyrin IX in vitro: A Spectroscopic Study. *Photochemistry and photobiology*, 2000, Vol. 72(2), pp. 186-192. https://doi.org/10.1562/0031-8655(2000)0720186POAAIP2.0.CO2
8. Ogbonna Sochi J., Y. York W.B., Nishimura T., Hazama H., Fukuhara H., Inoue K. and Awazu K. Increased fluorescence observation intensity during the photodynamic diagnosis of deeply located tumors by fluorescence photoswitching of protoporphyrin IX. *Journal of Biomedical Optics*, 2023, pp. 055001-055001. https://doi.org/10.1117/1. JBO.28.5.055001
9. Sidney Cox G., Bobillier C. and G. Whitten D. Photooxydation and singlet oxygen sensitization by protoporphyrin IX and its photooxydation products. *Photochemistry and Photobiology*, 1982, Vol. 36, pp. 401-407. https://doi.org/10.1111/j.1751-1097.1982.tb04393.x
10. Rick K., Sroka R., Stepp H., Kriegmair M.,. Huber R.M, Jacob K. and Baumgartner R. Phototransformations of 5-Aminolevulinic Pharmacokinetics of Saminolevulinic acid-induced protoporphyrin IX in skin and blood. *Journal of Photochemistry and Photobiology: Biology*, 1997, Vol. 40, pp. 313-319. https://doi.org/10.1016/S1011-1344(97)00076-6
11. Fritsch C., Lehmann P., Stahl W., Schulte K.W., Blohm E., Lang K., Sies H. and Ruzicka T. Optimum porphyrin accumulation in epithelial skin tumours and psoriatic lesions after topical application of δ-aminolaevulinic acid. *British Journal of Cancer*, 1999, Vol. 79, pp. 1603-1608. https://doi.org/10.1038/sj.bjc.6690255
12. Brault D., Aveline B., Delgado O. and Vever-Bizet Ch. Chlorin-type photosensitizers derived from vinyl porphyrins. *Photochemistry and Photobiology*, 2001, Vol. 73(4), pp. 331-338. https://doi.org/10.1117/12.199160
13. Robinson D. J., de Brujin H. S., van der Veen N., Stringer M. R., Brown S. B. and Star W. M. Fluorescence photobleaching of ALA-induced PpIX during photodynamic therapy of normal hairless mouse skin: the effect of light dose and irradiance and the resulting biological effect. *Photochemistry and Photobiology*, 1998, Vol. 67, pp. 140-149. https://doi.org/10.1111/j.1751-1097.1998.tb05177.x
14. Ogbonna, Sochi J., Katsuyoshi Masuda, and Hisanao Hazama. "The effect of fluence rate and wavelength on the formation of protoporphyrin IX photoproducts. *"Photochemical & Photobiological Sciences*, 2024, Vol. 23(9), pp.1627-1639. https://doi.org/10.1007/s43630-024-00611-9

5. Efendiev K., Alekseeva P.M., Bikmukhametova I.R., Piterskova L.S., Orudzhova K.F., Agabekova U.D., Slovokhodov E.K. and Loschenov V.B. Comparative investigation of 5-aminolevulinic acid and hexyl aminolevulinate-mediated photodynamic diagnostics and therapy of cervical dysplasia and vulvar leukoplakia // Laser Physics Letters. – 2021. – Vol. 18(6) . – P. 065601. DOI 10.1088/1612-202X/abf5cf
6. Kirillin, M., Khilov, A., Kurakina, D., Orlova, A., Perekatova, V., Shishkova, V., ... & Sergeeva, E. (2021). Dual-wavelength fluorescence monitoring of photodynamic therapy: from analytical models to clinical studies // Cancers. – 13(22). – P. 5807. https://doi.org/10.3390/cancers13225807
7. Bagdonas S., Ma L.W., Iani V., Rotomskis R., Juzenas P. and Moan J. Phototransformations of 5-Aminolevulinic Acid–induced Protoporphyrin IX in vitro: A Spectroscopic Study // Photochemistry and photobiology. – 2000. – Vol. 72(2). – P. 186-192. https://doi.org/10.1562/0031-8655(2000)0720186POAAIP2.0.CO2
8. Ogbonna Sochi J., Y. York W.B., Nishimura T., Hazama H., Fukuhara H., Inoue K. and Awazu K. Increased fluorescence observation intensity during the photodynamic diagnosis of deeply located tumors by fluorescence photoswitching of protoporphyrin IX // Journal of Biomedical Optics. – 2023. – P. 055001-055001. https://doi.org/10.1117/1.JBO.28.5.055001
9. Sidney Cox G., Bobillier C. and G. Whitten D. Photooxydation and singlet oxygen sensitization by protoporphyrin IX and its photooxydation products // Photochemistry and Photobiology. – 1982. – Vol. 36. – P. 401-407. https://doi.org/10.1111/j.1751-1097.1982.tb04393.x
10. Rick K., Sroka R., Stepp H., Kriegmair M.,. Huber R.M, Jacob K. and Baumgartner R. Phototransformations of 5-Aminolevulinic Pharmacokinetics of Saminolevulinic acid-induced protoporphyrin IX in skin and blood // Journal of Photochemistry and Photobiology: Biology. – 1997. – Vol. 40. – P. 313-319. https://doi.org/10.1016/S1011-1344(97)00076-6
11. Fritsch C., Lehmann P., Stahl W., Schulte K.W., Blohm E., Lang K., Sies H. and Ruzicka T. Optimum porphyrin accumulation in epithelial skin tumours and psoriatic lesions after topical application of δ-aminolaevulinic acid // British Journal of Cancer. – 1999. – Vol. 79. – P. 1603-1608. https://doi.org/10.1038/sj.bjc.6690255
12. Brault D., Aveline B., Delgado O. and Vever-Bizet Ch. Chlorin-type photosensitizers derived from vinyl porphyrins // Photochemistry and Photobiology. – 2001. – Vol. 73(4) . – P. 331-338. https://doi.org/10.1117/12.199160
13. Robinson D. J., de Brujin H. S., van der Veen N., Stringer M. R., Brown S. B. and Star W. M. Fluorescence photobleaching of ALA-induced PpIX during photodynamic therapy of normal hairless mouse skin: the effect of light dose and irradiance and the resulting biological effect // Photochemistry and Photobiology. – 1998. – Vol. 67. – P. 140-149. https://doi.org/10.1111/j.1751-1097.1998.tb05177.x
14. Ogbonna, Sochi J., Katsuyoshi Masuda, and Hisanao Hazama. "The effect of fluence rate and wavelength on the formation of protoporphyrin IX photoproducts. // "Photochemical & Photobiological Sciences. – 2024. – Vol. 23.9 – P.1627-1639. https://doi.org/10.1007/s43630-024-00611-9

MODERN METHODS OF INTRAOPERATIVE FLUORESCENT IMAGING OF THE PARATHYROID GLANDS IN ENDOCRINE SURGERY: A LITERARY REVIEW

Zinchenko S.V.[1], Shanazarov N.A.[2], Muratov N.F.[1], Kisikova S.D.[2], Seitbekova K.S.[2], Galiev I.Z.[2], Ibragim M.I.[3], Ahmetshin R.R.[1]
[1]Kazan (Volga Region) Federal University, Kazan, Russia
[2]Medical Centre Hospital of the President's Affairs Administration of the Republic of Kazakhstan RSE, Astana, the Republic of Kazakhstan
[3]MC "Aya" Astana, the Republic of Kazakhstan

Abstract

Hyperparathyroidism (primary, secondary and tertiary) is a common endocrine disease, often occurring with pronounced symptoms, in most cases caused by adenoma (rarely several adenomas) in primary hyperparathyroidism (pHPT) and chronic renal failure in patients on programmed hemodialysis with secondary (sHPT) and tertiary (tHPT) hyperparathyroidism. To date, the only radical treatment for hyperparathyroidism (HPT) is surgical removal of pathologically altered parathyroid glands. In this regard, there is a need to improve diagnostic search algorithms, including intraoperative ones, for altered parathyroid glands. The main objective of the review is to study current trends and techniques of intraoperative imaging of the parathyroid glands, compare these methods and evaluate their effectiveness. The use of qualitatively new technologies for the topical diagnosis of altered parathyroid glands, such as identification by autofluorescence in the near infrared spectrum (NIRAF), the technique of using indocyanine green (ICG) and 5-aminolevulinic acid under UV radiation, make it possible to visualize the localization of the parathyroid glands with more than 90% accuracy. However, the issue of their priority use remains open and unresolved.

Key words: primary, secondary, tertiary hyperparathyroidism, parathyroid gland, imaging, surgical treatment, ICG, NIRAF, 5-ALA.

Contacts: Zinchenko S.V., e-mail: zinchenkos.v@mail.ru.

For citations: Zinchenko S.V., Shanazarov N.A., Muratov N.F., Kisikova S.D., Seitbekova K.S., Galiev I.Z., Ibragim M.I., Ahmetshin R.R. Modern methods of intraoperative fluorescent imaging of the parathyroid glands in endocrine surgery: a literary review, *Biomedical Photonics*, 2025, vol. 14, no. 1, pp. 47–52. doi: 10.24931/2413–9432–2025–14–1–47–52

МЕТОДЫ ИНТРАОПЕРАЦИОННОЙ ФЛУОРЕСЦЕНТНОЙ ТОПИЧЕСКОЙ ДИАГНОСТИКИ ПАРАЩИТОВИДНЫХ ЖЕЛЕЗ: ЛИТЕРАТУРНЫЙ ОБЗОР

С.В. Зинченко[1], Н.А. Шаназаров[2], Н.Ф. Муратов[1], С.Д. Кисикова[2], К.С. Сейтбекова[2], М.И. Ибрагим[3], Р.Р. Ахметшин[1]
[1]Казанский (Приволжский) федеральный университет, Казань, Россия
[2]РГП на ПХВ «Больница Медицинского центра Управления делами Президента РК», Астана, Республика Казахстан
[3]Медицинский центр «Айя», Астана, Республика Казахстан

Резюме

Гиперпаратиреоз (первичный, вторичный и третичный) – распространенное эндокринное заболевание, часто протекающее с выраженной симптоматикой, в большинстве случаев обусловленное аденомой (реже несколькими аденомами) при первичном гиперпаратиреозе (пГПТ) и хронической почечной недостаточностью у пациентов на программном гемодиализе при вторичном (вГПТ) и третичном (тГПТ) гиперпаратиреозе. На сегодняшний день единственный радикальный метод лечения гиперпаратиреоза (ГПТ) – хирургическое удаление патологически измененных паращитовидных желез. В этой связи возникает необходимость совершенствования алгоритмов диагностического поиска, в том числе интраоперационного, измененых паращитовидных желез. Основная задача обзора – изучить современные тенденции и методики интраоперационной визуализации паращитовидных желез, сравнить данные способы и оценить их эффективность. Применение качественно новых технологий топической диагностики

измененных паращитовидных желез, таких как идентификация путем аутофлюоресценции в близком инфракрасном спектре (NIRAF), методика использования индоцианин-зеленого (ICG) и 5-аминолевулиновой кислоты при УФ-излучении позволяют с более чем 90% точностью визуализировать локализацию паращитовидных желез. Однако вопрос их приоритетного использования остается открытым и не решенным.

Ключевые слова: первичный, вторичный и третичный гиперпаратиреоз, паращитовидная железа, визуализация, хирургическое лечение, ICG, NIRAF, 5-АЛК.

Контакты: Зинченко С.В., e-mail: zinchenkos.v@mail.ru

Для цитирования: Зинченко С.В., Шаназаров Н.А., Муратов Н.Ф., Кисикова С.Д., Сейтбекова К.С., Ибрагим М.И., Ахметшин Р.Р. Методы интраоперационной флуоресцентной топической диагностики паращитовидных желез: литературный обзор // Biomedical Photonics. – 2025. – Т. 14, № 1. – С. 47–52. doi: 10.24931/2413–9432–2025–14–1–47–52

Introduction

Today, primary hyperparathyroidism (pHPT) after diabetes mellitus and thyroid diseases is the third most common disease of the endocrine organs, which occurs in 1% of the world's population [15]. Chronic kidney disease in the terminal stage is the cause of secondary hyperparathyroidism (sHPT) and tertiary hyperparathyroidism (tHPT), which is associated with a violation of phosphorus-calcium metabolism, altered metabolism of cholecalciferol due to a violation of its hydroxylation in the affected kidneys [1]. In this case, the secretion of parathyroid hormone (PTH) becomes independent of the concentration of calcium and phosphate ions. Together, this leads first to sHPT, and then to tHPT, which is expressed morphologically in the formation of autonomous hyperfunctioning adenomas of the parathyroid glands (PTG). Drug therapy of HPT in the form of taking drugs that suppress the synthesis of PTH from the cinocalcet group is quite effective in the early stages of sHPT, but has a number of significant drawbacks: 1) high cost; 2) the effectiveness does not extend to pHPT, tHPT and long-term persistent sHPT. Thus, surgical treatment remains the only effective treatment option for the latter category of patients [1].

Despite the fact that PTG surgery has been developing since the mid-20th century, generally accepted indications for parathyroidectomy are accepted only for pHPT; a unified and standardized surgical method, volume, and timing of the intervention for sHPT and tHPT have not yet been developed [1, 2, 3]. The most commonly used approaches are subtotal parathyroidectomy and total parathyroidectomy with autotransplantation. Thus, the analysis conducted by Triponez et al. proves a confident decrease in PTH levels in the postoperative period in patients with total parathyroidectomy, in contrast to patients who underwent subtotal resection [2]. Rothmund et al. also found a low rate of hyperparathyroidism recurrence in patients who underwent total parathyroidectomy with autotransplantation [3]. It is worth noting that autotransplanted PTG tissue will not function fully until it undergoes neovascularization, so transient hypoparathyroidism is more common and pronounced after such radical operations than after subtotal parathyroidectomy. Autotransplantation of PTG can also fail and lead to long-term hypoparathyroidism [4].

For adequate parathyroidectomy, a clear understanding of the PTG localization is necessary. Preoperative PTG visualization techniques such as ultrasound and PTG scintigraphy have not lost their importance to this day. Overweight patients, recurrent HPT, multiple lesions, atypical parathyroid gland location can reduce the accuracy of these methods. All these disadvantages are inherent in intraoperative ultrasound and gamma detection [5,6]. In this review, we discuss in detail the issues of intraoperative fluorescence navigation of the PTG when all available preoperative diagnostic methods have been exhausted.

One of the first methods of visual navigation of the PTG was the intravenous administration of a methylene blue solution in the preoperative period with the development of blue staining of the PTG [7]. However, according to a number of authors, methylene blue stains less than half of all PTG [8], and in some cases can lead to the development of acute neurological disorders [9,10]. Today, this technique is not used due to the above-mentioned shortcomings.

The use of indocyanine green (ICG) as a fluorescent dye has attracted the attention of surgeons due to its ability to improve the visualization of anatomical structures. ICG was first synthesized in 1955 and was initially used in ophthalmology to assess vascular perfusion. One of the first significant studies devoted to the use of ICG in PTG surgery was a study conducted in 2016 by Fortuny et al. [11]. Richard et al. showed that the use of ICG significantly increases the accuracy of PTG identification compared to traditional visualization methods and reaches, according to the authors, 94%. This is especially important in cases where the anatomical position of the glands may vary [12]. Raffaelli et al. found that the use of ICG in parathyroidectomy reduces the number of complications (persistent hypoparathyroidism up

to 9%, persistence of HPT up to 5%) [13]. However, this method also has its drawbacks in use: 1) the need for appropriate fluorescence imaging systems, which are not available in most medical institutions; 2) reduced efficiency of ICG imaging in cicatricial and tumorous changes in the anatomic location of the PTG; 3) the need for expensive training of medical staffl in the ICG imaging technique. The most important advantage of ICG over other techniques is the ability to determine the preservation of PTG vascularization with 99% sensitivity. This helps to determine which glands are functioning normally, which is important for improving calcium control after surgery [14, 15, 16, 17, 18, 19]. Fortuny et al. demonstrated that ICG angiography can reliably predict PTG vascularization and eliminate the possibility of persistent hypoparathyroidism. Using this technique in 13 patients with HPT, it was possible to visualize all 4 PTGs in all cases. A correlation was obtained between perfusion of the parathyroid remnant and its function in the postoperative period [20].

In 2012, Chissov V.I. et al. proposed a method for intraoperative identification of parathyroid gland using derivatives of 5-aminolevulinic acid (5-ALA) (Patent of the Russian Federation No. 2458689 Chissov V.I. et al., 2012). The method is based on the 5-ALA oral administrastion in the preoperative period at a dose of 30 mg/kg of body weight and a surgery performed 120-180 minutes after administration with irradiation of the surgical field with polarized blue light [21]. According to the results of the study by Dolidze et al., conducted as part of a study of the pre-, intra- and postoperative period of surgical treatment with intraoperative visualization in patients with PTG adenomas, it was proven that visualization of the PTG was achieved in 94% of patients. Normalization of ionized calcium levels was also noted within 6 months in 100% of patients, a decrease in PTH levels by more than 50%, and due to clear visualization of the PTG, no recurrent nerve injury was recorded in any of the cases. According to the authors, this approach significantly improves the results of surgical treatment of solitary PTG adenoma in patients with pHPT [22].

In 2020, Zinchenko S.V. et al. described a technique similar to the technique described by Chissov V.I. et al. (Patent of the Russian Federation No. 2019142608). The authors reported that high doses of the drug (10 mg/kg body weight of 5-ALA when administered orally) are not required for adequate parathyroidectomy in patients with sHPT and tHPT, since the excretion of 5-ALA is significantly slowed down in dialysis patients [23]. The promise of this visualization method is undeniable and many studies confirm this thesis. Kalashnikov A.A. et al. conducted a study in which they compared the technique of using 5-ALA in patients with parathyroid adenomas, 95% of which were visualized [24]. Vshivtsev D.O. et al. in their study of intraoperative visualization of the PTG using 5-ALA demonstrated that the fluorescence intensity of altered and hyperfunctioning glands was subjectively higher than that of unchanged glands. In all patients in the sample, the PTH level decreased to normal values within 24 hours after surgery. However, the authors of the study noted the development of a phototoxic reaction was detected in 2 patients with oral administration of 5-ALA at a rate of 30 mg/kg body weight [25].

The most "young" method of PTG visualization is near infrared autofluorescence (NIRAF). In 2011, Paras et al. presented a new technique for PTG detection in the near infrared range. The study demonstrated that the fluorescence intensity of PTG is higher than that of thyroid tissue [26]. In 2014, MacWade et al. presented the possibility of PTG visualization in the near infrared range using a modified Karl Storz camera [27]. Subsequently, a number of studies confirmed these findings that near infrared fluorescence can help in detecting PTG tissue during thyroid surgery. Early studies using near-infrared fluorescence imaging allowed surgeons to scan the surgical field for parathyroid tissue using a camera with a 25 cm field of view, but this requires turning off the operating room lights due to interference between ambient light and the light emitted by the intrinsic fluorophores of the PTG [28,29]. Despite the interest of surgeons in developing the technique, research studies are limited by small patient samples. Rossi et al. conducted a study on the use of NIRAF in parathyroidectomy in 11 patients with primary hyperparathyroidism. Histopathologic examination of 15 resected specimens confirmed 14 PTG adenomas and one schwannoma. All adenomas had a heterogeneous NIRAF pattern, distinct from the homogeneous pattern seen in the schwannoma. A bright "cap" was detected in 9 of 14 (64.3%) PTG adenomas, which proves the high efficiency of the method [30]. A large monocentric prospective study by Akgun et al., which examined NIRAF images in 1506 normal and 597 altered PTG, indicates that there are differences between the luminescence intensity of normal and hyperplastic PTG glands [31]. Despite the high sensitivity and accuracy (92-99%) declared by the authors, cases of negative use of the method have been described. Thus, small adenomas can be verified by the surgeon as normally functioning PTGs. Lee et al. in their study examined NIRAF data in patients with a history of parathyroidectomy. From 2017 to 2021, 151 parathyroidenomas were removed from 131 patients with pHPT. The mean intensity of PTG autofluorescence in the near infrared range had a negative correlation with the weight of patients and a positive correlation with age (glands in elderly patients fluoresced more strongly). However, no correlations were found with the level of calcium in the blood before surgery, PTH, BMI, or gender [32].

Таблица 1.
Сравнение методик интраоперационной визуализации паращитовидных желез

Table 1.
Comparison of intraoperative imaging techniques for parathyroid glands

Методика Methodo-logy	Преимущества Advantages	Недостатки Disadvantages	Чувствительность Sensitivity	Специфичность Specificity	Точность Accuracy
Метиленовый синий [7,8,9,10] Methylene blue [7,8,9,10]	Достаточно четкая визуализация. Sufficiently clear visualization.	Может приводить к развитию острых неврологических нарушений после операции. Can lead to the development of acute neurological disorders after surgery.	Чувствительность 46% Sensitivity 46%	–	–
ICG [11-20] ICG [11-20]	Улучшенная идентификация анатомических структур. Снижение риска послеоперационных осложнений. Интраоперационная оценка васкуляризации. Минимизация инвазивности и сокращение времени операции. Improved identification of anatomical structures. Reduced risk of postoperative complications. Intraoperative assessment of vascularization. Minimization of invasiveness and reduction of surgical time.	Возможен риск возникновения аллергической реакции у пациентов с аллергией на йод. Для проведения методики требуется специальное оборудование. Возможно ограничение визуализации при наличии анатомических особенностей. Possible risk of allergic reaction in patients with iodine allergy. Special equipment is required to perform the technique. Visualization may be limited in the presence of anatomical features.	85%–100%	90%–100%	93%–98%
5-АЛК [21-25] 5-ALA [21-25]	Высокий уровень интраоперационной визуализации. Визуализация гиперплазированных ПЩЖ выше, чем у нормальных. Относительно низкий процент осложнений, минимизация инвазивности, оптимизация времени операции. High level of intraoperative visualization. Visualization of hyperplastic PTG is higher than that of normal ones. Relatively low percentage of complications, minimization of invasiveness, optimization of surgical time	Ограниченная доступность Наличие возможного осложнения в виде фотодерматозов Требует особых условий проведения, учета времени введения препарата Limited availability Presence of a possible complication in the form of photodermatoses Requires special conditions for implementation, taking into account the time of drug administration	85%–95%	90%–98%	88%–95%
NIRAF [26-32] NIRAF [26-32]	Для визуализации ПЩЖ не нужен контраст. Сравнительно большая глубина проникновения спектра. Визуа-лизация не зависит от патологического статуса. Отсутствие побочных эффектов. No contrast needed for PTG imaging. Relatively large spectrum penetration depth. Visualization is independent of pathological status. No side effects.	Ограничивает оценку перфузии ПЩЖ. Требуются особые условия освещения во время операции. Высокие экономические затраты, несовершенное оборудование. Limits PTG perfusion assessment. Requires special lighting conditions during surgery. High economic costs, imperfect equipment.	85%	80%–90%	90%–95%

The resulting data on the comparison of existing methods of intraoperative visualization of the PTG are presented in Table 1.

Conclusion

The main method of treating HPT (primary, secondary and tertiary) remains surgical. Even for an experienced surgeon, visualization of the PTG and their complete removal is often an impossible task. Despite the large number of scientific papers on the topic of intraoperative navigation of the PTG, the cheapest and most effective method of fluorescent visualization of the PTG are techniques using 5-ALA. They do not require the purchase of expensive equipment and fluorescent agents, and are associated with low rates of side effects and complications. Further research on this issue is necessary in order to minimize side effects and improve the effectiveness and safety of surgical treatment of pHPT, sHPT and tHPT

REFERENCES

1. Tjahjono R., Nguyen K., Phung D., Riffat F., Palme C.E. Methods of identification of parathyroid glands in thyroid surgery: A literature review. *ANZ J Surg*, 2021, Vol. 91(9), pp. 1711-1716. doi:10.1111/ans.17117
2. Triponez F., Kebebew E., Dosseh D., et al. Less-than-subtotal parathyroidectomy increases the risk of persistent/recurrent hyperparathyroidism after parathyroidectomy in tertiary hyperparathyroidism after renal transplantation. *Surgery*, 2006, Vol. 140(6), pp. 990-999. doi:10.1016/j.surg.2006.06.039
3. Rothmund M., Wagner P.K., Schark C. Subtotal parathyroidectomy versus total parathyroidectomy and autotransplantation in secondary hyperparathyroidism: a randomized trial. *World J Surg*, 1991, Vol. 15(6), pp. 745-750. doi:10.1007/BF01665309
4. Steinl G.K., Kuo J.H. Surgical Management of Secondary Hyperparathyroidism. *Kidney Int Rep*, 2020, Vol. 6(2), pp. 254-264. doi:10.1016/j.ekir.2020.11.023
5. Epstein E.V. Educational atlas «Ultrasound examination of the thyroid gland // Atlas-manual» / E.V. Epstein, S.I. Matyashchuk. – Kiev, 2004. 2nd ed., p. 382.
6. Mitkov V.V. Clinical guidelines for ultrasound diagnostics / V.V. Mitkov, Moscow, 2005, Vol. 4, pp. 120.
7. Klopper P.J., Moe R.E. Demonstration of the parathyroids during surgery in dogs, with preliminary report of results in some clinical cases. *Surgery*, 1966, Vol. 59(6), pp. 1101-1107.
8. Kuriloff D.B., Sanborn K.V. Rapid intraoperative localization of parathyroid glands utilizing methylene blue infusion. *Otolaryngol Head Neck Surg*, 2004, Vol. 131(5), pp. 616-622. doi:10.1016/j.otohns.2004.04.026
9. Sweet G., Standiford S.B. Methylene-blue-associated encephalopathy. *J Am Coll Surg*, 2007, 204(3), pp. 454-458. doi:10.1016/j.jamcollsurg.2006.12.030
10. Ng B.K., Cameron A.J., Liang R., Rahman H. Serotonin syndrome following methylene blue infusion during parathyroidectomy: a case report and literature review. *Can J Anaesth*, 2008, 55(1), pp. 36-41. doi:10.1007/BF03017595
11. Vidal Fortuny J., Karenovics W., Triponez F., Sadowski S.M. Intra-Operative Indocyanine Green Angiography of the Parathyroid Gland. *World J Surg*, 2016, Vol. 40(10), pp. 2378-2381. doi:10.1007/s00268-016-3493-2
12. Richard M., Rizo P. Feasibility of parathyroid gland autofluorescence imaging after indocyanine green fluorescence angiography. *Front Endocrinol (Lausanne)*, 2023, Vol. 14, pp. 1248449. doi:10.3389/fendo.2023.1248449
13. Lombardi C.P., Raffaelli M., Princi P., et al. Parathyroid hormone levels 4 hours after surgery do not accurately predict post-thyroidectomy hypocalcemia. *Surgery*, 2006, Vol. 140(6), pp. 1016-1025. doi:10.1016/j.surg.2006.08.009
14. Mannoh E.A., Baregamian N., Thomas G., Solórzano C.C., Mahadevan-Jansen A. Comparing laser speckle contrast imaging and indocyanine green angiography for assessment of parathyroid perfusion. *Sci Rep*, 2023, Vol. 13(1), pp. 17270. doi:10.1038/s41598-023-42649-2
15. Aygün N., Uludağ M. Intraoperative Adjunct Methods for Localization in Primary Hyperparathyroidism. *Sisli Etfal Hastan Tip Bul*, 2019, Vol. 53(2), pp. 84-95. doi:10.14744/SEMB.2019.37542

ЛИТЕРАТУРА

1. Tjahjono R., Nguyen K., Phung D., Riffat F., Palme C.E. Methods of identification of parathyroid glands in thyroid surgery: A literature review // ANZ J Surg. – 2021. – Vol. 91(9). – P. 1711-1716. doi:10.1111/ans.17117
2. Triponez F., Kebebew E., Dosseh D., et al. Less-than-subtotal parathyroidectomy increases the risk of persistent/recurrent hyperparathyroidism after parathyroidectomy in tertiary hyperparathyroidism after renal transplantation // Surgery. – 2006. – Vol. 140(6). – P. 990-999. doi:10.1016/j.surg.2006.06.039
3. Rothmund M., Wagner P.K., Schark C. Subtotal parathyroidectomy versus total parathyroidectomy and autotransplantation in secondary hyperparathyroidism: a randomized trial // *World J Surg*. – 1991. – Vol. 15(6). – P. 745-750. doi:10.1007/BF01665309
4. Steinl G.K., Kuo J.H. Surgical Management of Secondary Hyperparathyroidism // Kidney Int Rep. – 2020. – Vol. 6(2). – P. 254-264. doi:10.1016/j.ekir.2020.11.023
5. Эпштейн Е.В. Учебный атлас «Ультразвуковое исследование щитовидной железы // Атлас-руководство» / Е.В. Эпштейн, С.И. Матящук. – Киев, 2004. изд. 2-е. – С. 382.
6. Митьков В.В. Клиническое руководство по ультразвуковой диагностике / В.В. Митьков. – М., 2005. – Т. 4. – С. 120.
7. Klopper P.J., Moe R.E. Demonstration of the parathyroids during surgery in dogs, with preliminary report of results in some clinical cases // Surgery. – 1966. – Vol. 59(6). – P. 1101-1107.
8. Kuriloff D.B., Sanborn K.V. Rapid intraoperative localization of parathyroid glands utilizing methylene blue infusion // Otolaryngol Head Neck Surg. – 2004. – Vol. 131(5). – P. 616-622. doi:10.1016/j.otohns.2004.04.026
9. Sweet G., Standiford S.B. Methylene-blue-associated encephalopathy // J Am Coll Surg. – 2007. – Vol. 204(3). – P. 454-458. doi:10.1016/j.jamcollsurg.2006.12.030
10. Ng B.K., Cameron A.J., Liang R., Rahman H. Serotonin syndrome following methylene blue infusion during parathyroidectomy: a case report and literature review // Can J Anaesth. – 2008. – Vol. 55(1). – P. 36-41. doi:10.1007/BF03017595
11. Vidal Fortuny J., Karenovics W., Triponez F., Sadowski S.M. Intra-Operative Indocyanine Green Angiography of the Parathyroid Gland // World J Surg. – 2016. – Vol. 40(10). – P. 2378-2381. doi:10.1007/s00268-016-3493-2
12. Richard M., Rizo P. Feasibility of parathyroid gland autofluorescence imaging after indocyanine green fluorescence angiography // Front Endocrinol (Lausanne). – 2023. – Vol. 14. – P. 1248449. doi:10.3389/fendo.2023.1248449
13. Lombardi C.P., Raffaelli M., Princi P., et al. Parathyroid hormone levels 4 hours after surgery do not accurately predict post-thyroidectomy hypocalcemia // Surgery. – 2006. – Vol. 140(6). – P. 1016-1025. doi:10.1016/j.surg.2006.08.009
14. Mannoh E.A., Baregamian N., Thomas G., Solórzano C.C., Mahadevan-Jansen A. Comparing laser speckle contrast imaging and indocyanine green angiography for assessment of parathyroid perfusion // Sci Rep. – 2023. – Vol. 13(1). – P. 17270. doi:10.1038/s41598-023-42649-2
15. Aygün N., Uludağ M. Intraoperative Adjunct Methods for Localization in Primary Hyperparathyroidism // Sisli Etfal Hastan Tip Bul. – 2019. – Vol. 53(2). – P. 84-95. doi:10.14744/SEMB.2019.37542

16. Abdelrahman H., El-Menyar A., Peralta R., Al-Thani H. Application of indocyanine green in surgery: A review of current evidence and implementation in trauma patients. *World J Gastrointest Surg*, 2023, Vol. 15(5), pp. 757-775. doi:10.4240/wjgs.v15.i5.757
17. Rames J.D., Tran N.V., Hesley G.K., Fahradyan V., Lee C.U. An Allergic Reaction in Contrast-enhanced Ultrasound Lymphography for Lymphovenous Bypass Surgery. *Plast Reconstr Surg Glob Open*, 2024, Vol. 12(6), pp. e5908. doi:10.1097/GOX.0000000000005908
18. Namikawa K., Tsutsumida A., Tanaka R., Kato J., Yamazaki N. Limitation of indocyanine green fluorescence in identifying sentinel lymph node prior to skin incision in cutaneous melanoma. *Int J Clin Oncol*, 2014, Vol. 19(1), pp. 198-203. doi:10.1007/s10147-013-0524-y
19. Li H., Xie X., Du F., et al. A narrative review of intraoperative use of indocyanine green fluorescence imaging in gastrointestinal cancer: situation and future directions. *J Gastrointest Oncol*, 2023, Vol. 14(2), pp. 1095-1113. doi:10.21037/jgo-23-230
20. 20 Vidal Fortuny J., Guigard S., Diaper J., Karenovics W., Triponez F. Subtotal Parathyroidectomy Under Indocyanine Green Angiography. *VideoEndocrinology*, 2016, Vol. 3(1), pp. ve.2015.0056. doi:10.1089/ve.2015.0056
21. Method of intraoperative determination of the parathyroid glands / V.I. Chissov, I.V. Reshetov, A.K. Golubtsov, et al. – No. 2458689, announced on 28.03.2011; published on 20.08.2012, Byul. No. 21.
22. Dolidze D.D., Mumladze R.B., Vardanyan A.V., Dzhigkaev T.D., Siukaev O.N., Shieh M. An integrated approach for the surgical treatment of patients with primary hyperparathyroidism. *Endocrine Surgery*, 2013, Vol. 7(3), pp. 41-47. doi:10.14341/serg2013341-47
23. A method of intraoperative identification of hyperplasia and tumors of the parathyroid glands in patients with primary, secondary and tertiary hyperparathyroidism for adequate parathyroidectomy / S.V. Zinchenko, I.Z. Galiev, R.M. Minabutdinov, et al. – No. 2019142608; application dated 28.03.2011; published on 23.06.2020, Byul. No. 18.
24. Prevention of iatrogenic postoperative complications in thyroid and parathyroid surgery / A. A. Kalashnikov, S. S. Yashin, E. L. Ovchinnikov [et al.]. *Modern problems of science and education*, 2019, Vol. 6, pp. 135. – EDN ZQFDBJ.
25. Vshivtsev D.O. Intraoperative photodynamic visualization of the parathyroid glands using 5-aminolevulinic acid / Vshivtsev D.O., Shcherbakov V. R., Makhmudov Yu. R. *Proceedings of the Russian Military Medical Academy*, 2020, Vol. 39(S1–1), pp. 188-191. – EDN ZPVXKN.
26. Paras C., Keller M., White L., Phay J., Mahadevan-Jansen A. Near-infrared autofluorescence for the detection of parathyroid glands. *J Biomed Opt*, 2011, Vol. 16(6), pp. 067012. doi:10.1117/1.3583571
27. McWade MA, Paras C, White LM, et al. Label-free intraoperative parathyroid localization with near-infrared autofluorescence imaging. *J Clin Endocrinol Metab*, 2014, Vol. 99(12), pp. 574-4580.
28. Falco J., Dip F., Quadri P., de la Fuente M., Rosenthal R. Cutting edge in thyroid surgery: autofluorescence of parathyroid glands. *J Am Coll Surg*, 2016, Vol. 223(2), pp. 374-380.
29. Kim S.W., Lee H.S., Ahn Y-C., et al. Near-infrared autofluorescence image-guided parathyroid gland mapping in thyroidectomy. *J Am Coll Surg*, 2018, Vol. 226(2), pp. 165-172.
30. Rossi L., De Palma A., Papini P., et al. Near-infrared autofluorescence pattern in parathyroid gland adenoma. *Surg Endosc*, 2024, Vol. 38(11), pp. 6930-6937. doi:10.1007/s00464-024-11314-8
31. Akgun E., Ibrahimli A., Berber E. Near-Infrared Autofluorescence Signature: A New Parameter for Intraoperative Assessment of Parathyroid Glands in Primary Hyperparathyroidism. *J Am Coll Surg*. doi:10.1097/XCS.0000000000001147
32. Lee S.M., Dedhia P.H., Shen C., Phay J.E. Smaller parathyroids have higher near-infrared autofluorescence intensity in hyperparathyroidism. *Surgery*, 2022, Vol. 172(4), pp. 1114-1118. doi:10.1016/j.surg.2022.06.027

16. Abdelrahman H., El-Menyar A., Peralta R., Al-Thani H. Application of indocyanine green in surgery: A review of current evidence and implementation in trauma patients // World J Gastrointest Surg. – 2023. – Vol. 15(5). – P. 757-775. doi:10.4240/wjgs.v15.i5.757
17. Rames J.D., Tran N.V., Hesley G.K., Fahradyan V., Lee C.U. An Allergic Reaction in Contrast-enhanced Ultrasound Lymphography for Lymphovenous Bypass Surgery // Plast Reconstr Surg Glob Open. – 2024. – Vol. 12(6). – P. e5908. doi:10.1097/GOX.0000000000005908
18. Namikawa K., Tsutsumida A., Tanaka R., Kato J., Yamazaki N. Limitation of indocyanine green fluorescence in identifying sentinel lymph node prior to skin incision in cutaneous melanoma // Int J Clin Oncol. – 2014. – Vol. 19(1). – P. 198-203. doi:10.1007/s10147-013-0524-y
19. Li H., Xie X., Du F., et al. A narrative review of intraoperative use of indocyanine green fluorescence imaging in gastrointestinal cancer: situation and future directions // J Gastrointest Oncol. – 2023. – Vol. 14(2). – P. 1095-1113. doi:10.21037/jgo-23-230
20. 20 Vidal Fortuny J., Guigard S., Diaper J., Karenovics W., Triponez F. Subtotal Parathyroidectomy Under Indocyanine Green Angiography // VideoEndocrinology. – 2016. – Vol. 3(1). – P. ve.2015.0056. doi:10.1089/ve.2015.0056
21. Способ интраоперационного определения паращитовидных желез / В.И. Чиссов, И.В. Решетов, А.К. Голубцов, и др. №2458689, заявл. 28.03.2011; опубл. 20.08.2012, Бюл. №21.
22. Dolidze D.D., Mumladze R.B., Vardanyan A.V., Dzhigkaev T.D., Siukaev O.N., Shieh M. An integrated approach for the surgical treatment of patients with primary hyperparathyroidism // Endocrine Surgery. – 2013. – Vol. 7(3). – P. 41-47. doi:10.14341/serg2013341-47
23. Способ интраоперационной идентификации гиперплазии и опухолей паращитовидных желез у пациентов с первичным, вторичным и третичным гиперпаратиреозом для адекватной паратиреоидэктомии / С.В. Зинченко, И.З. Галиев, Р.М. Минабутдинов, и др. №2019142608; заявл. 28.03.2011; опубл. 23.06.2020, Бюл. №18.
24. Профилактика ятрогенных послеоперационных осложнений в тиреоидной и паратиреоидной хирургии / А. А. Калашников, С. С. Яшин, Е. Л. Овчинников [и др.] // Современные проблемы науки и образования. – 2019. – № 6. – С. 135. – EDN ZQFDBJ.
25. Вшивцев, Д. О. Интраоперационная фотодинамическая визуализация околощитовидных желез с применением 5-аминолевулиновой кислоты / Д. О. Вшивцев, В. Р. Щербаков, Ю. Р. Махмудов // Известия Российской военно-медицинской академии. – 2020. – Т. 39, № S1-1. – С. 188-191. – EDN ZPVXKN.
26. Paras C., Keller M., White L., Phay J., Mahadevan-Jansen A. Near-infrared autofluorescence for the detection of parathyroid glands // J Biomed Opt. – 2011. – Vol. 16(6). – P. 067012. doi:10.1117/1.3583571
27. McWade MA, Paras C, White LM, et al. Label-free intraoperative parathyroid localization with near-infrared autofluorescence imaging // J Clin Endocrinol Metab. – 2014. – Vol. 99(12). – P. 574-4580.
28. Falco J., Dip F., Quadri P., de la Fuente M., Rosenthal R. Cutting edge in thyroid surgery: autofluorescence of parathyroid glands // J Am Coll Surg. – 2016. – Vol. 223(2). – P. 374-380.
29. Kim S.W., Lee H.S., Ahn Y-C., et al. Near-infrared autofluorescence image-guided parathyroid gland mapping in thyroidectomy // J Am Coll Surg. – 2018. – Vol. 226(2). – P. 165-172.
30. Rossi L., De Palma A., Papini P., et al. Near-infrared autofluorescence pattern in parathyroid gland adenoma // Surg Endosc. – 2024. – Vol. 38(11). – P. 6930-6937. doi:10.1007/s00464-024-11314-8
31. Akgun E., Ibrahimli A., Berber E. Near-Infrared Autofluorescence Signature: A New Parameter for Intraoperative Assessment of Parathyroid Glands in Primary Hyperparathyroidism // J Am Coll Surg. doi:10.1097/XCS.0000000000001147
32. Lee S.M., Dedhia P.H., Shen C., Phay J.E. Smaller parathyroids have higher near-infrared autofluorescence intensity in hyperparathyroidism // Surgery. – 2022. – Vol. 172(4). – P. 1114-1118. doi:10.1016/j.surg.2022.06.027

ФОТОСЕНСИБИЛИЗАТОРЫ НОВОГО ПОКОЛЕНИЯ ДЛЯ ФОТОДИНАМИЧЕСКОЙ ТЕРАПИИ

«ФОТОДИТАЗИН®» концентрат для приготовления раствора для инфузий — лекарственное средство (РУ № ЛС 001246 от 18.05.2012 г.)
«ФОТОДИТАЗИН®» гель — изделие медицинского назначения (РУ № ФСР 2012/13043 от 03.02.2012 г.)
«ФОТОДИТАГЕЛЬ®» — косметическое средство (ДС ЕАЭС № RU Д-RU.НВ42.В.06108/20 от 24.09.2020 г.)

Препараты применяются для флюоресцентной диагностики и фотодинамической терапии злокачественных новообразований, а также патологий неонкологического характера в следующих областях медицины:

- гинекология
- урология
- нейрохирургия
- торакальная хирургия
- офтальмология
- травматология
- ортопедия
- комбустиология
- гнойная хирургия
- дерматология
- косметология
- стоматология

www.fotoditazin.com
www.фотодитазин.рф

@FOTODITAZIN

@FOTODITAGEL_FDT

ООО «ВЕТА-ГРАНД»
123056, г. Москва, ул. Красина, д. 27, стр. 2
Тел.: +7 (499) 250-40-00, +7 (929) 971-44-46
E-mail: veta-grand@mail.ru